EFFECT OF NANO FILLERS ON THE PRODUCTION AND PROPERTIES OF LLDPE USING *IN-SITU* POLYMERIZATION

BY

MUHAMMAD DAUD

A Dissertation Presented to the

DEANSHIP OF GRADUATE STUDIES

KING FAHD UNIVERSITY OF PETROLEUM & MINERALS

DHAHRAN, SAUDI ARABIA

In Partial Fulfillment of the
Requirements for the Degree of

DOCTOR OF PHILOSOPHY

In

CHEMICAL ENGINEERING

December 2016

KING FAHD UNIVERSITY OF PETROLEUM & MINERALS

DHAHRAN- 31261, SAUDI ARABIA

DEANSHIP OF GRADUATE STUDIES

This thesis, written by **Muhammad Daud** under the direction of his thesis advisor and approved by his thesis committee, has been presented and accepted by the Dean of Graduate Studies, in partial fulfillment of the requirements for the degree of **DOCTOR OF PHILOSOPHY IN CHEMICAL ENGINEERING.**

Dr. Mamdouh A. Al-Harthi
(Advisor)

Dr. Mohammed S. Ba-Shammakh
Department Chairman

Dr. Mohamed B. Amin
(Member)

Dr. Salam A. Zummo
Dean of Graduate Studies

Dr. Mohammed S.Ba-Shammakh
(Member)

4/1/17

Date

Dr. Mohammad M. Hossain
(Member)

Dr. Shaikh A. Razzak
(Member)

Dedicated

To my beloved father Mr. Murad Ali Khan

&

My kids,

Ibraheem Khan & Musa Khan

ACKNOWLEDGMENTS

First of all thanks to ALLAH, the most merciful and beneficent, Who gave me the strength and power to complete my thesis with great interest and well on time.

I am highly thankful to the Department of Chemical Engineering, King Fahad University of Petroleum & Minerals (KFUPM), Saudi Arabia for awarding me Ph.D scholarship. I am highly thankful to my parental institute i.e. Department of Chemical Engineering, University of Engineering & Technology (UET) Peshawar for their support and paid study leave, to persue my Ph.D.

I express sincere thanks to my advisor, Prof. Mamdouh A. Al-Harthi for his technical support, kind supervision and continuous guidance in my research. I am also very thankful for my committee members; Prof. Mohamed B. Amin, Dr. Mohammed S.Ba-Shammakh, Dr. Mohammad M. Hossain and Dr. Shaikh A. Razzak for their valuable and helpful suggestions.

An acknowledgment would not be complete without appreciating my parents and family for their encouragement, motivation and praying continuously for my successful Ph.D completion.

Finally, I would also like to present my acknowledgments to my university colleagues and close-friends especially Muhammad Yasir Khan, Muhammad Safdar Khan Afridi, Dr. Muhammad Sajid, Dr. Umer Mehmood, Farrukh Shehzad and Murad Ali who continuously motivate me in achieving my goals.

TABLE OF CONTENTS

LIST OF TABLES

LIST OF FIGURES

ABSTRACT

Full Name : MUHAMMAD DAUD

Thesis Title : *[EFFECT OF NANO FILLERS ON THE PRODUCTION AND PROPERTIES OF LLDPE USING IN-SITU POLYMERIZATION]*

Major Field : [CHEMICAL ENGINEERING]

Date of Degree : [December, 2016]

Linear low density polyethylene (LLDPE) was synthesized using in-situ polymerization of ethylene with various alpha olefins (comonomers). Zirconocene/MAO was used as catalyst/cocatalyst complex. The comonomers used under study were 1-hexene, 1-octene, and 1-decene. In this study, the effect of comonomers on the catalytic activity, melting temperature (T_m), degree of crystallinity (DOC), melt crystallization behavior and lamellar thickness distribution (LTD) were evaluated. A higher catalytic activity was recorded in the presence comonomers. Further, the comonomers have added more short chain branching (SCB) to the copolymers, which corresponds to lower DOC and T_m. The Mo crystallization model perfectly explained the crystallization behavior of the copolymers for all cooling rates under study. The modified Gibbs-Thomson equation was utilized to observe the melting behaviors and LTD of the copolymers. Moreover, the activation energies (E_A) were calculated using Kissinger method. The 1-hexene comonomer exhibited the lowest E_A. Overall, crystallization was found, to be more effected by the degree of branching rather than the comonomer type.

In another study, LLDPE nanocomposites were synthesized in the presence of nano titania doped with 1 % (TiO_2/Mn), used as a drop-in nanofiller. The comonomer selected for this study was 1-hexene, based on our previous findings. The nanofiller added more SCB to the polymer backbone and as result decreased the DOC and T_m. The non-isothermal crystallization behavior of the synthesized polymer nanocomposites were studied by Ozawa and Mo models. Additionally, the E_A of the nanocomposites were calculated using Kissinger method. An increased E_A profiles were observed, confirming a slower crystallization process in the presence of nano filler.

Further, graphene/layered double hydroxides (G/LDHs) hybrid nanofillers were synthesized by co-precipitation technique and were successfully characterized using different characterization techniques. The hybrid G/LDHs based ethylene-co-1-hexene nanocomposites were synthesized using in-situ polymerization. The activity of the zirconocene catalyst was boosted in the presence of hybrid nanofillers. Moreover, the synthesized polymer nanocomposites have shown improved thermal stability. E_A for the synthesized polymer nanocomposites were calculated using Friedman iso-conversional method. The G/LDHs based polymer nanocomposites have shown higher E_A (more thermal stability) compared to bare LDHs based nanocomposites, because of the superior thermal properties inherited by these hybrid nanofillers.

Keywords: Copolymers, Catalytic activity, Melt crystallization, Hybrid materials Graphene/Layered double hydroxides nanocomposites

ملخص الرسالة

الاسم الكامل: محمد داؤود

عنوان الرسالة: تاثير المواد المالئة النانوية فى تحسين انتاج وخصائص البولي اثيلين الخطي منخفض الكثافة باستخدام تقنية البلمرة في الموقع

التخصص: هندسة كيميائية

تاريخ الدرجة العلمية: ديسمبر 2016

في هذه الدراسة تم تصنيع البولي اثيلين الخطي منخفض الكثافة (LLDPE) باستخدام طريقة in-situ polymerization من الاثيلين وألفا الأوليفينات وقد استخدم zirconocene / MAO كمحفز معقد. تم استخدام جزيئات (comonomers) مختلفة مثل 1-hexene، 1-octene، و1-decene . ايضا في هذه الدراسه تمت دراسة تاثير comonomers على نشاط المحفز، ودرجة حرارة الانصهار (T_m) ودرجة التبلور (DOC) و lamellar thickness distribution. وجود comonomers زاد من نشاط المحفز. وعلاوة على ذلك، عند اضافة نسب أعلى من comonomer تزداد التفرعات السلسلية القصيرة (SCB)، والتي أدت بدورها الى انخفاض درجة التبلور (DOC) ودرجة الانصهار . وأوضحت طريقة Mo بصورة جيدة سلوك بلورة comonomers عند درجات تبريد مختلفة. استخدمت معادلة Gibbs Thomson المعدلة لدراسة سلوك الانصهار و lamellar thickness distribution. تم حساب طاقات التنشيط باستخدام طريقة Kissinger. أوضحت نتائج الدراسة ان 1-هيكسين comonomer له طاقة التنشيط الاقل وان عملية التبلور تعتمد بشكل اكبر على درجة التفرع بدلا من نوع comonomer.

وعلاوة على ذلك، تم في هذه الدراسة تصنيع البولي اثيلين الخطي منخفض الكثافة (LLDPE) باستخدام 1 % من المغنيز المطعم باوكسيد التيتانيوم (Mn/ TIO_2) كمادة مالئة نانونية. تم اختيار1-هيكسين (comonomer) لهذه الدراسة استنادا إلى النتائج السابقة التي توصلنا إليها. ادى اضافة المادة المالئة النانونية الى زيادة SCB وتقليل DOC ودرجة الانصهار. وايضا تم دراسة عملية التبلور (non-isothermal) للمواد المحضرة باستخدام النماذج المقترحة من قبل Ozawa وMo. بالإضافة إلى ذلك، تم حساب طاقة التنشيط (E_A) للبوليمر المتناهى الصغر

باستخدام طريقة Kissinger. واظهرت نتائج الدراسة الى وجود زيادة في طاقة التنشيط (E_A) ، مؤكدا ابطاء عملية التبلور بسبب وجود المادة المالئة النانونية.

تم ايضا في هذه الدراسة تصنيع مادة مالئة نانونية هجينه بنجاح من الجرافين / هيدروكسيدات مزدوجة الطبقات (G/LDHs) بواسطة تقنية co-precipitation. واستخدمت هذه المالئة النانومترية الهجينة كمادة مالئة في بلمرة الاثيلين و1-هيكسين . و أظهرت نتائج الدراسة وجود زيادة كبيرة في نشاط الحفاز (zirconocene) بسبب وجود هذه المالئة النانومترية الهجينة. وأظهرت نتائج البحث كذلك أن البوليمرات النانونية المحضرة لها استقرار حراري افضل . تم حساب طاقة التنشيط للبوليمرات المحضرة باستخدام طريقة iso-conversional Friedman. وقد اوضحت نتائج بأن البوليمرات النانونية المحضرة باستخدام G/LDHs لها طاقة تنشيط أعلى من البوليمرات النانونية المحضرة باستخدام LDHs بسب خواصها الحرارية الفائقة.

كلمات البحث: البوليمرات المشتركة، النشاط التحفيزي، تذويب التبلور، الجرافين / هيدرواوكسيدات الطبقات المزدوجة النانوية، المواد الهجينة.

CHAPTER 1

INTRODUCTION

1.1 Polyethylene synthesis

Single site metallocene complexes have gained great interest in the synthesis of polyethylene (PE). The complexes have opened new avenues for synthesizing polymers, having high catalytic activities, high comonomer incorporation, controlled polymer tacticity, efficient microstructure control and chemical composition distribution (CCD). An increased global demand has been noted during the last few decades for the polyethylene (PE) and especially for its derivatives that include high density polyethylene (HDPE), low density polyethylene (LDPE), and linear-low density polyethylene (LLDPE). Among them, the LLDPE has a very prominent demand because of its special applications such as food packaging, shopping bags and beverages bottling, etc. The LLDPE's synthesized with metallocene complexes exhibit several attractive properties depending on the nature and concentration of comonomer used during polymerization reactions [1,2].

1.2 Effect of comonomer

Commercially used comonomers mainly include α-olefins i.e. 1-hexene, 1-octene, and 1-decene. The comonomer has a noticeable effect on: catalytic activity, degree of

crystallinity (DOC), melting temperature (T_m) and several other properties. The catalytic activity of the higher α-olefins (1-decene) exhibit higher catalytic activity compared to 1-octene and 1-hexene under the same conditions of pressure, temperature and comonomer composition for polymerization reaction. However a contradictory results were observed by Mingkwan et al. (2011) by recording a slight decrease in catalytic activity while using 1-decene comonomer compared to 1-octene, due to steric hindrance effect caused by 1-decene comonomer. Higher amorphous contents were noted due to increase of comonomer ratio in the feed and vice versa [1].

1.3 Polymer nanocomposites

In order to enhance the mechanical properties, dielectric properties, heat resistance properties and strength of the PE, various nanofillers can be utilized either by melt blending or by *in-situ* polymerization. During the production of polymer nanocomposites the nanofiller remains in a discontinuous phase in the entire polymer matrix thus enabling them to have better properties than the unmodified polymer. The thus produced nanocomposites have high stiffness and tensile strength. These nanofillers also have high degree of interfacial interaction (due to their nano size) which provides high surface area compared to conventional fillers. Several nano fillers including; Titania (TiO_2), graphene, layered double hydroxides (LDHs) and hybrids of G/LDHs are studied in this thesis. Every nanofiller impart their own special characteristics to the polymer nanocomposites e.g. TiO_2 is the most promising inorganic nanofiller because of its versatile properties, such as unique optical properties, anti-static behavior (used as antibacterial agent), and interesting photo catalytic properties. TiO_2 bosts the catalytic performance of metallocene

catalyst and increases the activation energies. Similarly, the presence of graphene in the polymer nanocomposites made them mechanically strong and thermally more stable [1–4].

1.4 Melt crystallization

The polymer crystallization is an important phase transition process. In fact, the rate of crystallization and the degree of crystallinity are key factors in polymer processing. The comonomer composition and nanofiller both can affects the crystallization kinetics as well. The crystallization kinetics are very important, not only for polymer processing but also for obtaining the desired characteristics. The non-isothermal crystallization kinetics usually have more importance than the isothermal kinetics due to its practical operations and implementation in the industry. These non-isothermal melt studies successfully cover a wide range of kinetic models including Jeizorny, Ozawa and Mo models for the PE and their nanocomposites [2,5].

1.5 Thesis Summary

Thesis summary section highlight the summary of each chapter. Each chapter is discussed in the manuscript format.

Chapter-2 described the general literature related to the production of PE. Further, the importance of LLDPE and metallocene based complexes for LLDPE synthesis were discussed briefly. The chapter also includes the literature review for PE nanocomposites and their applications.

Chapter-3 described the impact of branching and comonomer type on the crystallization kinetics, lamellar thickness distribution and activity of zirconocene catalyst. The comonomers used for this study were: 1-hexene, 1-octene and 1-decene. The *in-situ* polymerization were adopted for the polymer synthesis. Initially equal amounts of each of the comonomer were added to the ethylene polymerization to analyze the comonomer type upon catalytic activity and non-isothermal crystallization kinetics of the synthesized copolymers. The comonomer amount in the reaction greatly influences the final product properties. The activation energies (E_A) were calculated using the Kissinger method and found to be lower for the 1-hexene comonomer, which empowers the 1- hexene copolymer to crystallize relatively easy as compared to other copolymers.

Chapter-4 described the synthesis of LLDPE using 1-hexene as a comonomer by *in-situ* polymerization in the presence of nano TiO_2. The catalytic activities and comonomer incorporation was significantly increased by the addition of nano-TiO_2. The crystallization analysis fractionation (CRYSTAF) profiles has revealed that the microstructure of the copolymers were altered due to TiO_2 nanofiller. The Mo-model perfectly explains the non-isothermal crystallization behavior of the copolymers. The activation energy (E_A) required for the polymerization process was found to be increased with the TiO_2 addition, showing difficulty in the crystallization process.

Chapter-5 described the various synthesis routes adopted for the hybrid graphene/layered double hydroxides (G/LDHs) nanocomposties. The chapter also summarized applications of hybrid materials in various arenas such as supercapacitors, catalysis and nanofillers for polymer nanocomposites. Further, future challenges to continuous mass production, uniform particulated sized were also discussed in detail.

Chapter-6 described the synthesis of G/MgAl hybrid nanofiller using co-precipitation method. The nanofiller was then characterized using different characterization techniques. The synthesized nanofiller was then used as drop-in filler for LLDPE synthesis. This chapter also studied the effect of catalytic activity, crystallinity and degradational kinetics of the as-synthesized LLDPE nanocomposites due the addition of G/MgAl nanofiller.

Chapter-7 described the brief summary of the conclusion and recommendations along with the research outcomes in the form of research publications obtained from this thesis.

1.6 References

[1] M. Daud, F. Shehzad, M.A. Al-Harthi, Crystallization behaviour and lamellar thickness distribution of metallocene-catalyzed polymer: Effect of 1-alkene comonomer and branch length, Can. J. Chem. Eng. (2016). doi:10.1002/cjce.22711.

[2] M. Daud, F. Shehzad, M.A. Al-Harthi, Non-isothermal crystallization kinetics of LLDPE prepared by in situ polymerization in the presence of nano titania, Polym. Bull. 72 (2015) 1233–1245. doi:10.1007/s00289-015-1335-2.

[3] M. Daud, M.S. Kamal, F. Shehzad, M.A. Al-Harthi, Graphene/layered double hydroxides nanocomposites: A review of recent progress in synthesis and applications, Carbon N. Y. 104 (2016) 241–252. doi:10.1016/j.carbon.2016.03.057.

[4] F. Shehzad, M. Daud, M.A. Al-Harthi, Synthesis, characterization and crystallization kinetics of nanocomposites prepared by in situ polymerization of ethylene and graphene, J. Therm. Anal. Calorim. 123 (2016) 1501–1511. doi:10.1007/s10973-015-5087-x.

[5] F. Shehzad, S.P. Thomas, M.A. Al-Harthi, Non-isothermal crystallization kinetics of high density polyethylene/graphene nanocomposites prepared by in-situ polymerization, Thermochim. Acta. 589 (2014) 226–234. doi:10.1016/j.tca.2014.05.039.

CHAPTER 2

LITERATURE REVIEW AND BACKGROUND

2.1 Ethylene polymerization

Polyethylene (PE) is a widely used polymer because of its low production cost and remarkable properties thus making them a favorite product to be used in variety of application such as toys, food packaging, home appliances *etc.* [1]. A huge increase in the production trends of PE has been noted over the last few decades due to its high demand in global plastic consumption [2].

PE are essentially be synthesize by ethylene polymerization/copolymerization with α-olefins (comonomers) including 1-hexene, 1-octene and 1-octene *etc.* [3]. The PEs are sub-categorized as high density PE (HDPE), low density PE (LDPE) and linear-low density PE (LLDPE) or sometimes called very-low density PE (VLDPE) illustrated in Figure 2-1 [1,4]. The short chain branching (SCB) and long chain branching (LCB) attached with ethylene backbone are the basis for the classification of PE. The differences between HDPE/LLDPE and LDPE are further summarized in Table 2-1.

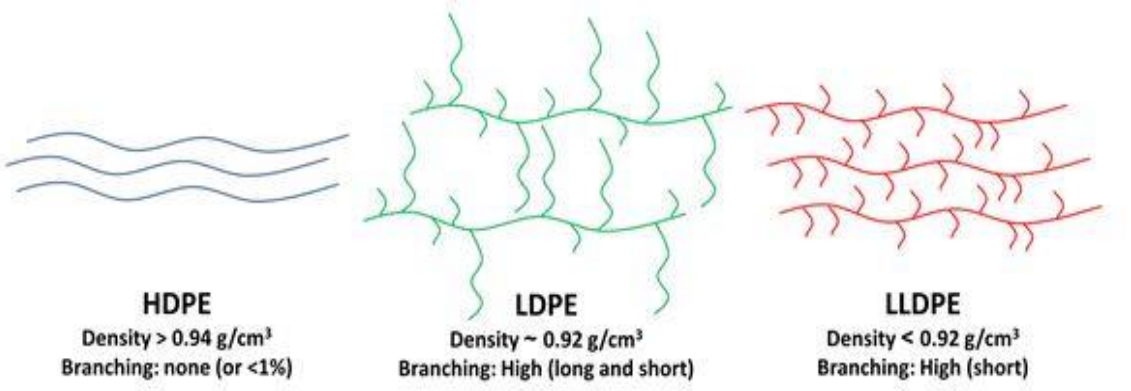

Figure 2-1. Classification of PE on the basis of branching structure and densities range [1] with permission from John Wiley and Sons

Table 2-1. Sketch of differences between HDPE/LLDPE and LDPE [1]

HDPE/LLDPE	**LDPE**
Produced at relatively lower temperature and pressure by copolymerization of ethylene with α-olefin.	Produced by high temperature, high pressure process by polymerization of ethylene without any co-monomer.
Follow Co-ordination polymerization.	Free radical polymerization is involved in the production of LDPE.
SCB are the results of copolymerization of α-olefin.	LCB are formed due to polymer chain transfer reactions. SCB are the results of backbiting reactions.

2.2 Linear low density polyethylene (LLDPE)

Linear low density PE (LLDPE) is synthesized by the copolymerization of ethylene in the presence of comonomer. Commercially used comonomers for the production of LLDPE are α-olefin including 1-butene, 1-hexene and 1-octene [5,6]. The olefins or monomers coordinate with the catalyst active sites and get inserted to the growing polymer chain shown in Figure 2-2. The final copolymer chemical composition distribution (CCD) is highly dependent on different comonomer coordinations and insertion rates [4,7]. LLDPE is one of the most important emerging resins of PE not only because of their low production cost but also due to the properties that make them of remarkable interest to the consumers [8,9]. The most prominent applications of LLDPE including food packaging, shopping bags and beverages bottling, etc. [10]. The addition of the comonomer greatly affects the final product properties, including the catalytic activity, melting temperature, the microstructure of the end polymer and aslo effects the crystallization kinetics [6,11–13].

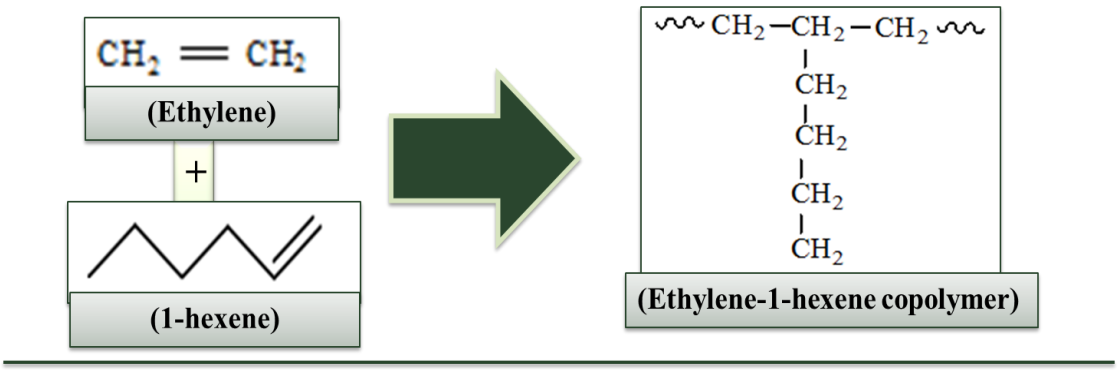

Figure 2-2. Structural design of LLDPE ethylene/1-hexene copolymer

2.3 High activity catalysts for LLDPE production

Single site (metallocene catalysts) or multiple sites (Ziegler-Natta or Phillips) catalysts are widely used for polymerization of HDPE and LLDPE. These catalyst are also known as coordination polymerization catalyst, since they polymerized the product through coordination polymerization [4,7]. The discovery of Zieglar-Natta (ZN) catalyst in the early 1950's was a major breakthrough to the polyolefin industry. The high catalytic activity and selectivity of ZN catalysts makes them favorite for the LLDPE production commercially [2,14]. Selection of process (gas phase, slurry & solution) and catalyst selection (Ziegler-Natta, Phillips or Metallocene) are the important parameters that influence the properties of PE and also control the economics of the system. But due to the single siteness of the metallocene catalyst, it is preferred over Ziegler Natta catalyst, as it gives uniform and narrow microstructure distribution for the copolymers [15,16]. The CCD greatly affects the properties of the copolymers, thus a fast and reliable quantitative technique is mandatory for CCD analysis rapidly [17,18].

2.4 Mettallocene catalyst/cocatalyst complex studies

The LLDPE synthesized with metallocene catalyst/cocatalyst complexes exhibit several attractive properties depending on the nature and concentration of comonomer used during polymerization reactions [19]. Kaminisky and his coworkers in 1998 suggested that, the methylaluminoxane (MAO) is more effective cocatalyst as compared to trimethylaluminium (TMA) while using metallocenes as a catalyst [11]. Further in his studies, he discovered that metallocene/MAO complex can be used to synthesized

LLDPE with high degree of microstructure control, uniform CCD, which cannot be possible to achieve while using the conventional heterogeneous Ziegler-Natta catalyst [20]. MAO is sometimes modified with glycol, ethers or polyethers to synthesized the LLDPE, these polymers have high melt flow index and better thermal processability [21]. The modified methylaluminoxane type 3 (MMAO) and activated modified methylaluminoxane (AMMAO) activators can preferably be used with metallocene catalysts for high yield of LLDPE [3,22–24]. Other activators/cocatalyst that are widely used for synthesis of LLDPE using metallocene catalyst includes; Borane type (polyisobutylaluminoxane and tris(pentafluorophenyl)borane) and Borates type (tetrakis(pentafluorophenyl) and Lithium tetrakis(pentafluorophenyl) borates) [25–28].

2.5 Polymer nanocomposites

In order to enhance the mechanical, electrical and heat resistance properties of the PE, various nano fillers are utilized either by melt blending or by *in-situ* polymerization [29,30]. During the production of polymer nanocomposites the nano filler remains in a discontinuous phase in the entire polymer matrix thus enabling them to have better properties than the unmodified polymer. The thus produced nanocomposites have high stiffness and tensile strength [31,32]. The nano fillers have a high degree of interfacial interaction (due to their nano size) which provides high surface area compared to conventional fillers [31]. Several nano fillers including SiO_2 [32–34], TiO_2 [29,30,35,36], Al_2O_3 [37], LDHs [38] and graphene [39] are widely studied in literature.

2.5.1 PE/TiO_2 nanocomposites

TiO_2 is the most promising inorganic nano filler because of its versatile properties, such as unique optical properties, anti-static behavior (used as antibacterial agent), and interesting photo catalytic properties [29,35]. A detail literature study of PE/TiO_2 are tabulated in Table 2-2.

Table 2-2. PE/TiO_2 Nanocomposites properties and applications

Authors	**Study**	**Findings**
Wang Z et al., 2005 [29]	Preparation and characterization of polyethylene/TiO_2 nanocomposites.	Significant improvement in the impact strength and tensile strength of the polyethylene by the addition of filler by melt compounding.
Wathanyoo O. et al., 2010 [40]	Synthesis of LLDPE/TiO_2 nanocomposites by *in-situ* polymerization with zirconocene/dMMAO catalyst.	The dMMAO is impregnated on TiO_2 to get white powder of dMMAO/TiO2. The catalytic activity is increased by four times as compared to rutile TiO_2.

Kaleel A. et al., 2012 [30]	Effect of Mn doped-titania on the activity of metallocene catalyst by *in-situ* ethylene polymerization	*In-situ* polymerization is the most promising technique to produce polymer nanocomposites with homogeneous distribution of the nanoparticles inside the polymer matrix. Polymerization temperature greatly effect catalytic activity. The filler addition has less effect on Tm. Doped titania has four folding effect on the catalytic activity.
Chaichana E. et al., 2012 [35]	LLDPE/TiO_2 nano composites produced from different crystallite sizes of TiO_2 via *in-situ* polymerization	Different nano crystallite sizes of TiO_2 influences the catalytic activity and co-monomer incorporation in the polymer nano composites. Larger the crystallite size of the nano filler provided better catalytic activity while lesser comonomer incorporation and vice versa.
Daud M. et al., 2015 [41]	Non-Isothermal Crystallization Kinetics of LLDPE Prepared by In-Situ Polymerization in the Presence of Nano Titania.	Doped titania has drastic effect on the activity of the zirconocene catalyst by increasing the 1-hexene incorporation. The optimum dose of the nano filler is found to be 15mg. The activation energies facts revealed that the crystallization process get slower with filler addition. Mo

		model perfectly explain the crystallization behavior of the copolymer.

2.5.2 PE/Graphene nanocomposites

Graphene is one of the new emerging carbon based material of the modern era with Sp2 hybridized carbon atoms arranged in honey comb hexagonal structure. Thermal and mechanical properties of the polymers are dramatically enhanced even with low graphene content [42–44]. Detailed literatures of the effect of graphene on the PE nanocomposites are tabulated below in Table 2-3.

Table 2-3. Graphene/PE nanocomposites properties and applications

Authors	**Study**	**Findings**
Khanam PN. et al., 2015 [45]	Electrical Properties of Graphene Polymer Nanocomposites	Significant improvement in the electrical properties has been recorded with low dosages of graphene addition. The dispersion of graphene greatly influences the Polymer graphene nanocomposites electrical properties.
Farrukh S. et al., 2015 [46]	Synthesis, Characterization and Crystallization Kinetics of Nanocomposites Prepared by *in-situ* Polymerization of Ethylene and Graphene	Thermal and mechanical properties of the nanocomposites are greatly improved with graphene loading. Decrease catalytic activities and increase weight average molecular weight (M_w) is observed for the PE/Graphene nanocomposites.

Kuila T. et al., 2011 [47]	Effect of functionalized graphene on the physical properties of linear low density polyethylene nanocomposites	An increase in the dimension stability, crystallization temperature, storage modulus and thermal stability of the LLDPE/Dodecyl-amine-modified graphene nanocomposites were noted over neat LLDPE. However, the % crystallinity and oxygen/nitrogen permeability decreases.
Kim H. et al., 2010 [48]	Graphene/polyethylene nanocomposites: Effect of polyethylene functionalization and blending methods	Graphene/PE nanocomposites possess better mechanical and electrical properties but the effective dispersion of graphene is difficult to achieve. The LLDPE functionalized with amine and nitrile groups can uniformly disperse graphene nanosheets using solvent based melt blending. The unmodified LLDPE/graphene nanocomposites have higher electrical conductivity as compared to modified one.
Fim F. et al., 2012 [49]	Thermal, Electrical, and Mechanical Properties of Polyethylene–Graphene Nanocomposites Obtained by	Effective dispersion can be achieved using *in-situ* polymerization of PE using zirconocene and MAO complex. The onset degradation temperature of the nanocomposites is increased by 30°C for

	in-Situ Polymerization	20 weight percent. Percolation threshold is recorded at a loading of 8.4 weight percent of graphene. The glass transition temperature is increased from -111°C (neat PE) to -106 °C (6.6 wt. % of graphene loading).
Stürzel M. et al., 2012 [50]	Novel Graphene UHMWPE Nanocomposites Prepared by Polymerization Filling Using Single-Site Catalysts Supported on Functionalized Graphene Nanosheet Dispersions	UHMWPE is synthesized using *in-situ* polymerization filling having functionalized graphene as a support for MAO activated single site chromium (Cr1) catalyst. The complex gives excellent catalytic activities and morphological to the synthesized UHMWPE. The general safety and handling problems associated to the dispersion of graphene using the conventional PE/graphene nanocomposites can be much reduced using FG/MAO/Cr1 complex.

2.5.3 PE/LDHs Nanocomposites

On the other hand, layered double hydroxides (LDHs) have 2D highly tunable brucite-like lamellar crystal structure [51]. They are also commonly known as anionic clays with metallic hydroxides positive layers with charge neutralizer anions (Cl, NO_3, CO_3 etc.). The water associated within the lamellar geometry comes from the synthesis routes followed [52]. Like graphene, LDHs are also employed as nanofillers for the synthesis of polymer nanocomposites [53]. These LDHs based polymer nanocomposites have shown better thermal stability and flame retardancy [54,55]. PE/LDHs nanocomposites properties and applications literature is summarized in Table 2-4.

Table 2-4. PE/TiO2 Nanocomposites properties and applications

Authors	**Study**	**Findings**
Wei Chen. and Baojun Qu. 2004 [56]	LLDPE/ZnAl LDH-exfoliated nanocomposites: effects of nanolayers on thermal and mechanical properties	The ZnAl LDHs were synthesized using Self-assembly technique. The NO_3 anions were replaced with dodecyl sulfate (DS) through intercalation technique for better dispersion of nano LDHs in the polymer matrix. Polymer nanocomposites with 5 wt. % and 20 wt. % were synthesized by solution intercalation technique. The as-synthesized LLDPE/ZnAl nanocomposites has shown better thermal stability having corresponding activation energies as 94, 215 and 150 kJ mol^{-1} for control, 5 and 20 wt. % respectively. Also

		the decomposition temperatures were recorded as 384, 440 and 426 °C respectively, at 30 % wt. loss was considered as reference. Further, the young modulus of 20 wt. % was increased by 59 % over control LLDPE. However, the strength and elongation at break slightly decreased due to decrease crystallinity.
Longchao Du. and Baojun Qu. 2004 [57]	Structural characterization and thermal oxidation properties of LLDPE/ MgAl-LDH nanocomposites	The MgAl LDHs were synthesized using co-precipitation method and was successfully characterized. The LLDPE/LDHs nanocomposites were fabricated using melt blending. The 10 wt. % nano blend has shown better thermal stability by enhancing the degradation temperatures up to 42 °C over control LDLPE at 40 wt. % loss analysis. These LLDPE/MgAl nanocomposites are exhibiting interesting fire retardant properties. Further, the charring process initiated by MgAl LDHs compels the blend to be slowly thermally oxidized in the temperature range of 200

		to 320 ^{0}C.
Peng Ding. And Baojun Qu. 2006 [58]	Structure, Thermal Stability, and Photocrosslinking Characterization of HDPE/LDH Nanocomposites Synthesized by Melt-Intercalation	The co-precipitation synthesis route were followed for ZnAl LDHs. The organomodification of these LDHs were done using the DS. The ZnAl (DS) LDHs were used in 1, 5, 10 and 20 wt. % loading in HDPE. Approx. 40 °C increased were recorded in the decomposition temperature for 5 wt. loaded blend, when taking reference at 50 wt. % loss. Further, these LDHs have the tendency to absorb UV-irradiation and thus the gel contents of 20 wt. % blend at 2s exposure is 1.4 % compared to control HDPE (64.9). Moreover, the photo cross linking efficiency of HDPE/LDHs blends has shown significant decrease due to high uptake of UV light at higher LDHs loading.
Francis RC. et al., 2007 [59]	LDPE/MgAl layered double hydroxide nanocomposite: Thermal and flammability	The melt blend of LDPE/MgAl LDHs is fabricated using twin screw extruder. A 20 °C increased in the decomposition temperature were recorded with just 2.43 wt. % LDHs addition having a peak heat

	properties	release rate (PHRR) value of 600 kW m^{-2}. The PHRR for virgin LDPE was recorded to be 800 kW m^{-2}. This reduction in PHRR corresponds to better flame retardant property of PE nanocomposites. Moreover, at high loading of LDHs (16 wt. %) the PHRR recorded was 300 kW m^{-2} with a 44 % reduction in total heat release (THR). Further, the burning rate of 16.2 wt. % has decreased from 33 to 22 mm/min. These results have shown that better flame retardant polymers can thus be fabricated using LDHs as nanofillers.
Lei Ye. and Qianghua Wu. 2011 [60]	Effects of an Intercalating Agent on the Morphology and Thermal and Flame-Retardant Properties of Low-Density Polyethylene/Layered Double Hydroxide Nanocomposites Prepared by Melt	Three types of anion intercalated MgAl LDHs were successfully synthesized by the authors. These anions include NO_3, dodecyl sulfate anion (DS) and stearate anion (SA). The LDPE/MgAl nanocomposites were synthesized using melt intercalation technique. A better dispersion and morphology can be achieved with MgAl-SA LDHs. Further, the thermal stability and fire retardancy of the PE nanocomposites obey the order as

	Intercalation	PE/SA > PE/DS > PE/NO_3.
Jean CB. et al., 2016 [38]	Metallocene supported core @LDH catalysts for slurry phase ethylene polymerization	The slurry phase polymerization was conducted with metallocene catalysts supported on hybrids of silica@LDHs and zeolite@LDHs using MAO as a cocatalyst. The synergistic effect of LDHs has significantly affected the catalytic activity both in temperature and time domain. As a result of hybridization with LDHs, the activity of the metallocene catalyst has increased up to three times by supporting the accessibility, stability of metallocene based catalysts.

2.6 References

[1] J.B.P. Soares, T.F.L. McKenna, Polyolefin Reaction Engineering, Wiley-VCH Verlag GmbH & Co. KGaA, Weinheim, Germany, Germany, 2012. doi:10.1002/9783527646944.

[2] P.S. Chum, K.W. Swogger, Olefin polymer technologies—History and recent progress at The Dow Chemical Company, Prog. Polym. Sci. 33 (2008) 797–819. doi:10.1016/j.progpolymsci.2008.05.003.

[3] M.-L. Gao, Y.-F. Gu, C. Wang, X.-L. Yao, X.-L. Sun, C.-F. Li, et al., Ethylene homopolymerization and copolymerization with α-olefins catalyzed by titanium complexes bearing [O−NSR] tridentate ligands, J. Mol. Catal. A Chem. 292 (2008) 62–66. doi:10.1016/j.molcata.2008.06.006.

[4] J.B.P. Soares, T. Mckenna, C.P. Cheng, Coordination Polymerization, Handb. Polym. React. Eng. Willey-VCH (2008) 365–430.

[5] R. Quijada, G.B. Galland, R.S. Mauler, The influence of the comonomer in the copolymerization of ethylene with α-olefins using $C_2H_4[ind]_2ZrCl_2$/methylaluminoxane as catalyst system, Macromol. Chem. Phys. 197 (1996) 3091–3098. doi:10.1002/macp.1996.021971003.

[6] J.A.M. Awudza, P.J.T. Tait, The "comonomer effect" in ethylene/α-olefin copolymerization using homogeneous and silica-supported Cp_2ZrCl_2/MAO catalyst systems: Some insights from the kinetics of polymerization, active center studies, and polymerization temperature, J. Polym. Sci. Part A Polym. Chem. 46

(2008) 267–277. doi:10.1002/pola.22378.

[7] W. Kuran, Principles of Coordination Polymerisation, John Wiley & Sons, Ltd, Chichester, UK, UK, 2001. doi:10.1002/047084583X.

[8] O. Pérez, J.B.P. Soares, M. García, V.E. Comparán, J. McCoy, G. Cadenas, Heterogeneous Ethylene and Alpha-Olefin Copolymerization Using Zirconocene Aluminohydride Complexes, Macromol. Symp. 325–326 (2013) 71–76. doi:10.1002/masy.201200041.

[9] H. Wang, Z. Ma, Y. Ke, Y. Hu, Synthesis of linear low density polyethylene (LLDPE) byin situ copolymerization with novel cobalt and zirconium catalysts, Polym. Int. 52 (2003) 1546–1552. doi:10.1002/pi.1282.

[10] S.T. Harini, S. Padmavathi, A. Satish, B. Raj, Food compatibility and degradation properties of pro-oxidant-loaded LLDPE film, J. Appl. Polym. Sci. 131 (2014) n/a-n/a. doi:10.1002/app.39756.

[11] W. Kaminsky, Highly active metallocene catalysts for olefin polymerization, J. Chem. Soc. Dalt. Trans. (1998) 1413–1418. doi:10.1039/a800056e.

[12] I.A. Hussein, Influence of Composition Distribution and Branch Content on the Miscibility of m-LLDPE and HDPE Blends: Rheological Investigation †, Macromolecules. 36 (2003) 2024–2031. doi:10.1021/ma0257245.

[13] M.A. Islam, I.A. Hussein, M. Atiqullah, Effects of branching characteristics and copolymer composition distribution on non-isothermal crystallization kinetics of metallocene LLDPEs, Eur. Polym. J. 43 (2007) 599–610.

doi:10.1016/j.eurpolymj.2006.10.019.

[14] A.K.S.T. Kumar, Handbook of Polyolefins, Second Edition, CRC Press, 2000.

[15] Y. Choi, J.B.P. Soares, Supported single-site catalysts for slurry and gas-phase olefin polymerisation, Can. J. Chem. Eng. 90 (2012) 646–671. doi:10.1002/cjce.20583.

[16] W. Kaminsky, M. Fernandes, Discovery and development of metallocene-based polyolefins with special properties, Polyolefins J. 2 (2015) 1–16.

[17] B. Monrabal, Polyolefins: 50 years after Ziegler and Natta I, Springer Berlin Heidelberg, Berlin, Heidelberg, Heidelberg, 2013. doi:10.1007/978-3-642-40808-3.

[18] J.B.P. Soares, S. Anantawaraskul, Crystallization analysis fractionation, J. Polym. Sci. Part B Polym. Phys. 43 (2005) 1557–1570. doi:10.1002/polb.20441.

[19] M. Wannaborworn, P. Praserthdam, B. Jongsomjit, Observation of Different Catalytic Activity of Various 1-Olefins during Ethylene/1-Olefin Copolymerization with Homogeneous Metallocene Catalysts, Molecules. 16 (2011) 373–383. doi:10.3390/molecules16010373.

[20] W. Kaminsky, C. Piel, K. Scharlach, Polymerization of Ethene and Longer Chained Olefins by Metallocene Catalysis, Macromol. Symp. 226 (2005) 25–34. doi:10.1002/masy.200550803.

[21] S.W. Shao-Hua Guo, Polymerization catalyst system containing polyether-modified aluminoxane, 2005.

[22] M. Wannaborworn, P. Praserthdam, B. Jongsomjit, Z. Cai, H. Yano, T. Shiono, Copolymerization of Ethylene and 1-Hexene with Ansa - Dimethylsilylene(fluorenyl) (t-butylamido)Dimethyltitanium Complexes Activated by Modified Methylaluminoxane, Macromol. Chem. Phys. 214 (2013) 2584–2590. doi:10.1002/macp.201300446.

[23] K. Nishii, S. Hayano, Y. Tsunogae, Z. Cai, Y. Nakayama, T. Shiono, Highly Active Copolymerization of Ethylene and Dicyclopentadiene with [(η 1 - t - BuN)SiMe 2 (η 1 -C 29 H 36)]TiMe 2 (THF) Complex, Chem. Lett. 37 (2008) 590–591. doi:10.1246/cl.2008.590.

[24] M.M. Mortazavi, S. Ahmadjo, J.H.Z. Dos Santos, H. Arabi, M. Nekoomanesh, G.H. Zohuri, et al., Characterization of MAO-Modified Silicas for Ethylene Polymerization, J. Appl. Polym. Sci. (2013) n/a-n/a. doi:10.1002/app.39737.

[25] P.-G. Lassahn, C. Janiak, J.-S. Oh, Borane Activators for Late-Transition Metal Catalysts in Norbornene Polymerization, Macromol. Rapid Commun. 23 (2002) 16–20. doi:10.1002/1521-3927(20020101)23:1<16::AID-MARC16>3.0.CO;2-K.

[26] M.C. Baier, M.A. Zuideveld, S. Mecking, Post-Metallocenes in the Industrial Production of Polyolefins, Angew. Chemie Int. Ed. 53 (2014) 9722–9744. doi:10.1002/anie.201400799.

[27] A. Laine, B.B. Coussens, J.T. Hirvi, A. Berthoud, N. Friederichs, J.R. Severn, et al., Effect of Ligand Structure on Olefin Polymerization by a Metallocene/Borate Catalyst: A Computational Study, Organometallics. 34 (2015) 2415–2421. doi:10.1021/om501185x.

[28] R.S. Rojas, B.C. Peoples, A.R. Cabrera, M. Valderrama, R. Fröhlich, G. Kehr, et al., Synthesis and Structure of Bifunctional Zirconocene/Borane Complexes and Their Activation for Ethylene Polymerization, Organometallics. 30 (2011) 6372–6382. doi:10.1021/om200536z.

[29] Z. Wang, X. Wang, G. Xie, G. Li, Z. Zhang, Preparation and characterization of polyethylene/TiO2 nanocomposites, Compos. Interfaces. 13 (2006) 623–632. doi:10.1163/156855406778440730.

[30] S.H. Abdul Kaleel, B. Kottukkal Bahuleyan, S.K. De, M. Jabarulla Khan, R. Sougrat, M. a. Al-Harthi, Effect of Mn doped-titania on the activity of metallocene catalyst by in situ ethylene polymerization, J. Ind. Eng. Chem. 18 (2012) 1836–1840. doi:10.1016/j.jiec.2012.04.010.

[31] J. Jordan, K.I. Jacob, R. Tannenbaum, M. a. Sharaf, I. Jasiuk, Experimental trends in polymer nanocomposites—a review, Mater. Sci. Eng. A. 393 (2005) 1–11. doi:10.1016/j.msea.2004.09.044.

[32] E. Kontou, M. Niaounakis, Thermo-mechanical properties of LLDPE/SiO2 nanocomposites, Polymer (Guildf). 47 (2006) 1267–1280. doi:10.1016/j.polymer.2005.12.039.

[33] H. Zou, S. Wu, J. Shen, Polymer/Silica Nanocomposites: Preparation, Characterization, Properties, and Applications, Chem. Rev. 108 (2008) 3893–3957. doi:10.1021/cr068035q.

[34] K.-T. Li, C.-L. Dai, C.-W. Kuo, Ethylene polymerization over a nano-sized silica

supported Cp2ZrCl2/MAO catalyst, Catal. Commun. 8 (2007) 1209–1213. doi:10.1016/j.catcom.2006.11.011.

[35] E. Chaichana, S. Pathomsap, O. Mekasuwandumrong, J. Panpranot, A. Shotipruk, B. Jongsomjit, LLDPE/TiO2 nanocomposites produced from different crystallite sizes of TiO2 via in situ polymerization, Chinese Sci. Bull. 57 (2012) 2177–2184. doi:10.1007/s11434-012-5021-6.

[36] Z. Wang, G. Li, G. Xie, Z. Zhang, Dispersion Behavior of TiO2 Nanoparticles in LLDPE/LDPE/TiO2 Nanocomposites, Macromol. Chem. Phys. 206 (2005) 258–262. doi:10.1002/macp.200400309.

[37] M.C. Kuo, C.M. Tsai, J.C. Huang, M. Chen, PEEK composites reinforced by nano-sized SiO2 and Al2O3 particulates, Mater. Chem. Phys. 90 (2005) 185–195. doi:10.1016/j.matchemphys.2004.10.009.

[38] J.-C. Buffet, C.F.H. Byles, R. Felton, C. Chen, D. O'Hare, Metallocene supported core@LDH catalysts for slurry phase ethylene polymerisation, Chem. Commun. 52 (2016) 4076–4079. doi:10.1039/C6CC00280C.

[39] F. Shehzad, S.P. Thomas, M.A. Al-Harthi, Non-isothermal crystallization kinetics of high density polyethylene/graphene nanocomposites prepared by in-situ polymerization, Thermochim. Acta. 589 (2014) 226–234. doi:10.1016/j.tca.2014.05.039.

[40] W. Owpradit, O. Mekasuwandumrong, J. Panpranot, A. Shotipruk, B. Jongsomjit, Synthesis of LLDPE/TiO_2 nanocomposites by in situ polymerization with

zirconocene/dMMAO catalyst: effect of [Al]/[Zr] ratios and TiO_2 phases, Polym. Bull. 66 (2011) 479–490. doi:10.1007/s00289-010-0287-9.

[41] M. Daud, F. Shehzad, M.A. Al-Harthi, Non-isothermal crystallization kinetics of LLDPE prepared by in situ polymerization in the presence of nano titania, Polym. Bull. 72 (2015) 1233–1245. doi:10.1007/s00289-015-1335-2.

[42] R. Verdejo, M.M. Bernal, L.J. Romasanta, M.A. Lopez-Manchado, Graphene filled polymer nanocomposites, J. Mater. Chem. 21 (2011) 3301–3310. doi:10.1039/C0JM02708A.

[43] T.K. Das, S. Prusty, Graphene-Based Polymer Composites and Their Applications, Polym. Plast. Technol. Eng. 52 (2013) 319–331. doi:10.1080/03602559.2012.751410.

[44] H. Kim, A.A. Abdala, C.W. MacOsko, Graphene/polymer nanocomposites, Macromolecules. 43 (2010) 6515–6530.

[45] K.K. Sadasivuni, D. Ponnamma, J. Kim, S. Thomas, eds., Graphene-Based Polymer Nanocomposites in Electronics, Springer International Publishing, Cham, 2015. doi:10.1007/978-3-319-13875-6.

[46] F. Shehzad, M. Daud, M.A. Al-Harthi, Synthesis, characterization and crystallization kinetics of nanocomposites prepared by in situ polymerization of ethylene and graphene, J. Therm. Anal. Calorim. 123 (2016) 1501–1511. doi:10.1007/s10973-015-5087-x.

[47] T. Kuila, S. Bose, A.K. Mishra, P. Khanra, N.H. Kim, J.H. Lee, Effect of

functionalized graphene on the physical properties of linear low density polyethylene nanocomposites, Polym. Test. 31 (2012) 31–38. doi:10.1016/j.polymertesting.2011.09.007.

[48] H. Kim, S. Kobayashi, M.A. Abdurrahim, M.J. Zhang, A. Khusainova, M.A. Hillmyer, et al., Graphene/polyethylene nanocomposites: Effect of polyethylene functionalization and blending methods, Polymer (Guildf). 52 (2011) 1837–1846.

[49] F. de C. Fim, N.R.S. Basso, A.P. Graebin, D.S. Azambuja, G.B. Galland, Thermal, electrical, and mechanical properties of polyethylene-graphene nanocomposites obtained by in situ polymerization, J. Appl. Polym. Sci. 128 (2013) 2630–2637. doi:10.1002/app.38317.

[50] M. Stürzel, F. Kempe, Y. Thomann, S. Mark, M. Enders, R. Mülhaupt, Novel Graphene UHMWPE Nanocomposites Prepared by Polymerization Filling Using Single-Site Catalysts Supported on Functionalized Graphene Nanosheet Dispersions, Macromolecules. 45 (2012) 6878–6887. doi:10.1021/ma301376q.

[51] Q. Wang, D. Ohare, Recent advances in the synthesis and application of layered double hydroxide (LDH) nanosheets, Chem. Rev. 112 (2012) 4124–4155. doi:10.1021/cr200434v.

[52] M. Sajid, C. Basheer, Layered double hydroxides: Emerging sorbent materials for analytical extractions, TrAC Trends Anal. Chem. 75 (2016) 174–182. doi:10.1016/j.trac.2015.06.010.

[53] F.R. Costa, M. Saphiannikova, U. Wagenknecht, G. Heinrich, Layered double

hydroxide based polymer nanocomposites, Wax Cryst. Control Nanocomposites, Stimuli-Responsive Polym. 210 (2008) 101–168. doi:10.1007/12_2007_123.

[54] C. a. W. and D.O. Yanshan Gao, Jingwen Wu,QiangWang, Flame retardant polymer/layered double hydroxide nanocomposites, J. Mater. Chem. A. (2014) 10996–11016. doi:10.1039/c4ta01030b.

[55] Z. Matusinovic, C. a. Wilkie, Fire retardancy and morphology of layered double hydroxide nanocomposites: a review, J. Mater. Chem. 22 (2012) 18701.

[56] W. Chen, B. Qu, LLDPE/ZnAl LDH-exfoliated nanocomposites: effects of nanolayers on thermal and mechanical properties, J. Mater. Chem. 14 (2004) 1705–1710. doi:10.1039/B401790K.

[57] L. Du, B. Qu, Structural characterization and thermal oxidation properties of LLDPE/MgAl-LDH nanocomposites, J. Mater. Chem. 16 (2006) 1549. doi:10.1039/b514319e.

[58] P. Ding, B. Qu, Structure, thermal stability, and photocrosslinking characterization of HDPE/LDH nanocomposites synthesized by melt-intercalation, J. Polym. Sci. Part B Polym. Phys. 44 (2006) 3165–3172. doi:10.1002/polb.20959.

[59] F.R. Costa, U. Wagenknecht, G. Heinrich, LDPE/Mg–Al layered double hydroxide nanocomposite: Thermal and flammability properties, Polym. Degrad. Stab. 92 (2007) 1813–1823. doi:10.1016/j.polymdegradstab.2007.07.009.

[60] L. Ye, Q. Wu, Effects of an intercalating agent on the morphology and thermal and flame-retardant properties of low-density polyethylene/layered double

hydroxide nanocomposites prepared by melt intercalation, J. Appl. Polym. Sci. 123 (2012) 316–323. doi:10.1002/app.33770.

CHAPTER 3

Crystallization behavior and lamellar thickness distribution of metallocene-catalyzed polymer: Effect of 1-alkene comonomer and branch length

Muhammad Daud[1], Farrukh Shehzad[1], Mamdouh A. Al-Harthi[1,2*]

[1] Department of Chemical Engineering, King Fahd University of Petroleum and Minerals, Dhahran 31261, Saudi Arabia

[2] Center of Research Excellence in Petroleum Refining and Petrochemicals (CoRE-PRP), King Fahd University of Petroleum and Minerals, Dhahran 31261, Kingdom of Saudi Arabia

[*]Corresponding Author: Mamdouh A. Al-Harthi

E-mail address: mamdouh@kfupm.edu.sa

This chapter has been accepted in "The Canadian Journal of Chemical Engineering" on 7th June 2016.

ABSTRACT

The effect of comonomer and branching on the melt crystallization and lamellar thickness distribution was studied for ethylene and 1-alkene copolymers. The comonomers used in this study are 1-hexene, 1-octene, and 1-decene. A notable influence of the comonomer ratio in the feed was observed on the crystallization and melting behavior. The Ozawa and Mo models were found suitable for these copolymers. However, variation of relative crystallinity at different heating rates preferred the Mo method over the Ozawa method. The melting behavior and lamellar thickness distribution of the copolymers were analyzed by the help of modified Gibbs-Thomson equation. The activation energies (E_A) for the melt crystallization were calculated using the Kissinger method. It was observed that 1-hexene comonomer exhibits lower E_A, indicating an easier crystallization process as compared to other comonomers used. Overall, crystallization was found to be more influenced by the degree of branching rather than the comonomer type.

Keywords: metallocene catalyst, crystallization kinetics, copolymer, lamellar thickness distribution.

3.1 INTRODUCTION

Single site metallocene complexes have gained great interest in the synthesis of polyethylene (PE). The complexes have opened new paths for synthesizing polymer having high catalytic activities, high comonomer incorporation, controlled polymer tacticity, efficient microstructure control and chemical composition distribution (CCD) [1–4]. An increased global demand has been noted during the last few decades for the PE and especially for its derivatives that include high density polyethylene (HDPE), low density polyethylene (LDPE), and linear-low density polyethylene (LLDPE). LLDPE has very prominent demand because of its special applications such as food packaging, plastic bags, wraps, and pipes etc. [5,6]. The LLDPE synthesized with metallocene complexes exhibits several attractive properties depending on the nature and concentration of comonomer used during polymerization reactions [7–10]. PE and all its derivatives are semi crystalline in nature, and solidify easily during its crystallization. Since the addition of comonomer increases the amorphous contents in the copolymer, thus affecting the crystal structure and morphology and as a result the crystallization kinetics behavior is altered. Therefore, the knowledge of polymer crystallization kinetics and resulting degree of crystallinity are helping tools for its processing and desired characteristics [11,12]. Several studies have been done for better understanding of the concepts linked with isothermal and non-isothermal crystallization behavior of PE [13,14]. The non-isothermal crystallization kinetics has more practical significance over the isothermal kinetics study due to its industrial applications [15]. These non-isothermal melt studies successfully cover a wide range of kinetic models including Jeizorny, Ozawa and Mo models [16–18] for the HDPE, LDPE and LLDPE [14,19,20]. The modeling of

melting behaviors is utilized to study the lamellar thickness distribution (LTD) and average lamellar thickness for the PEs using modified Gibbs-Thomson (MGT) equation [21–23]. Adamu et al. studied the LTD and average lamellar thickness of the ethylene-α-olefin homo- and copolymers using metallocene complexes. It was found that the lamellar thickness of the homopolymer is much widely distributed than the copolymers; with a high weight average lamellar thickness (WALT) calculated using Flory and GT equations. This could be ascribed to the resulting decrease in longer lamellae by the butyl branching of the copolymer [24].

In this research work, in-situ polymerization of ethylene with variant amounts of α-olefins is performed using zirconocene and methyl aluminoxane (MAO) as catalyst/cocatalyst complex. The aim is to study the effect of branching and comonomer type on crystallization behavior, lamellar thickness distribution and activation energies (E_A). The crystallization kinetics and the quantitative effect of branching were analyzed by the Ozawa and Mo models. The LTD and mathematical correlation of WALT with the degree of crystallinity (DOC) was obtained using MGT equation. Activation energy (E_A) was evaluated using Kissinger method [25] and compared with all the samples.

3.2 EXPERIMENTAL

3.2.1 Chemical Reagents

All chemical reagents sensitive to oxygen were stored and manipulated in a glove box under nitrogen atmosphere. Zirconocene ($C_{10}H_{10}Cl_2Zr$) Bis(cyclopentadienyl zirconium (IV) dichloride) > 98 %, methyl aluminoxane (MAO), α-olefins (1-hexene, 1-octene, and

1-decene) and other solvents (toluene and methanol) were provided by the Sigma Aldrich Company and were used as received.

3.2.2 Polymerization Reaction

A Schlenk reactor was charged with 6 mg (20 μmol) of the zirconocene catalyst with subsequent addition of varying amount of α-olefins in 100 mL of solvent (toluene), inside the glove box. The reactor equipped with magnetic stirrer and recipe of the copolymer formation was air tightened using rubber septum and connected to the ethylene line and left for 5 min to get ethylene saturation. After saturation, the MAO was injected into the reactor to initiate the polymerization reaction for 25 minutes. The polymerization conditions were fixed for all reactions i.e. 303 K and 1.3 bar polymerization temperature and ethylene pressure respectively. After a total of 30 min. reaction time, the septum was then removed and the copolymer was quenched with acidified methanol (5 Vol %) for 45 min. The copolymer thus formed was filtered and dried for 24 hours in an oven set at 333 K [19]. The abbreviations used for the LLDPE in the current studies are: HEX-1, HEX-2, OCT-1, OCT-2, OCT-4, DEC-1, DEC-2 and DEC-4, whereas the HEX, OCT and DEC represented the comonomers used while the integers associated with them showed that the milliliters utilized of that particular comonomer in the copolymer synthesis.

3.2.3 Polymer Characterization

The melting and crystallization behavior of the copolymers were characterized by using a DSC Q-1000, TA instruments. The equipment was calibrated using Indium samples. The copolymers were analyzed using conventional heat-cool-heat cycle; at a heating rate of 10 K/min. Melting temperature (T_m) and DOC were recorded from the 2nd heating cycle. For the study of crystallization kinetics, the samples were first heated to 423 K and kept

isothermal for 3 min. to minimize the effect of thermal history [26,27]. The samples were then cooled down at variant cooling rates (β), i.e. 1, 2, 3, 5, 10, 20, and 30 K/min. For baseline and integration of the recorded scans, software (Universal Analysis 2000, TA Instruments) was used provided by the vendor.

Crystallization analysis fractionation (CRYSTAF) was utilized for finding the chemical composition distribution (CCD) of the synthesized copolymers (provided by Polymer Char Instrument model-200). The samples were first dissolved in 1, 2, 4 trichlorobenzene (TCB) at a concentration of 0.1 mg/mL at 423 K for 60 min. The dissolved copolymer was then allowed to cool at 0.1 K/min. passing through a dual wavelength infrared detector to determine the polymer being crystallized in the solution [28,29].

The comonomer incorporation was determined using carbon 13 nuclear magnetic resonance (^{13}C NMR). Approx. 70 to 80 mg of the copolymer was dissolved in TCB at 393 K in 5 mm standard NMR tube with 0.5 mL of deuterated benzene-d6 (lock) [30]. The comonomer mole percentage was determined using ASTM method 5017-96 based on integration of peaks relative to main methylene resonance at 30.0 ppm on x-axis [31].

3.3 RESULTS AND DISCUSSION

3.3.1 Catalytic Activity and Crystallinity

The comonomer concentration in the feed greatly affects the properties of the synthesized copolymers. This effect is very prominent in terms of activity trends for the copolymer (See Figure 3-1). Increased activities of 18 %, 19 % and 15 % were recorded with just a single milliliter addition of comonomers 1-hexene, 1-octene and 1-decene respectively (See Table 3-1). A slight decrease in activity of DEC-4 compared to OCT-4 is due to the

steric hindrance caused by 1-decene (1-C_{10}) atoms [32]. Furthermore, higher amounts of comonomer added up the short chain branching (SCB) to the copolymers, and corresponds to lower DOC and T_m [33]. However, this effect is not that much prominent and approximately 1 K ± 0.4 K decrease was noted in T_m for each milliliter comonomer addition. The comparative CRYSTAF profiles for the copolymers (See Figure 3-2) uphold the ^{13}C NMR results, (See Table 3-1).

Table 3-1. Experimental conditions and properties for ethylene copolymers prepared by *in-situ* copolymerization using zirconocene complex with varying comonomers contents [a]

Sample No.	Comonomer in feed		Activity [b] (kg PE mole^{-1} hr^{-1} bar^{-1})	DOC [c]	T_m [d] (K)	A_{peak} [e]	*Branch Density* (per 1000C) [f]	Weight average lamellar thickness [g] (WALT) (nm)
	(mL)	mole %						
HEX-1	1	0.85	396 ± 6	52.12 ± 0.65	396.1	69.3	7.77	7.8
HEX-2	2	1.70	468 ± 12	31.62 ± 0.46	393.5	53.1	16.2	6.8
OCT-1	1	0.67	424 ± 12	43.14 ± 0.56	394.0	79.5	12.20	7.3
OCT-2	2	1.34	508 ± 6	34.16 ± 0.84	393.8	61.5	18.17	6.7
OCT-4	4	2.68	702 ± 8	24.65 ± 0.97	393.4	37.6	28.65	6.4
DEC-1	1	0.56	452 ± 8	43.84 ± 0.36	395.5	72.1	8.12	7.1
DEC-2	2	1.12	522 ± 11	32.32 ± 0.56	395.2	46.3	17.69	6.5
DEC-4	4	2.24	668 ± 8	30.65 ± 0.86	392.5	43.7	25.60	6.2

[a] Copolymerization conditions: temp = 303 K; ethylene pressure = 1.3 bar; solvent used (toluene) = 100 mL; catalyst used (zirconocene) = 6 mg (20 μmol); polymerization time = 30 min
[b] calculated from obtained yields
[c] determined by DSC based on enthalpy of melting of 100 % crystalline PE, 293.6 J/g
[d] calculated using 2nd heating cycle of DSC
[e] calculated using area under the peaks of the CRYSTAF profiles
[f] determined by ^{13}C NMR
[g] calculated using modified Gibbs-Thomson equations using 2nd heating cycle of DSC

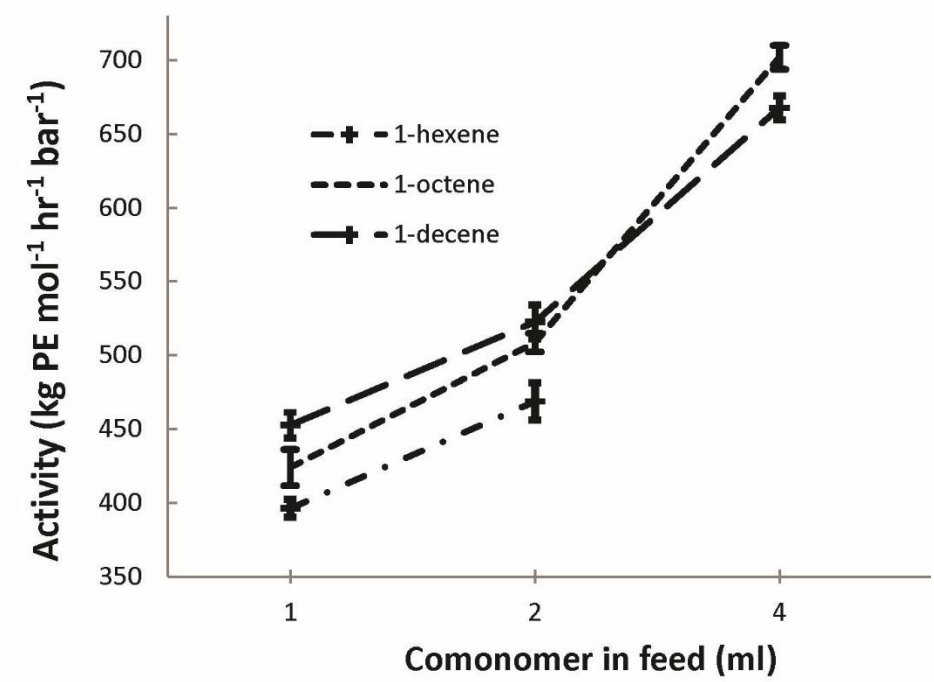

Figure 3-1. Catalytic activity variance with comonomer type and composition in the feed

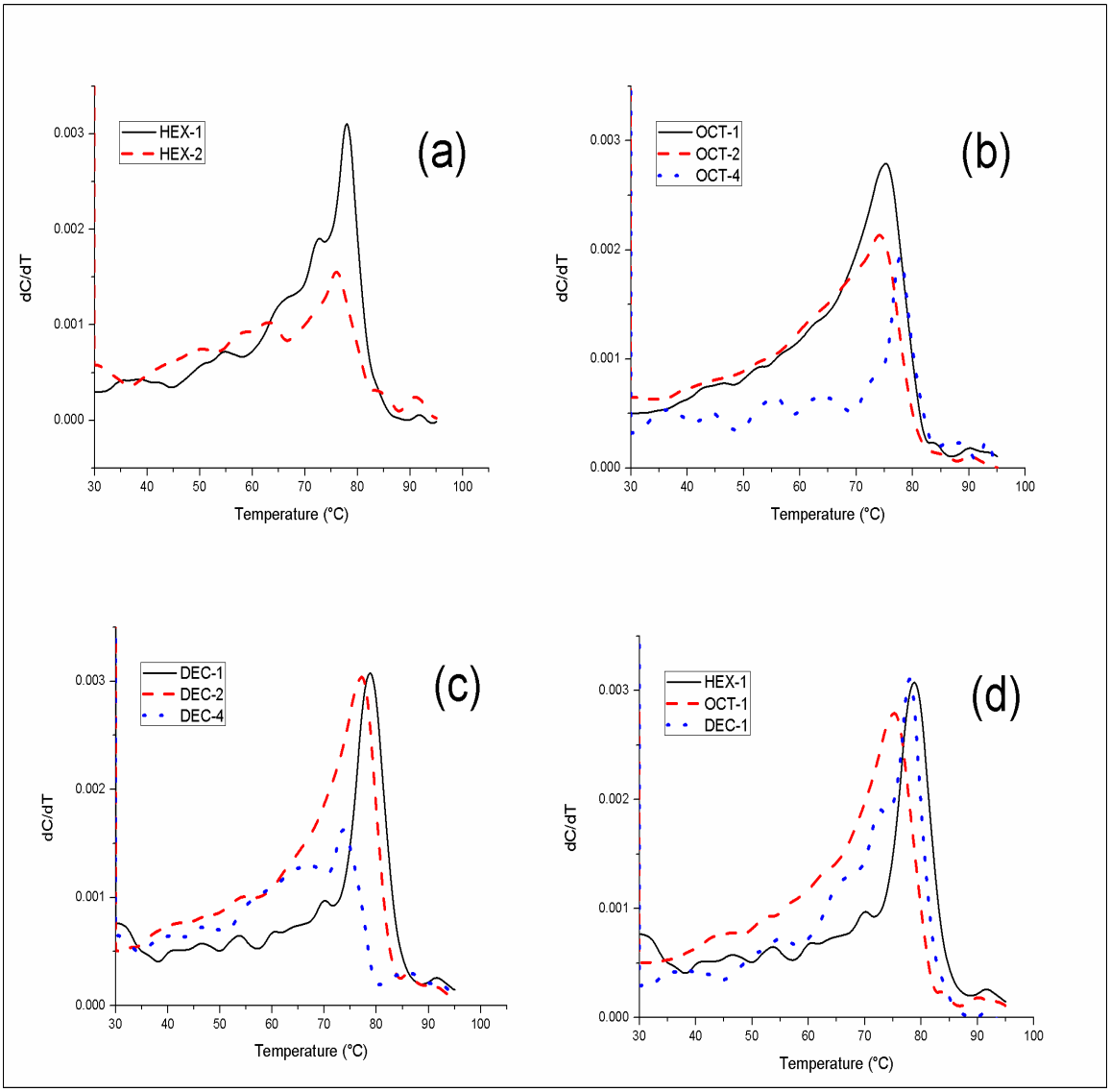

Figure 3-2. Effect of comonomer addition on the CRYSTAF results of the as-synthesized copolymers: a) 1-hexene b) 1-octene c) 1-decene d) comparative profiles using 1 mL comonomer

3.3.2 Thermal Analysis

The crystallization behavior of the copolymers was studied by DSC Q-1000 model equipment. The endotherms obtained for DEC-1 crystallization at different cooling rates (β) are shown in Figure 3-3a. The peak crystallization temperature (T_p) decreases with an increase in β, indicating that at lower cooling rates, the polymer chains have sufficient time to move from the melt phase to the crystal structure phase [14]. On the other hand, the high comonomer content in the feed decreases the crystallization onset and peak temperatures as shown in Figure 3-3b for different concentrations of 1-decene comonomer. The DEC-1 crystallizes earlier followed by DEC-2 and DEC-4, showing relatively less ethylene long chains in DEC-2 and DEC-4 because of the increase in the non-crystallizable fractions constituted by branched octyl- groups [See Table 3-1]. Figure 3-3c illustrates the comparative endotherms profiles for the comonomers HEX-1, OCT-1 and DEC-1, with the ^{13}C NMR analysis given in Table 3-1. The analysis of the results presented in Table 3-1 has shown that HEX-1 sample has the least comonomer incorporation and thus has the longest ethylene sequences compared to OCT-1 and DEC-1. The half-time for crystallization ($t_{½}$) increased with an increase in comonomer contents indicating that the high comonomer contents retarded the crystallization process (See Table 3-2).

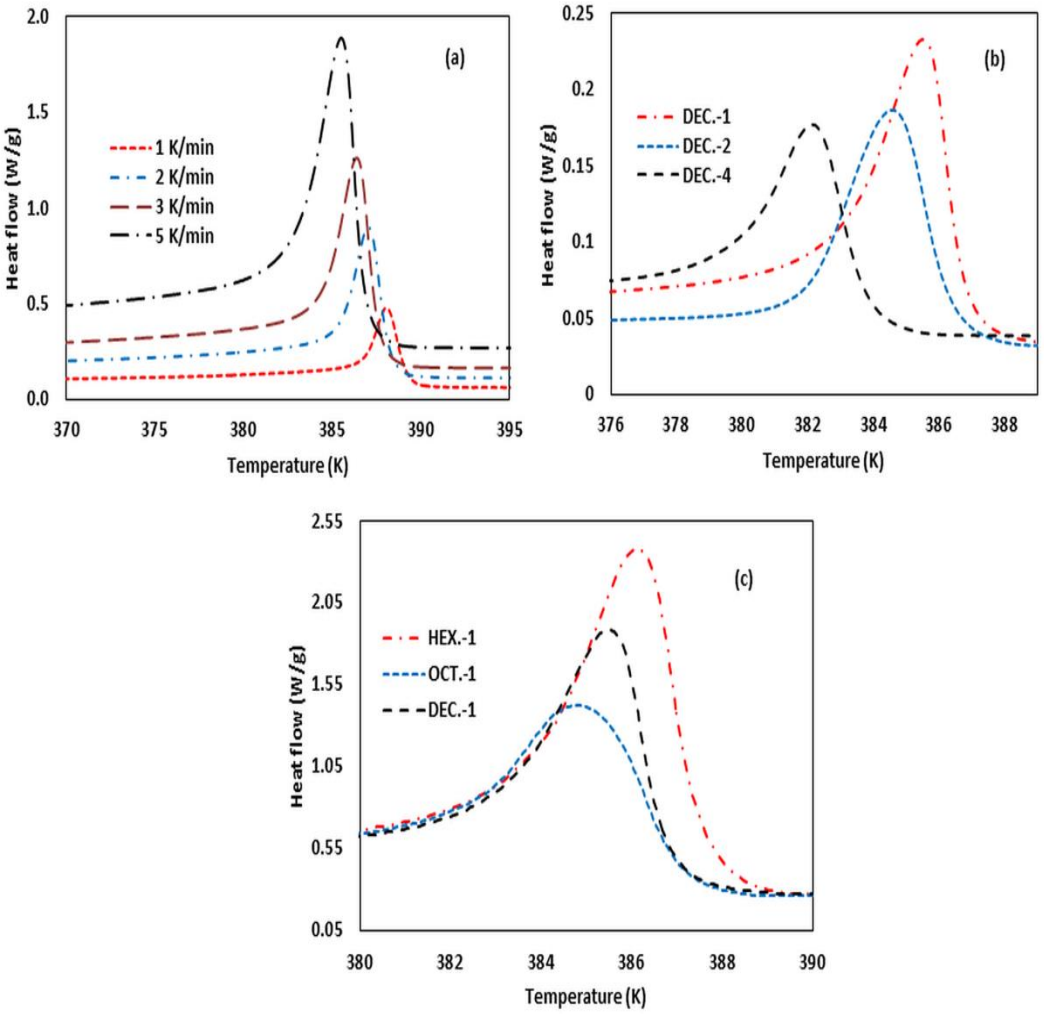

Figure 3-3. Differential Scanning Calorimetry (DSC) endotherms for: (a) different cooling rates; (b) different comonomer compositions; (c) different comonomer type.

Table 3-2. Evaluated half time for crystallization ($t_{½}$) at different cooling rates for all copolymers

β (K/min) Sample	1	2	3	5	10	20	30
	t½ (min)						
HEX-1	15.23	6.28	4.03	2.14	1.03	0.49	0.31
HEX-2	19.79	9.66	6.28	3.55	1.26	0.51	0.28
OCT-1	21.38	9.36	6.22	3.43	1.34	0.63	0.40
OCT-2	22.18	9.35	5.80	3.39	1.53	0.74	0.45
OCT-4	27.68	12.65	7.90	4.49	2.21	1.04	0.58
DEC-1	18.34	8.42	5.56	3.21	1.40	0.65	0.42
DEC-2	22.18	9.77	6.14	3.46	1.16	0.61	0.47
DEC-4	22.82	9.79	6.17	3.56	1.20	0.65	0.53

3.3.3 Melt Crystallization

The crystallization kinetics of polymers can be explained by the well-known Avrami model which relates nucleation rate and lamellar crystal growth of the polymer as a function of crystallization time. The Avrami model is given by Equation (1).

$$X_t = 1 - \exp(-kt^n) \qquad (1)$$

The term X_t represents the volume fraction of the polymer being transformed, *n and k* stands for the Avrami exponent and crystallization rate constant respectively. The parameter *n* is a function of nucleation process and it provides qualitative information about the nature of nucleation and growth process while *k* is the rate constant and it depends on the nucleation and crystal growth. For the non-isothermal crystallization kinetics study, direct use of Avrami model is not suitable since it holds good for the isothermal case and also excludes the secondary crystallization process. Thus for the non-isothermal process, a modified model in the growth rate constant is proposed by Jeizorny [16]. Further modification to the basic Avrami model is done by Ozawa [17] by considering that the crystallization process occurred in an infinite small isothermal steps at a constant cooling rate. The Ozawa model is given by the expression below:

$$X_t = 1 - \frac{\exp\left(-K\left(T\right)\right)}{\beta^m} \qquad (2)$$

K(T) is the crystallization rate constant which is cooling rate dependent function, β is a cooling rate and *m* is the Ozawa exponent. Normally, Ozawa model is preferred over the conventional Jeizorny-Avrami model while operating at non-isothermal crystallization

conditions [34]. The relative crystallinity X_t can be calculated from the DSC exotherm. The weight fraction α_t is calculated using the following expression:

$$\alpha_t = \frac{\Delta H(t)}{\Delta H_{total}} = \frac{\int_{T_o}^{T_i}\left(\frac{dH}{dt}\right)dt}{\int_{T_o}^{T_\infty}\left(\frac{dH}{dt}\right)dt} * 100 \qquad (3)$$

Whereas, ΔH_{total} and $\Delta H(t)$ are the total heat released and heat released at a time *t* for the crystallization process respectively. The relation between weight fractions to volume fraction for the relative crystallinity is evaluated using the following formula:

$$X_t = \frac{\alpha_t}{\alpha_t + \frac{\rho_c}{\rho_a}\left[1-\alpha_t\right]} \qquad (4)$$

The crystalline phase and amorphous phase densities for the PEs are given by ρ_c = 1.004 and ρ_a = 0.853 respectively [19]. The melt crystallization was studied using DSC. The effect of comonomer type and the degree of branching were evaluated by using the Ozawa and Mo models.

Analysis by Ozawa Model

The Ozawa model given by equation (2) can be linearized to the following form

$$Ln\left[-Ln\left[1-X_t\right]\right] = Ln\left[K(T)\right] - mLn\left[\beta\right] \qquad (5)$$

Equation 5 can be fitted to data obtained at different cooling rates. The data can be arranged in the form of $Ln(-Ln(1- X_t))$ vs. $Ln(\beta)$ at different temperatures. The slope and intercept of the Ozawa-plots corresponds to *m* and $Ln(K(T))$ respectively. The Ozawa-plots can be easily generated for any selected temperatures (T_a) and plotting the

crystallinity at that temperature against the corresponding β. For the current study, four temperatures were used for the analysis. Since, the fraction of the total transformation of any copolymer is strictly a function of temperature, it is different from each copolymer at that specified temperature as shown in Figure 3-4, and therefore, undermining the comparison of different copolymers by Ozawa analysis albeit, the temperature is same. The temperatures for the analysis were selected in the close vicinity of the onset crystallization temperature for all the copolymers. The Ozawa-plots are shown in Figure 3-5, with the corresponding values of m and $K(T)$ listed in Table 3-3. For the Ozawa analysis, four cooling rates were used i.e. 1, 2, 3, and 5 K/min. as these heating rates provided better fitting. The suitability of the Ozawa model decreased with large variation in the cooling rates such as 1-30 K/min. This behavior can be due to the negligence of the secondary crystallization in the Ozawa theory, as the cooling rates are increased the crystallization peak is shifted towards a lower temperature. Therefore, when the difference in cooling rates is high, the phase of crystallization can be different for the copolymer at a specific temperature, which leads to the inapplicability of the Ozawa model [35]. For instance, let us consider HEX-1, at 1 K/min. and 380 K, the fraction of the total transformation is nearly 40%, while at 20 and 30 K/min., the fraction of the total transformation is nearly 23% and 11% respectively. Therefore, to avoid this issue, we have used only four cooling rates for the Ozawa analysis. Sajkiewicz et al. also reported that linear function by Ozawa model is obtained at lower cooling rates only, which was due to the fact that higher cooling rates, reduces the absolute crystallinity and an increase in the amorphous phase within the spherulites. Similarly, the crystallinity at which the spherulites impingement become dominant also increases with the cooling rate [36].

From the results listed in Table 3-3, it is evident that, for all the copolymers *K(T)* decreases with an increase in temperature indicating a slower crystallization process at higher temperatures. The value of *m* was found close to 2, in the early stage of crystallization of all the copolymers indicating a 2 dimensional crystal growth. However, this value decreased rapidly with the decreasing temperature. The reason for this decrease can be the spherulites impingements which is dominant at low temperature. As stated earlier, the comparison of crystallization process for the different copolymers cannot be carried out through the Ozawa method. Therefore, for more quantitative analysis of the crystallization process, Mo-method should be evaluated.

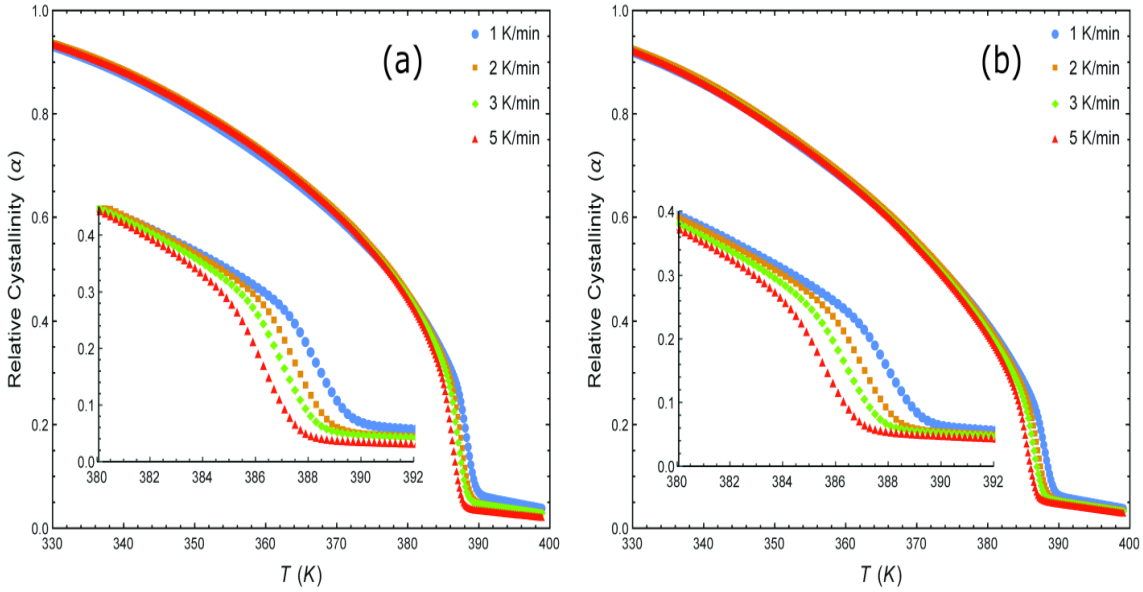

Figure 3-4. Variation of relative crystallinity with temperature for: (a) HEX-1; (b) DEC-1

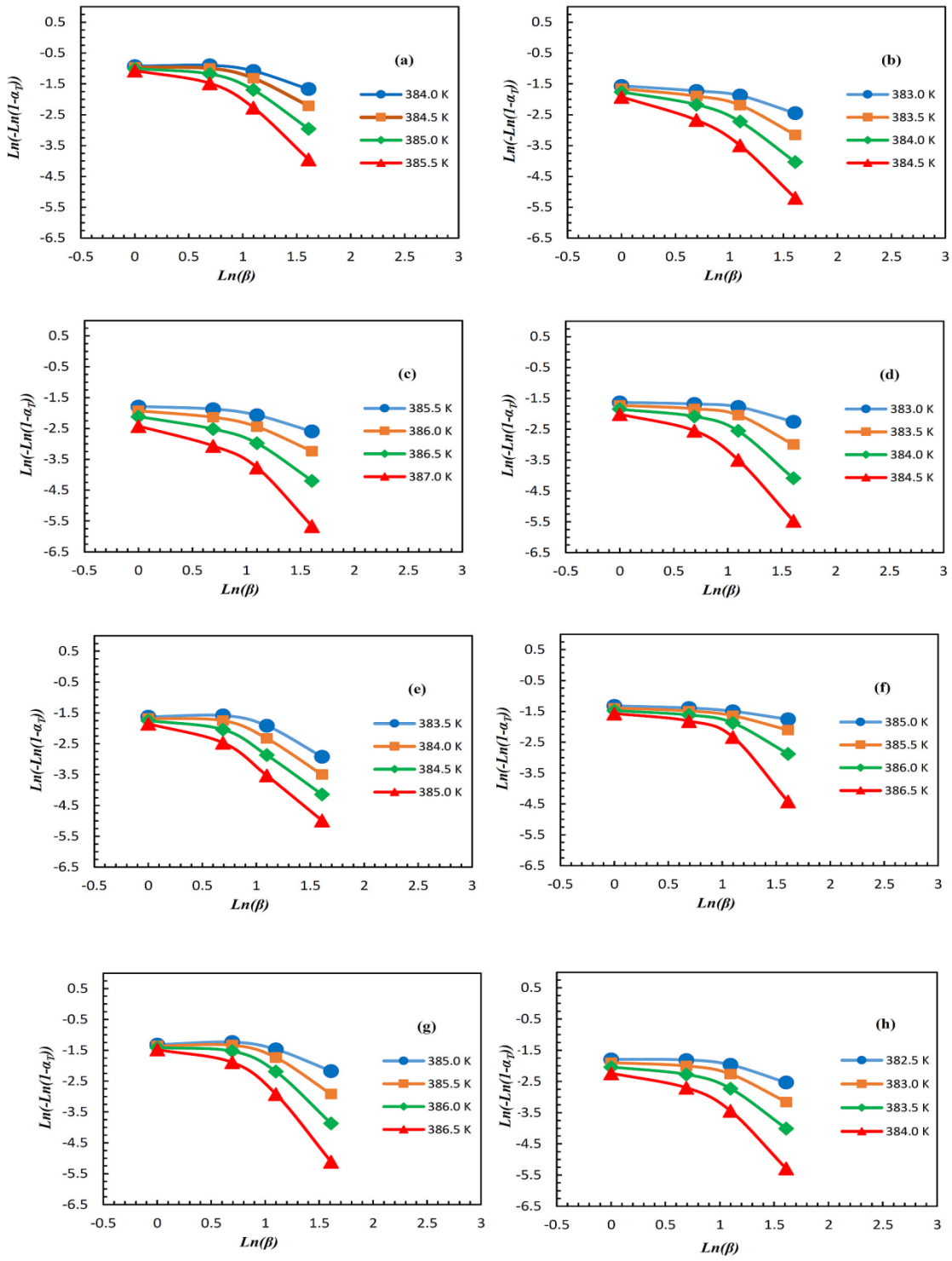

Figure 3-5. Ozawa-plots for: (a) HEX-1; (b) HEX-2; (c) OCT-1; (d) OCT-2; (e) OCT-4; f) DEC-1; (g) DEC-2; (h) DEC-4

Table 3-3. Resulting values for m and *K(T)* from Ozawa analysis

HEX-1	Temp (K)	386.00	385.50	385.00	384.00
	m	2.85	1.62	1.10	0.70
	K(T)	0.47	0.48	0.49	0.56
HEX-2	Temp (K)	384.50	384.00	383.50	383.00
	m	1.99	1.36	0.90	0.53
	K(T)	0.18	0.21	0.22	0.23
OCT-1	Temp (K)	387.00	386.50	386.00	385.50
	m	1.94	1.24	0.78	0.48
	K(T)	0.13	0.15	0.17	0.18
OCT-2	Temp (K)	384.50	384.00	383.50	383.00
	m	2.09	1.32	0.74	0.36
	K(T)	0.20	0.22	0.22	0.23
OCT-4	Temp (K)	385.00	384.50	384.00	383.50
	m	1.96	1.47	1.10	0.76
	K(T)	0.21	0.23	0.25	0.26
DEC-1	Temp (K)	386.50	386.00	385.50	385.00
	m	1.87	1.02	0.43	0.26
	K(T)	0.26	0.27	0.28	0.32
DEC-2	Temp (K)	386.50	386.00	385.50	385.00
	m	2.20	1.47	0.92	0.50
	K(T)	0.32	0.34	0.36	0.38
DEC-4	Temp (K)	384.00	383.50	383.00	382.50
	m	1.83	1.17	0.74	0.43
	K(T)	0.16	0.17	0.18	0.19

Analysis by Mo Model

Mo method was first proposed by Liu et al. [18]. The Mo model equation can be derived by linearization and addition of Equation 1 and Equation 2.

$$nLn(t) + Ln(k_t) = Ln(K(T)) - mLn(\beta) \qquad (6)$$

$$Ln[\beta] = Ln[F(T)] - \alpha Ln[t] \qquad (7)$$

Equation (7) represents the straight line, with slope α = n/m and intercept $F(T) = \left[\frac{K(T)}{k_t}\right]^{1/m}$ α is the ratio of Avrami and Ozawa exponent. The parameter *F (T)* represents the degree of super cooling required to obtain a specific degree of crystallinity in unit time which simply indicates the degree of difficulty found in the crystallization process [18] . Mo plots can be generated by plotting *Ln(β)* vs. *Ln(t)* for any selected value of the fraction of total transformation. These relative crystallinities are used in calculating the time required to achieve that particular relative crystallinity at different cooling rates *β*. The calculated values for time thus obtained i.e. *Ln(t)* is then plotted against *Ln(β)*. To successfully describe the crystallization process, Mo plots must be linear and straight line for a specific value of crystallinity [14]. For the current study, the Mo plots for all the samples were generated by selecting the relative crystallinities value of 0.2 to 0.8 with a step size of 0.2, which are shown in Figure 3-6 and the corresponding values obtained from model are listed in Table 3-4. The Mo plots are perfectly aligned and straight for all the copolymers samples which indicate that Mo method can suitably describe the crystallization process. From the analysis of the results in Table 3-4, it can be seen that *F* (*T*) value increased more with the comonomer addition (degree of branching) as

compared to comonomer type, which reveals that the crystallization is more affected by the degree of branching rather than comonomer type. The value of α is almost constant indicating that Mo method is suitably describing the crystallization process.

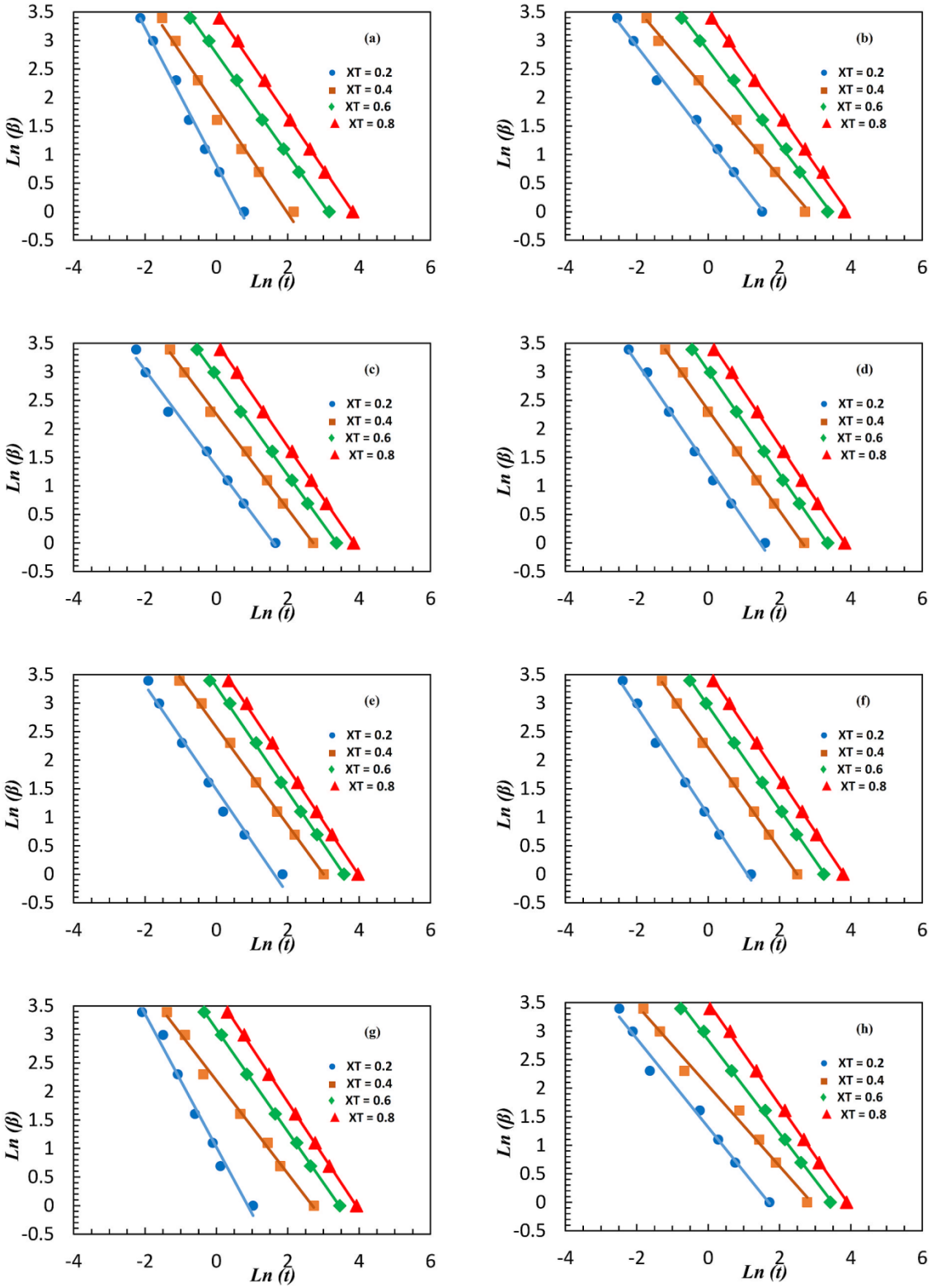

Figure 3-6. Mo-plots for: (a) HEX-1; (b) HEX-2; (c) OCT-1; (d) OCT-2; (e) OCT-4; f) DEC-1; (g) DEC-2; (h) DEC-4

Table 3-4. Summary of Mo model results

Sample		Relative crystallinity			
		0.2	0.4	0.6	0.8
HEX-1	F(T)	2.27	6.31	15.96	33.57
	α(T)	1.20	0.93	0.88	0.92
HEX-2	F(T)	3.56	9.80	18.91	34.96
	α(T)	0.82	0.72	0.84	0.90
DEC-1	F(T)	2.82	7.72	19.08	34.97
	α(T)	0.95	0.89	0.90	0.93
DEC-2	F(T)	3.51	9.43	17.17	33.19
	α(T)	1.11	0.87	0.90	0.95
DEC-4	F(T)	3.73	12.11	22.00	40.14
	α(T)	0.78	0.70	0.82	0.89
OCT-1	F(T)	3.87	9.35	19.42	35.02
	α(T)	0.84	0.83	0.87	0.91
OCT-2	F(T)	3.95	11.05	20.40	36.13
	α(T)	0.92	0.88	0.90	0.93
OCT-4	F(T)	4.60	14.14	26.65	42.97
	α(T)	0.91	0.85	0.91	0.94

3.3.4 ACTIVATION ENERGY

Activation energy (E_A) is the amount of energy that is released during the propagation of the crystalline chains within the polymer matrix during the phase transition. Kissinger method can be used for the calculation of E_A for LLDPE [19], which includes T_p and β [25]. E_A is calculated using the following expression:

$$\frac{d\left(Ln\left(\frac{\beta}{T_p^{\,2}}\right)\right)}{d\left(\frac{1}{T_p}\right)} = -\frac{E_A}{R} \qquad (8)$$

Where, R is the universal gas constant. The values E_A can be evaluated from the slopes of $Ln\left(\frac{\beta}{T_p^{\,2}}\right)$ vs. $\frac{1}{T_p}$ (See Figure 3-7) for the as-synthesized copolymers. Whereas, the negative sign is representing that the crystallization process is exothermic in nature. Thus the lower values of E_A corresponds to easier crystallization process [19]. It is found that, for higher comonomer composition in the feed increases E_A, thus indicating a difficult crystallization process, (See Table 3-5). The E_A for the comonomers follows the order as HEX-1<OCT-1<DEC-1.

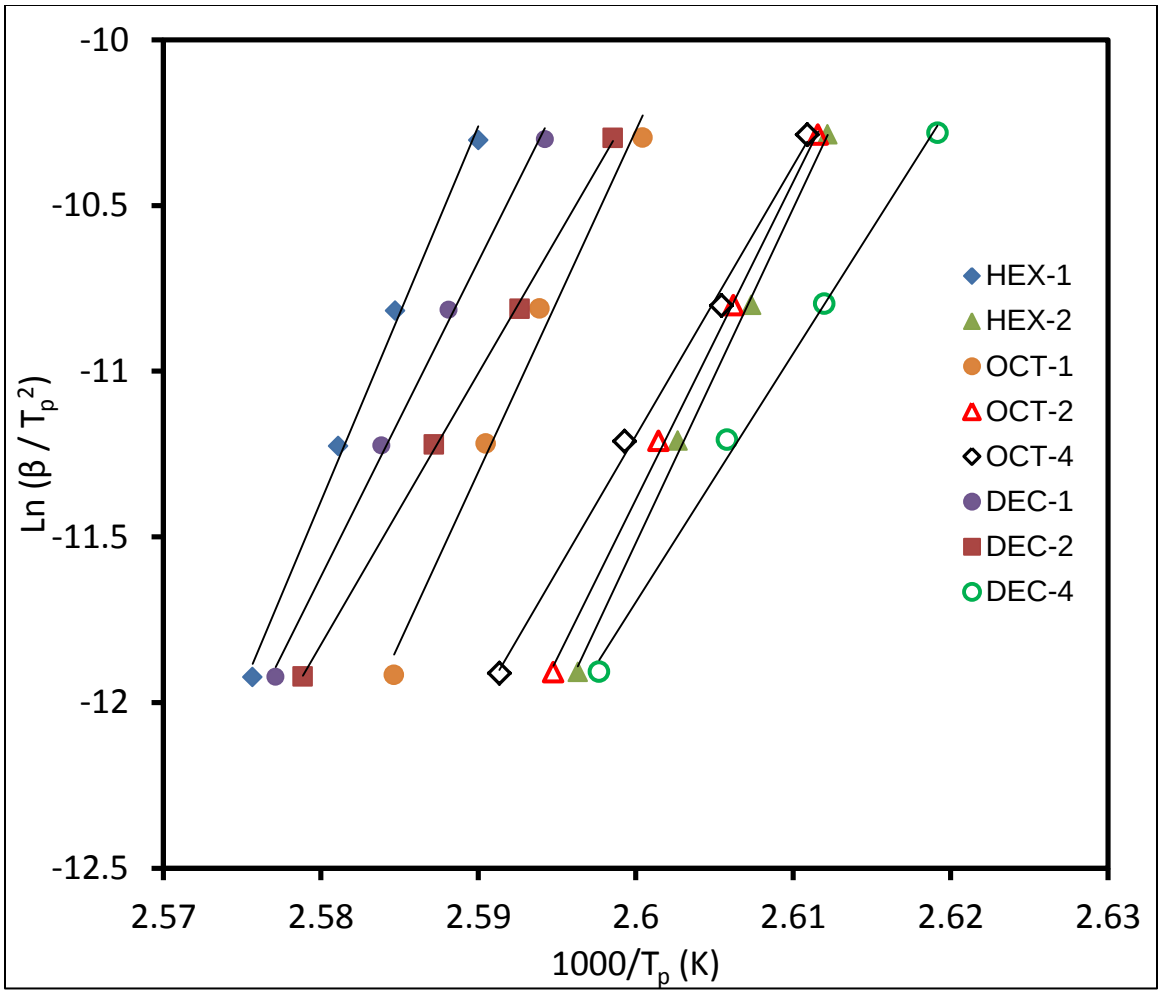

Figure 3-7. Kissinger plots for ethylene copolymers

Table 3-5. Summarized activation energies (E_A) obtained from Kissinger-plots

Sample No.	HEX-1	HEX-2	OCT-1	OCT-2	OCT-4	DEC-1	DEC-2	DEC-4
(E_A) kJ/mol	-940.1	-840.4	-856.8	-797.3	-677.8	-789.6	-681.1	-623.6

3.4 CRYSTAL THICKNESS DISTRIBUTION

The copolymers synthesized from polymerization of ethylene-1-alkene are semi crystalline in nature. The DOC of the copolymers decreases with addition of comonomers (See Table 1). The melting temperatures (T_m) at each point can thus be related to the equivalent dimensions of that crystal lamella (crystallite) by using Flory and GT equations also termed as MGT equation, given by Equation 9 [21,37,38].

$$T_m = T_m^o\left(1-\frac{2\sigma_{ssfe}}{\Delta H_f^o L_{fclamella}}\right) \qquad (9)$$

Where, T_m^o (equilibrium melting temperature of perfect crystal of ethylene homopolymer) = 418.65K; $\Delta H_f{}^o$ (heat of fusion per unit volume for the perfect crystal) = 290 J cm^{-3}; $L_{fclamella}$ is the folded crystal lamellar thickness and σ_{ssfe} (crystallite specific surface free energy) = 90 mJm^{-2} [24,39]. However, for the T_m^o for the copolymer ($T_{m,copolym}^o$) Equation 10 is used [22,23,39]. The main flaw in using MGT to calculate copolymer lamellar thickness distributions arise from the exclusion of branches from the copolymer crystalas. The comonomer composition in the melt around the crystals changes during melting, hence, using the same $T_{m,copolym}^o$ to calculate L values along the whole melting curve, which might cause some error [38,40].

$$\frac{1}{T_{m,copolym}^o} = \frac{1}{T_m^o} + \frac{R}{\Delta H_u}\left(lnX_A\right) \qquad (10)$$

Where, ΔH_u is the heat of fusion of ethylene repeat unit and X_A is the mole fraction of ethylene in copolymer.

The LTD for various copolymers is shown in the Figure 3-8, and the WALT is summarized in Table 3-1. The MGT equation was implemented for studying the comonomer induced structural/enchainment defects in the copolymers. The LTD profile shrinks and narrows upon the further addition of comonomer, shows less crystallite in the polymer lattice due to high SCB. Therefore the additional branching effect acted as to break the relatively longer lamellae, resulting in an overall decrease in the width of the distribution [41]. This conforms to the positive effect of DOC on the WALT i.e. higher WALT is recorded for higher crystalline polymer and vice versa (See Table 3-1).

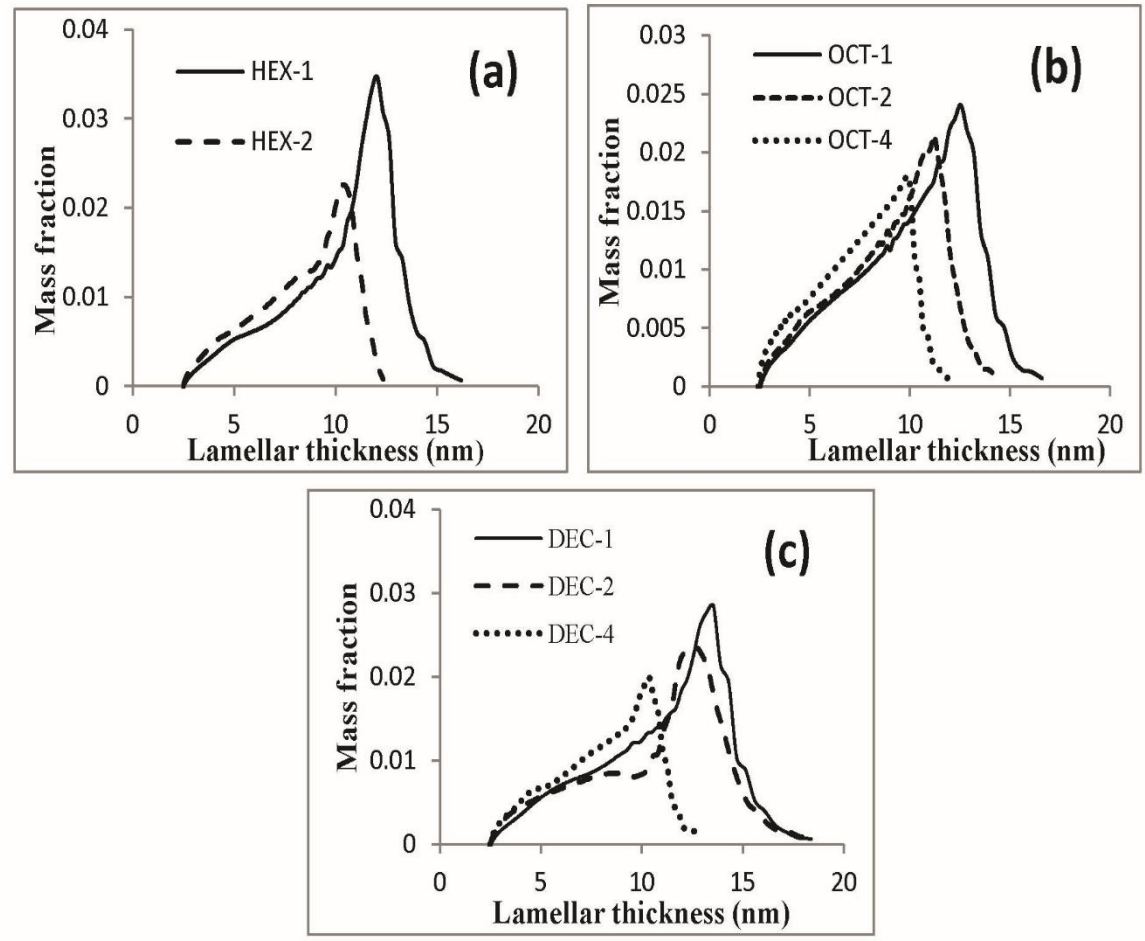

Figure 3-8. Lamellar thickness distribution (LTD) for: (a) 1-hexene; (b) 1-octene; (c) 1-decene; comonomers.

3.5 CONCLUSION

Ethylene-co-α-olefin polymerization was carried out using zirconocene complex with varying comonomer compositions. The comonomers (α-olefins) considerably influenced the melt crystallization and lamellar thickness distribution (LTD) of the copolymers. Mo method was found suitable for the copolymers melt crystallization, under study. The weight average lamellar thickness was found to decrease with comonomer addition. For the current study, Kissinger's activation energy (E_A) indicates that the crystallization process is more affected by the degree of branching rather than the comonomer type.

3.6 NOMENCLATURE

Table 3-6. Nomenclature

Symbols	**Meaning (Units)**
T_m	Peak melting temperature (K)
T_p	Peak crystallization temperature (K)
E_A	Activation energy (kJ/mol)
$t_{½}$	Half time for crystallization (min)
n	Avrami exponent
$K(T)$	Crystallization rate constant at any given temperature
m	Ozawa exponent
ΔH_{total}	Total heat released
$\Delta H(t)$	heat released at a time t
$F(T)$	Mo parameter also called degree of super cooling
α	Mo parameter (Ratio of Avrami and Ozawa exponent n and m respectively)
β	Cooling rate (K/min)
α_t	Weight fraction crystallized from melt
ρ_c	Crystalline phase density (kg/m^3)

ρ_a	Amorphous phase density (kg/m^3)

3.7 REFERENCES

[1] M.O. Kristen, Supported metallocene catalysts with methylalumoxane and boron activators., Top. Catal. 7 (1999) 89–95. doi:10.1023/A:1019195229418.

[2] W. Kaminsky, Highly active metallocene catalysts for olefin polymerization, J. Chem. Soc. Dalt. Trans. (1998) 1413–1418. doi:10.1039/a800056e.

[3] K.-J. Chu, J.B.P. Soares, A. Penlidis, Polymerization mechanism for in situ supported metallocene catalysts, J. Polym. Sci. Part A Polym. Chem. 38 (2000) 462–468. doi:10.1002/(SICI)1099-0518(20000201)38:3<462::AID-POLA10>3.0.CO;2-O.

[4] T.F.L. McKenna, E. Tioni, M.M. Ranieri, A. Alizadeh, C. Boisson, V. Monteil, Catalytic olefin polymerisation at short times: Studies using specially adapted reactors, Can. J. Chem. Eng. 91 (2013) 669–686. doi:10.1002/cjce.21684.

[5] S.T. Harini, S. Padmavathi, A. Satish, B. Raj, Food compatibility and degradation properties of pro-oxidant-loaded LLDPE film, J. Appl. Polym. Sci. 131 (2014) 1–8. doi:10.1002/app.39756.

[6] P.S. Chum, K.W. Swogger, Olefin polymer technologies—History and recent progress at The Dow Chemical Company, Prog. Polym. Sci. 33 (2008) 797–819. doi:10.1016/j.progpolymsci.2008.05.003.

[7] J.A.M. Awudza, P.J.T. Tait, The “comonomer effect” in ethylene/α-olefin copolymerization using homogeneous and silica-supported Cp2ZrCl2/MAO catalyst systems: Some insights from the kinetics of polymerization, active center studies, and

polymerization temperature, J. Polym. Sci. Part A Polym. Chem. 46 (2008) 267–277. doi:10.1002/pola.22378.

[8] K.T. Li, C.L. Dai, C.Y. Li, Synthesis of linear low density polyethylene with a nano-sized silica supported Cp2ZrCl2/MAO catalyst, Polym. Bull. 64 (2010) 749–759. doi:DOI 10.1007/s00289-009-0167-3.

[9] M.L. Gao, Y.F. Gu, C. Wang, X.L. Yao, X.L. Sun, C.F. Li, et al., Ethylene homopolymerization and copolymerization with ??-olefins catalyzed by titanium complexes bearing [O-NSR] tridentate ligands, J. Mol. Catal. A Chem. 292 (2008) 62–66. doi:10.1016/j.molcata.2008.06.006.

[10] C. Piel, P. Starck, J. V. Seppälä, W. Kaminsky, Thermal and mechanical analysis of metallocene-catalyzed ethene-α-olefin copolymers: The influence of the length and number of the crystallizing side chains, J. Polym. Sci. Part A Polym. Chem. 44 (2006) 1600–1612. doi:10.1002/pola.21265.

[11] R.M. Patel, Crystallization kinetics modeling of high density and linear low density polyethylene resins, J. Appl. Polym. Sci. 124 (2012) 1542–1552. doi:10.1002/app.35177.

[12] W. Liu, B. Liu, X. Wang, Morphology, Rheological Properties, and Crystallization Behavior of Polypropylene/Clay Nanocomposites, Int. J. Polym. Mater. 62 (2013) 164–171. doi:10.1080/00914037.2011.610061.

[13] F. Shehzad, M. Daud, M.A. Al-Harthi, Synthesis, characterization and crystallization kinetics of nanocomposites prepared by in situ polymerization of ethylene

and graphene, J. Therm. Anal. Calorim. 123 (2016) 1501–1511. doi:10.1007/s10973-015-5087-x.

[14] F. Shehzad, S.P. Thomas, M.A. Al-Harthi, Non-isothermal crystallization kinetics of high density polyethylene/graphene nanocomposites prepared by in-situ polymerization, Thermochim. Acta. 589 (2014) 226–234. doi:10.1016/j.tca.2014.05.039.

[15] Y.-H. Shi, Q. Dou, Non-isothermal crystallization kinetics of β-nucleated isotactic polypropylene, J. Therm. Anal. Calorim. 112 (2013) 901–911. doi:10.1007/s10973-012-2611-0.

[16] A. Jeziorny, Parameters characterizing the kinetics of the non-isothermal crystallization of poly(ethylene terephthalate) determined by d.s.c., Polymer (Guildf). 19 (1978) 1142–1144. doi:10.1016/0032-3861(78)90060-5.

[17] T. Ozawa, Kinetics of non-isothermal crystallization, Polymer (Guildf). 12 (1971) 150–158. doi:10.1016/0032-3861(71)90041-3.

[18] Z. Qiu, Z. Mo, Y. Yu, H. Zhang, S. Sheng, C. Song, Nonisothermal melt and cold crystallization kinetics of poly(aryl ether ketone ether ketone ketone), J. Appl. Polym. Sci. 77 (2000) 2865–2871. doi:10.1002/1097-4628(20000923)77:13<2865::AID-APP7>3.0.CO;2-2.

[19] M. Daud, F. Shehzad, M.A. Al-Harthi, Non-isothermal crystallization kinetics of LLDPE prepared by in situ polymerization in the presence of nano titania, Polym. Bull. 72 (2015) 1233–1245. doi:10.1007/s00289-015-1335-2.

[20] X. Cao, J. Gao, X. Dai, Y. Liu, X. He, Kinetics of thermal degradation of nanometer calcium carbonate/linear low-density polyethylene nanocomposites, J. Appl. Polym. Sci. 126 (2012) 1159–1164. doi:10.1002/app.36949.

[21] M. Atiqullah, I. Hussain, M. Al-Harthi, M.J. Khan, A.H. and A. Fazal, Changes in Melting Behaviors of a Residual Catalyst-Cum-UV Degraded Polyethylene Film: A New Insight Through Experiment and Modeling, Curr. Catal. 1 (2012) 2–13. doi:http://dx.doi.org/10.2174/2211544711201010002.

[22] S. Hosoda, Y. Nozue, Y. Kawashima, K. Suita, S. Seno, T. Nagamatsu, et al., Effect of the sequence length distribution on the lamellar crystal thickness and thickness distribution of polyethylene: Perfectly equisequential ADMET polyethylene vs ethylene/??-Olefin Copolymer., Macromolecules. 44 (2011) 313–319. doi:10.1021/ma102072p.

[23] F. Chen, R.A. Shanks, G. Amarasinghe, Molecular distribution analysis of melt-crystallized ethylene copolymers, Polym. Int. 53 (2004) 1795–1805. doi:10.1002/pi.1583.

[24] S. Adamu, M. Atiqullah, Z.O. Malaibari, M.A. Al-Harthi, A.-H.M. Emwas, A. Ul-Hamid, Metallocene-catalyzed ethylene-α-olefin isomeric copolymerization: A perspective from hydrodynamic boundary layer mass transfer and design of MAO anion, J. Taiwan Inst. Chem. Eng. 60 (2016) 92–105. doi:10.1016/j.jtice.2015.10.031.

[25] H.E. Kissinger, Reaction Kinetics in Differential Thermal Analysis, Anal. Chem. 29 (1957) 1702–1706. doi:10.1021/ac60131a045.

[26] B.O. Reid, M. Vadlamudi, A. Mamun, H. Janani, H. Gao, W. Hu, et al., Strong Memory Effect of Crystallization above the Equilibrium Melting Point of Random Copolymers, Macromolecules. 46 (2013) 6485–6497. doi:10.1021/ma400839d.

[27] A. Mamun, X. Chen, R.G. Alamo, Interplay between a Strong Memory Effect of Crystallization and Liquid–Liquid Phase Separation in Melts of Broadly Distributed Ethylene–1-Alkene Copolymers, Macromolecules. 47 (2014) 7958–7970. doi:10.1021/ma501937c.

[28] J.B.P. Soares, S. Anantawaraskul, Crystallization analysis fractionation, J. Polym. Sci. Part B Polym. Phys. 43 (2005) 1557–1570. doi:10.1002/polb.20441.

[29] S. Anantawaraskul, J.B.P. Soares, P.M. Wood-Adams, Fractionation of semicrystalline polymers by crystallization analysis fractionation and temperature rising elution fractionation, in: Adv. Polym. Sci., 2005: pp. 1–54. doi:10.1007/b135559.

[30] E.F. Connor, T.R. Younkin, J.I. Henderson, S. Hwang, R.H. Grubbs, W.P. Roberts, et al., Linear functionalized polyethylene prepared with highly active neutral Ni(II) complexes, J. Polym. Sci. Part A Polym. Chem. 40 (2002) 2842–2854. doi:10.1002/pola.10370.

[31] S.T. Method, Standard Test Method for Determination of Linear Low Density Polyethylene (LLDPE) Composition by Carbon-13 Nuclear Magnetic Resonance 1, 10 (1977) 1–7. doi:10.1520/D5017-96R09E01.2.

[32] M. Wannaborworn, P. Praserthdam, B. Jongsomjit, Observation of different catalytic activity of various 1-olefins during ethylene/1-olefin copolymerization with

homogeneous metallocene catalysts, Molecules. 16 (2011) 373–383. doi:10.3390/molecules16010373.

[33] M.R. Kamal, L. Feng, T. Huang, A generalized equation for the prediction of melting temperatures of homopolymers and copolymers, Can. J. Chem. Eng. 80 (2002) 432–442. doi:10.1002/cjce.5450800312.

[34] Z. Zhang, C. Xiao, Z. Dong, Comparison of the Ozawa and modified Avrami models of polymer crystallization under nonisothermal conditions using a computer simulation method, Thermochim. Acta. 466 (2007) 22–28. doi:10.1016/j.tca.2007.10.004.

[35] M. Run, J. Gao, Z. Li, Nonisothermal crystallization and melting behavior of mPE/LLDPE/LDPE ternary blends, Thermochim. Acta. 429 (2005) 171–178. doi:10.1016/j.tca.2005.03.007.

[36] P. Sajkiewicz, L. Carpaneto, A. Wasiak, Application of the Ozawa model to non-isothermal crystallization of poly(ethylene terephthalate), Polymer (Guildf). 42 (2001) 5365–5370. doi:10.1016/S0032-3861(00)00934-4.

[37] K. Shin, E. Woo, Y.G. Jeong, C. Kim, J. Huh, K.-W. Kim, Crystalline Structures, Melting, and Crystallization of Linear Polyethylene in Cylindrical Nanopores, Macromolecules. 40 (2007) 6617–6623. doi:10.1021/ma070994e.

[38] L. Lu, R.G. Alamo, L. Mandelkern, Lamellar Thickness Distribution in Linear Polyethylene and Ethylene Copolymers, Macromolecules. 27 (1994) 6571–6576. doi:10.1021/ma00100a048.

[39] H. Zhou, G.L. Wilkes, Comparison of lamellar thickness and its distribution determined from d.s.c., SAXS, TEM and AFM for high-density polyethylene films having a stacked lamellar morphology, Polymer (Guildf). 38 (1997) 5735–5747. doi:10.1016/S0032-3861(97)00145-6.

[40] B. Crist, P.R. Howard, Crystallization and melting of model ethylene-butene copolymers, Macromolecules. 32 (1999) 3057–3067. doi:10.1021/ma9816362.

[41] M. Atiqullah, S. Adamu, Z.O. Malaibari, M.A. Al-Harthi, A.-H.M. Emwas, (nBuCp)2ZrCl2-catalyzed ethylene-4M1P copolymerization: Copolymer backbone structure, melt behavior, and crystallization, AIChE J. 62 (2016) 1688–1706. doi:10.1002/aic.15159.

CHAPTER 4

Non-isothermal crystallization kinetics of LLDPE prepared by *in-situ* polymerization in the presence of nano titania

Muhammad Daud[1], Farrukh Shehzad[1], Mamdouh A. Al-Harthi[1,2*]

[1] Department of Chemical Engineering, King Fahd University of Petroleum and Minerals, Dhahran 31261, Saudi Arabia

[2] Center of Research Excellence in Petroleum Refining and Petrochemicals (CoRE-PRP), King Fahd University of Petroleum and Minerals, Dhahran 31261, Kingdom of Saudi Arabia

[*]Corresponding Author: Mamdouh A. Al-Harthi

E-mail address: mamdouh@kfupm.edu.sa

This chapter has been published in "Polymer Bulletin" on 11 Feburary 2015

ABSTRACT

In this research work, a zirconocene/MAO complex was used as a catalyst for the copolymerization of 1-hexene and ethylene in the presence of nano titania doped with 1% of manganese (TiO_2/Mn), which was used as a drop in filler. It was investigated from the ^{13}CNMR analysis that 1-hexene incorporation increases with the addition of nano filler. The degree of crystallinity (DOC), catalytic activity and molecular weight of the nanocomposites were studied by a differential scanning calorimeter (DSC), yield analysis and gel permeation chromatography (GPC) respectively. It was found that DOC, catalytic activity, molecular weight and molecular weight distribution were strongly influenced by the addition of nano filler due to the increase of 1-hexene incorporation. As a result, an increase in catalytic activity and a decrease in DOC were observed due to the addition of nano filler. The non-isothermal crystallization kinetics of the produced copolymer was studied using a model proposed by Ozawa and Mo *et al*. It was observed that the crystal growth rate is slowed by the nano filler. The Activation energy (E_A) was determined by the Kissinger method, and it was found that E_A is increased incrementally with the loadings of the nano filler, confirming a slower crystallization process.

Keywords: polymer nanocomposites, crystallization kinetics, nano-titania, catalytic activity

4.1 INTRODUCTION

Polyethylene (PE) is a widely used polymer because of its low production cost and remarkable properties. A huge increase in the production trends of PE has been noted over the last few decades due to its high demand in global plastic consumption [1]. The discovery of the metallocene catalyst has opened a new era of ethylene polymerization as it gives precisely designed products [2–6]. Linear Low Density Polyethylene (LLDPE) is one of the most important emerging resins of PE [7, 8]. In order to enhance heat resistance properties and strength of the PE, various nano fillers are utilized either by melt blending or by in-situ polymerization [9, 10]. During the production of polymer nanocomposites the nano filler remains in a discontinuous phase in the entire polymer matrix thus enabling them to have better properties than the unmodified polymer. The thus produced nanocomposites have high stiffness and tensile strength [1, 11]. The nano fillers have a high degree of interfacial interaction (due to their nano size) which provides high surface area compared to conventional fillers [11]. Several nano fillers including SiO_2 [1, 12, 13], TiO_2 [9, 10, 14, 15], Sepiolite ($Mg_4Si_6O_{15}(OH)_2$) [16], Al_2O_3 [17] and ZrO_2 [18, 19] are widely studied in literature. Among these nano fillers TiO_2 is the most promising inorganic nano filler because of its versatile properties, such as unique optical properties, anti-static behavior (used as antibacterial agent), and interesting photo catalytic properties [9, 14].

The crystallization of polymers is an important phase transition process. In fact, the rate of crystallization and the degree of crystallinity are key factors in polymer processing [20]. The crystallization process can be isothermal or non-isothermal. Generally most industrial processing is non-isothermal, and because of this, non-isothermal

crystallization kinetics has practical significance [21]. Various nano fillers, which impart unique characteristics to polymers, also affect the crystallization process. For instance, it has been reported that carbon nanotubes (CNTs) act as nucleating agents in the crystallization of LLDPE. It is also observed during isothermal crystallization the presence of a small amount of CNTs alter the morphology of LLDPE [22]. Similarly, it has also been observed that Carbon Nano Fibers (CNF) alter the lamellar thickness and lamellar thickness distribution [23].

Many Models such as Jeizorny, Ozawa and Mo [24–27] were used to describe non-isothermal crystallization kinetics of all derivatives of PE (high density PE (HDPE), low density PE (LDPE), linear low density PE (LLDPE), and ultra-high molecular weight PE (UHMWPE)). In this study the Mo-Model is applied to the analysis of non-isothermal crystallization kinetics of LLDPE-TiO_2 nanocomposites.

4.2 EXPERIMENTAL METHODS

4.2.1 Chemicals

A Bis(chclopentadienyl zirconium (IV) dichloride) > 98% ($C_{10}H_{10}Cl_2Zr$), Methylaluminoxane (MAO), nano titania doped with 1% manganese (TiO_2/Mn) (<100 nm) and all other chemicals were provided by Sigma Aldrich and were used as received.

4.2.2 *In-Situ* Polymerization Reaction

Ethylene/1-hexene copolymerization was carried out in a 250 mL round bottom flask (semi batch reactor) equipped with a magnetic stirrer. Inside the glove box the reactor was charged with 20 μmoles (6 mg) of a zirconocene catalyst and different dosages (5, 15 and 30 mg) of the nano filler and 80 ml of solvent (toluene). The airtight reactor was then

immersed in a constant temperature bath at 30 °C. Once the temperature of the bath and reactor reached equilibrium, the nitrogen was removed from the reactor using a vacuum pump. The ethylene gas at a pressure of 1.3 bar was fed to the reactor in order to start the polymerization process. After two minutes of saturation with ethylene, 1 mL of the comonomer (1-hexene) was introduced into the reactor. Five mL of cocatalyst (MAO) was added to reactor just after 3 minutes of saturation with the comonomer. The total reaction time was 30 minutes with a stirring speed of 600 rpm, after which the polymerization process was quenched by adding acidified methanol (5 vol. % HCl) followed by stirring for 45 minutes. The copolymer thus obtained from the copolymerization of ethylene/1-hexene was filtered and kept in an oven at 50 °C for 10 hours before weighing to calculate the activity. The abbreviations used in this section are E-H-0 (control), E-H-5, E-H-15 and E-H-30, where the numbers represent the amount of nano filler in milligrams.

4.2.3 Polymer Characterization

1. The thermal behavior of the copolymer was determined using a DSC-Q1000, instrument. The heating rate used in this study was 10 °C /min. The melting temperature (T_m) was obtained from the heating cycle while the crystallization temperature (T_c) was obtained from the different cooling cycles.
2. Crystallization analysis fractionation (CRYSTAF) (model 200 CRYSTAF instrument provided by Polymer ChAR) was employed for the analysis of the chemical composition distribution (CCD) of ethylene/1-hexene copolymer and its nanocomposites. The samples were dissolved in 1, 2, 4 trichloro-benzene (TCB) at 150

°C for 60 minutes and then allowed to cool at 0.1 °C /min. The infrared detector (dual wavelength) determined the polymer crystallize in the solution.

3. The carbon13 nuclear magnetic resonance (^{13}C-NMR) technique was utilized to study the copolymer microstructure. The samples were prepared by dissolving 25 mg of polymer in TCB at 120 °C with a few drops of deuterated benzene. The comonomer mole fraction was determined by using the integration of peaks relative to the isolated methylene resonance on the spectroscopy (largest peak assigned at 30ppm on the x-axis scale) [28, 29].

4. The gel permeation chromatography (GPC) technique was used to find the molecular weight (M_w) of the polymer nanocomposites. Nearly 5 mg of the polymer was dissolved in 10 mL TCB at 160 °C for 3 hours in a 40 mL glass vial, sealed with a Teflon coated cap. The equipment was calibrated using polystyrene (PS) standards.

4.3 RESULTS AND DISCUSSION

4.3.1 Catalytic Activity

From the yield analysis, catalytic activity was calculated and is tabulated in Table 4-1. The catalytic activity increases with the increase in the nano filler amount and reaches its maximum value at 15 mg of the nano filler. Similar results were reported for HDPE with the same nano filler [10]. The high catalytic activity and lower molecular weight (M_w) was observed at the optimum dose of the nano filler. The increase in catalytic activity is reported due to the high surface area of the nano particles which provide better distribution of catalytically active centers throughout the particle as a result monomers get easy access to coordinate with each other [14]. The doped manganese (Mn) also plays a vital role for getting high catalytic activity because of having the intrinsic activity of the

active species itself (i.e. Mn) present on doped TiO_2 [30]. The cocatalyst MAO adsorbed on the surface of nano filler by physical interaction. The adsorption phenomenon lowers the intrinsic activity of the active species as well as the availability of MAO at high doses of filler addition. Furthermore the presence of a high amount of the filler (as compared to the catalyst) boosts the agglomeration process of filler around the catalyst. As a result, a relatively lower yield is obtained during the lateral stages i.e. 30 mg of filler addition. The phenomena is termed as steric hindrance [31, 32]. Figure 4-1 shows the error bars for the variance in activities and crystallinities for the repeated runs. The change in the molecular weights of the polymer nanocomposites due to filler addition is not significant.

Table 4-1. Experimental activity data and Characteristics for LLDPE-TiO_2/Mn nanocomposites [a] using zirconocene catalyst

S/No.	Sample Name	Filler Amount (mg)	Activity [b] (kg PE $mole^{-1}$ hr^{-1} bar^{-1})	DOC [c]	T_m [d] (°C)	M_w [e] (g/mol)
1	E-H-0	0	354.24 ± 5.21	48.14 ± 0.72	122.15	20,072
2	E-H-5	5	364.74 ± 5.57	44.85 ± 0.85	122.12	22,873
3	E-H-15	15	509.2 ± 9.55	43.95 ± 0.32	122.05	18,286
4	E-H-30	30	362.19 ± 5.72	36.38 ± 0.36	119.99	21,957

[a] T = 30 °C; P_{guage} = 1.3 bar; solvent = toluene (80 mL); zirconocene amount = 6 mg (20 μmol); comonomer (1-hexene) amount = 1 mL; polymerization time = 30 min
[b] calculated from yields
[c] determined by DSC, based on enthalpy of melting of 100 % crystalline PE, 293.6 J/g
[d] determined by DSC
[e] determined by GPC

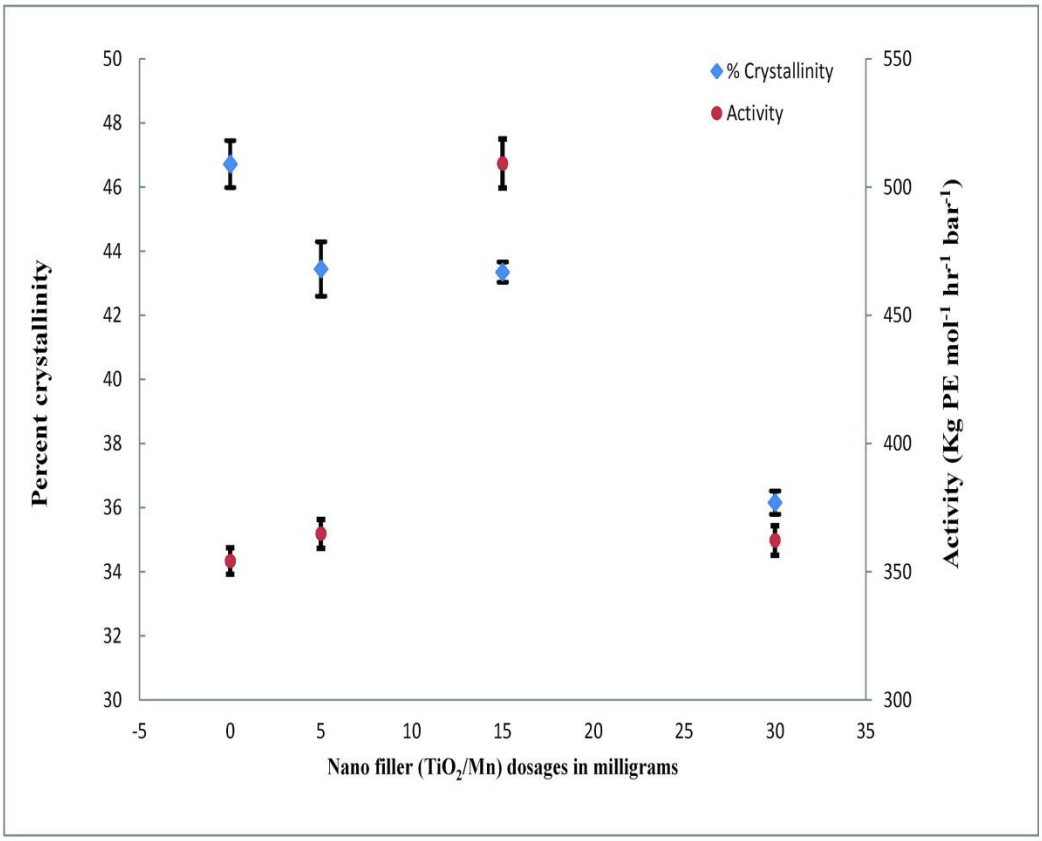

Figure 4-1. Catalytic activity and percent crystallinity variance

4.3.2 Crystallinity of LLDPE- TIO_2/Mn Nanocomposites

The DOC and T_m are tabulated in Table 1 obtained from DSC results. The decreasing trend in the crystallinity is observed as a result of filler addition and reaches its minimum value at a filler dosage of 30 mg. CRYSTAF is utilized for finding the CCD for the synthesized nanocomposites as shown in Figure 4-2. The broadness in the peak increases across the increase in the filler addition along with a slight decrease in the peak temperature, which clearly indicates that there is the addition of more short chain branching to the polymer structure due to 1-hexene incorporation [33]. The DOC is highly influenced by 1-hexene incorporation [29, 34]. At 30 mg of the filler dosage, there is very prominent change in the peak temperature of the nanocomposites which is due to the high comonomer incorporation supported by ^{13}C-NMR results obtained, tabulated in Table 4-2. The nano-TiO_2/Mn thus alters the structure of the polymer by attributing more 1-hexene incorporation and lowering the DOC. The minimum effect of nano-TiO2/Mn on crystallinity could be related to the effect of TiO_2/Mn on the low crystalline active sites only. This is supported by the negligible change in peak temperature of the high crystalline fraction on the CRYSTAF curves.

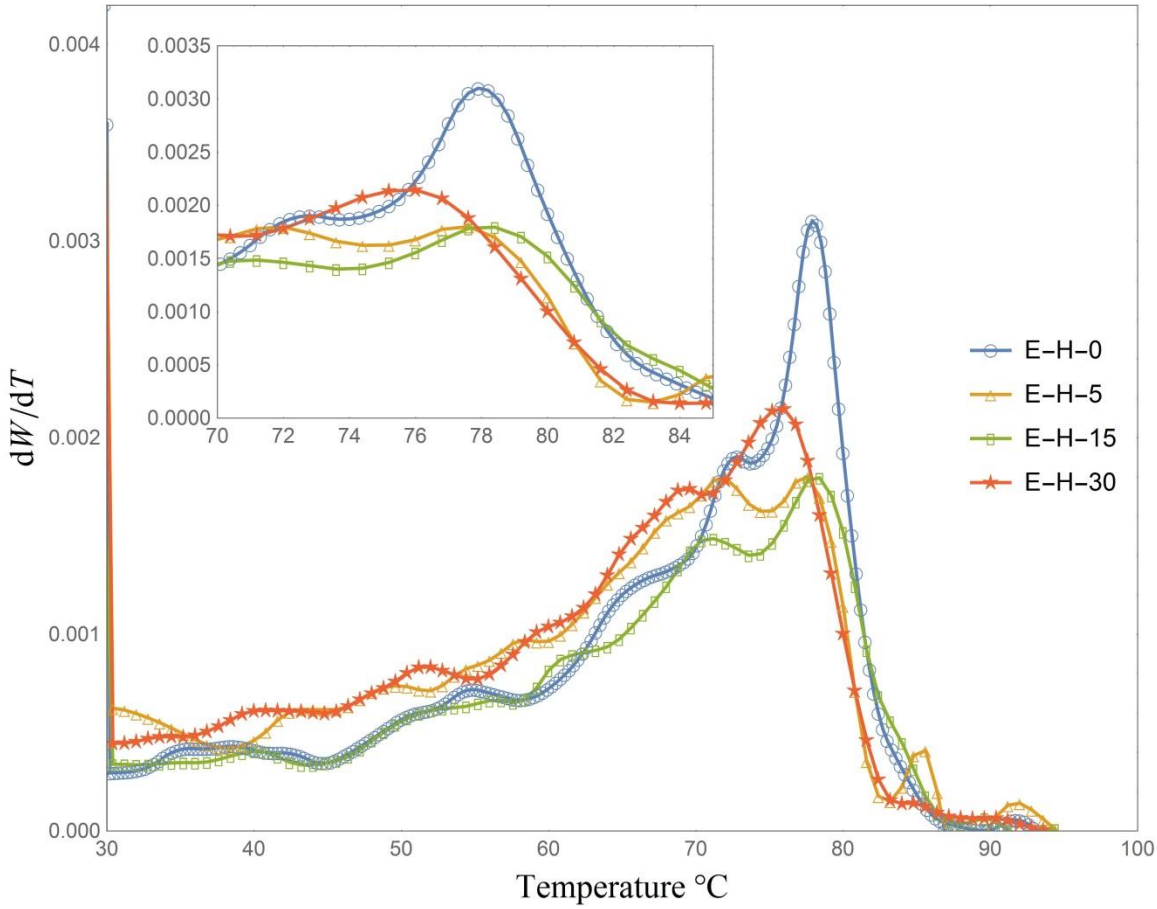

Figure 4-2 CRYSTAF profiles for LLDPE-TiO_2/Mn nanocomposites

Table 4-2. Effect of nano filler concentration on CRYSTAF Profiles

Sample ID	E-H-0	E-H-5	E-H-15	E-H-30
T_{Peak} (°C)	78.0	77.8	77.7	75.8
Mole % of 1-hexene (^{13}C NMR)	1.310	1.312	1.315	1.776

4.3.3 Melt Crystallization

The melt crystallization of polymer can be explained by the well-known Avrami model. The Avrami theory relates the nucleation rate and lamellar crystal growth to the volume fraction of transformed material and the crystallization time. Avrami model is given by Eq.1

$$X_t = 1 - e^{-kt^n} \qquad (1)$$

X_t is the volume fraction of transformed material, *n* is the Avrami exponent and *k* is crystallization rate constant. n is a function of nucleation process while k is the growth function and it depends on the nucleation and crystal growth. *n* provides qualitative information about the nature of nucleation and growth process. Since the Avrami model deals with the isothermal crystallization process, it is not suitable to be applied directly in non-isothermal case. Likewise this model excludes the effect of growth site impingement and secondary crystallization process. For the analysis of non-isothermal process Jeizorny [26] proposed a modification in the growth rate constant. Similarly, Ozawa [27] extended the Avrami theory for prediction of non-isothermal process. The Ozawa model is based on the assumption that the crystallization process occurs in infinitesimally small isothermal steps at a constant cooling rate. The Ozawa model is given by Eq.2 as followed.

$$X_t = 1 - \frac{exp\big(-K(T)\big)}{\beta^m} \qquad (2)$$

Where *K(T)* is a function of the cooling rate β and the Ozawa exponent *m*. It is reported that as compared to Jeizorny-Avrami model, the Ozawa model works well in case of non-

isothermal crystallization [35]. The relative crystallinity X_t can be calculated from the DSC exotherm. First the weight fraction α_t is obtained by the following relation.

$$\alpha_t = \frac{\Delta H(t)}{\Delta H_{total}} = \frac{\int_{T_o}^{T_i}\left(\frac{dH}{dt}\right)dt}{\int_{T_o}^{T\infty}\left(\frac{dH}{dt}\right)dt} * 100 \qquad (3)$$

Where $\Delta H(t)$ is the heat released at time *t* while ΔH_{total} is the total heat released during the crystallization process. The weight fraction can be transformed to volume fraction by the formula given below

$$X_t = \frac{\alpha_t}{\alpha_t + \frac{\rho_c}{\rho_a[1-\alpha_t]}} \qquad (4)$$

Where, $\rho_c$and ρ_a are the densities of crystalline and amorphous phases respectively. The values of $\rho_c$and ρ_a are 1.004 and 0.853 for PE [36].

Analysis by Ozawa model

The Ozawa model can be applied to the non-isothermal crystallization process, carried out at different cooling rates. Eq.5 can be can be simplified by linearization as shown below.

$$Ln\left[-Ln[1-X_t]\right] = Ln[K(T)] - mLn[\beta] \qquad (5)$$

The parameters of the model i.e. *m* and *K*(T) can be obtained from the slope and intercept of plot of $Ln\left[-Ln[1-X_t]\right]$ vs. $Ln[\beta]$. The Ozawa model plots can be generated by considering a temperature and then plotting the relative crystallinity at that temperature to the corresponding cooling rate. The temperatures selected here are, 365, 368, 371, 374,

377 and 380 K. The Ozawa plots are shown in Figure 4-3 (a-d) and the results are listed in Table 4-3.

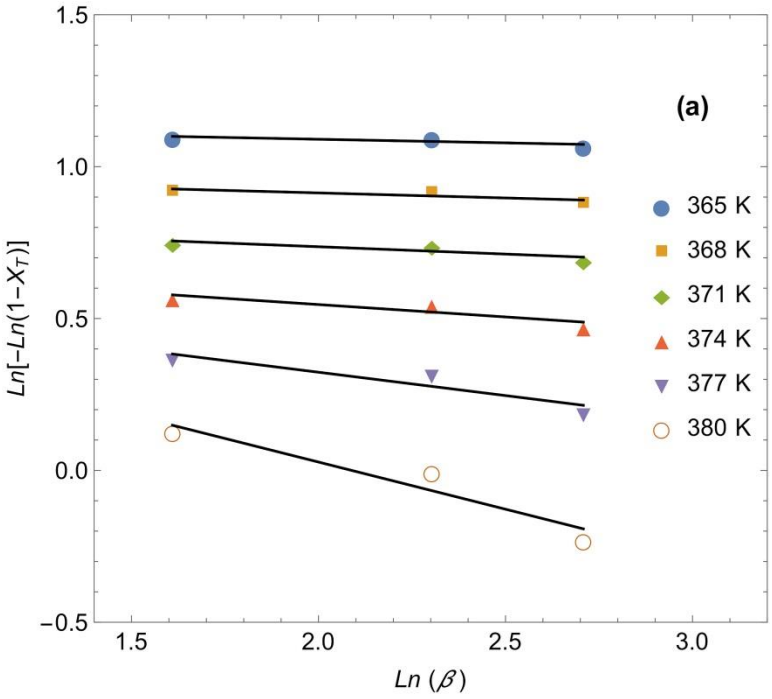

Figure 4-3 a. Ozawa-analysis plots for E-H-0

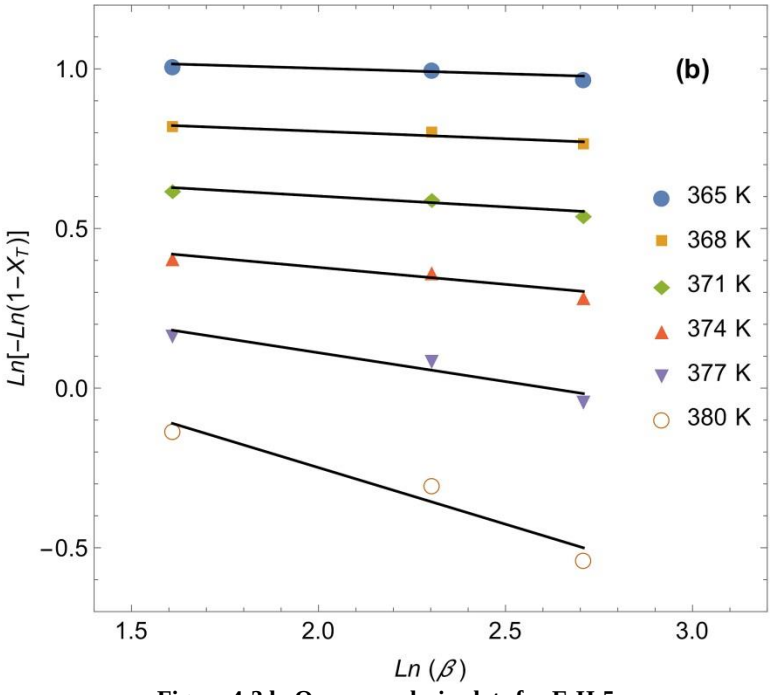

Figure 4-3 b. Ozawa-analysis plots for E-H-5

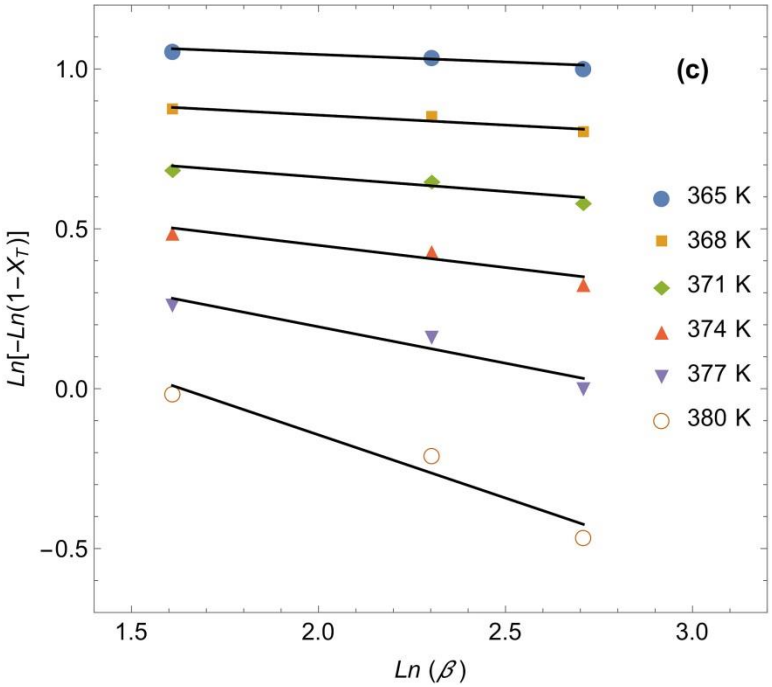

Figure 4-3 c. Ozawa-analysis plots for E-H-15

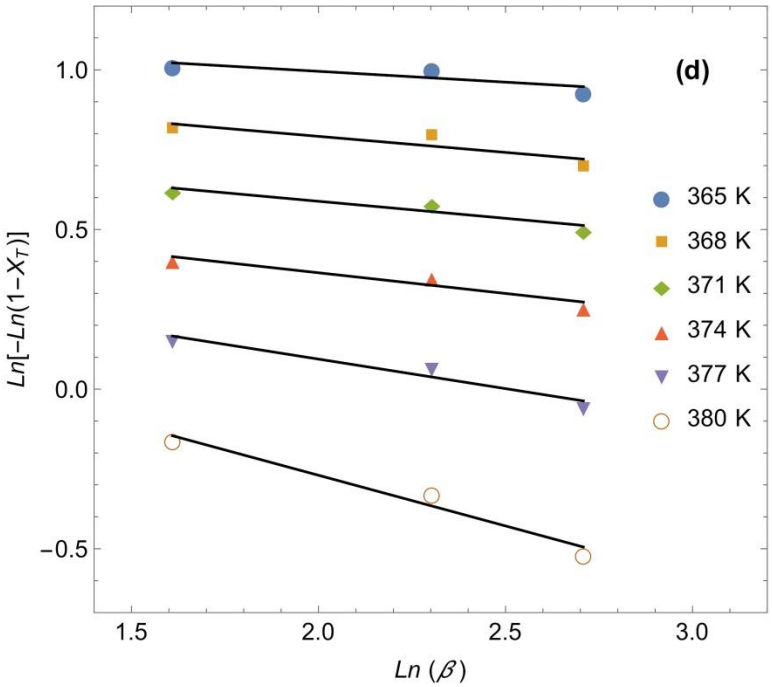

Figure 4-3 d. Ozawa-analysis plots for E-H-30

Table 4-3. Resulting values of *m* and *K*(T) from Ozawa analysis

Sample	Crystallization temperature T (*K*)											
	365		**368**		**371**		**374**		**377**		**380**	
	m	**k**	**m**	**k**	**m**	**k**	**m**	**k**	**m**	**k**	**m**	**k**
E-H-0	0.023	3.12	0.033	2.88	0.048	2.30	0.082	2.03	0.154	1.87	0.310	1.91
E-H-5	0.034	2.91	0.046	2.45	0.067	2.09	0.106	1.80	0.180	1.60	0.354	1.62
E-H-15	0.046	3.02	0.062	2.63	0.089	2.31	0.138	2.06	0.227	1.91	0.394	1.58
E-H-30	0.067	3.09	0.110	2.68	0.107	2.22	0.129	1.86	0.184	1.59	0.317	1.44

Analysis by Mo-model

The crystallization kinetics model proposed by Liu *et al*. [24] is derived from the Jeizorny-Avrami equation given by Eq. 1 and the Ozawa equation given by Eq.2 [25, 38].

After linearization and addition of Eq.1 & 2, the equation becomes

$$nLn(t) + Ln(k_t) = Ln\big(K(T)\big) - m\,Ln(\beta) \qquad (6)$$

Upon simplification, the above equation is reduced to

$$Ln[\beta] = Ln[F(T)] - \alpha Ln[t] \qquad (7)$$

Whereas, $F(T) = \left[\frac{K(T)}{k_t}\right]^{1/m}$ and α = n/m i.e. the ratio of the Avrami exponent to the Ozawa exponent. *F (T)* represents the degree of super cooling required to obtain a specific degree of crystallinity in unit time. A higher *F (T)* refers to a comparably difficult crystallization process and vice versa [24]. According to Eq.7 for Mo-model to successfully describe the crystallization process, plots of $Ln[\beta]$ against $Ln[t]$ should be linear. The Mo-model plots can be generated by considering a percent relative crystallinity and then calculate the time required to achieve that crystallinity at different cooling rates. The corresponding values of Ln (*t*) can then be plotted against $Ln[\beta]$. For the present case similar Mo-model plots were generate according to Eq.4. The plots are presented in Figure 4-4 (a-d) and the summarized results are listed in Table 4-4. The linearity of the plots shows that this model is valid for the LLDPE and LLDPE-TiO_2/Mn nanocomposites. *F(T)* and α were obtained from the intercept and slope of lines in Figure 4 respectively. As stated above that *F(T)* refers to the degree of super cooling required for a unit degree of crystallinity, it can be observed from the results in Table 4-4, that as the relative crystallinity increases the *F(T)* increases as well, which indicates that at higher

relative crystallinity more super cooling is required to crystallize the polymer melt. Similarly, it can also be observed that at a specific value of X_t, the *F (T)* for LLDPE-TiO_2/Mn nanocomposites is high as compared to neat LLDPE. This means the crystal growth process is slower for LLDPE-TiO_2/Mn nanocomposites. This conclusion is consistent with the Ozawa analysis.

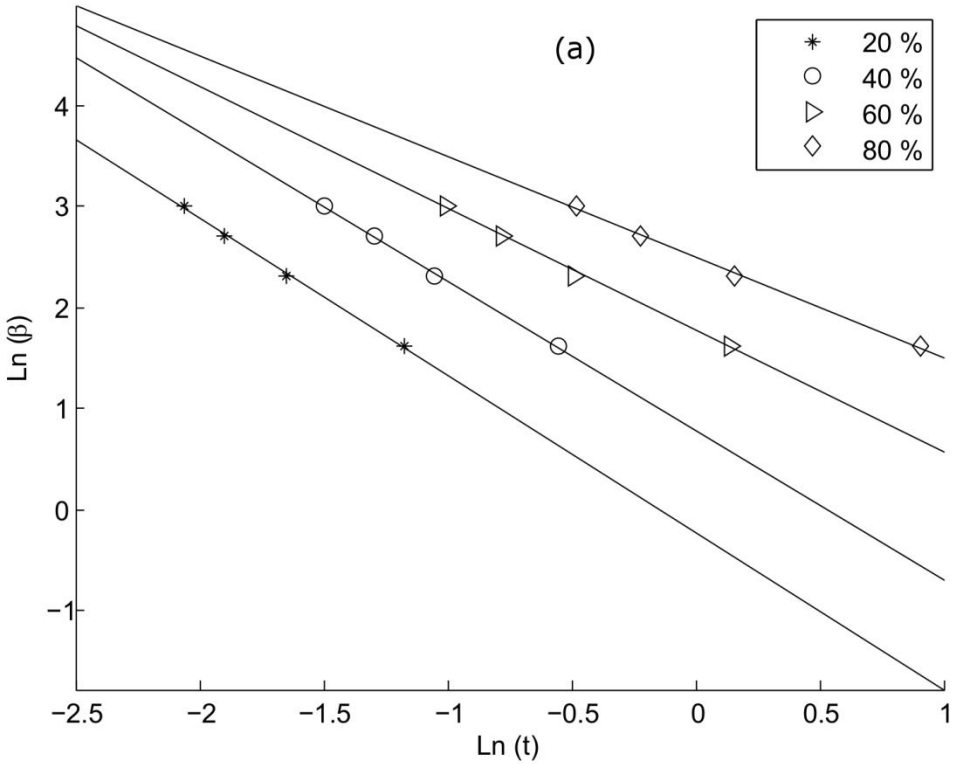

Figure 4-4 a. Mo-analysis plots for E-H-0

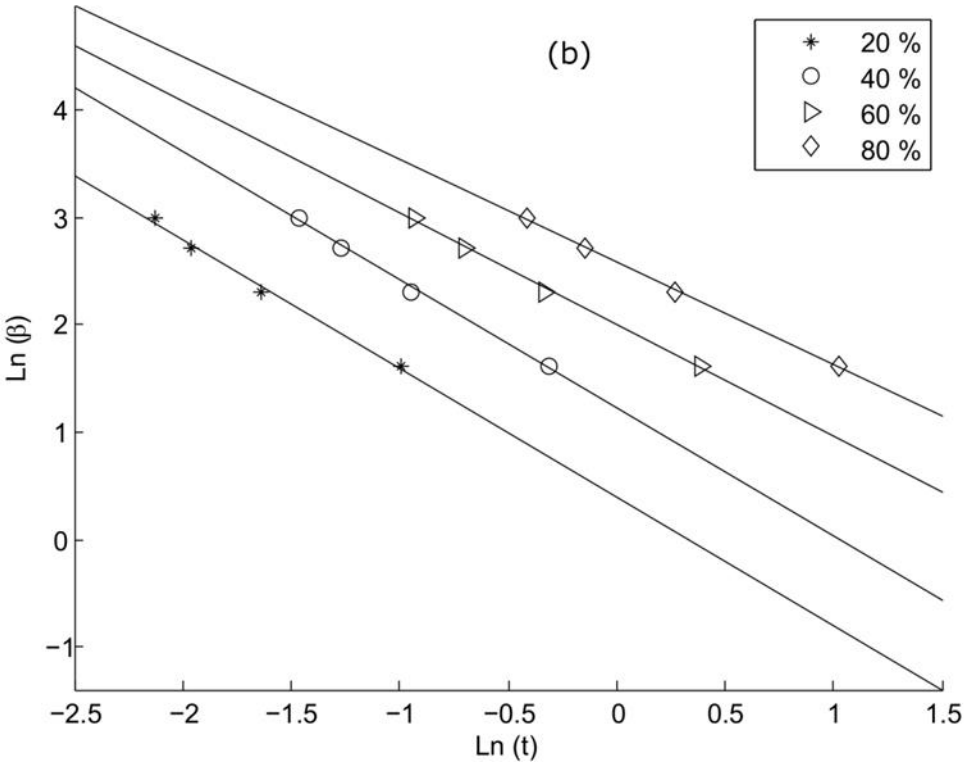

Figure 4-4 b. Mo-analysis plots for E-H-5

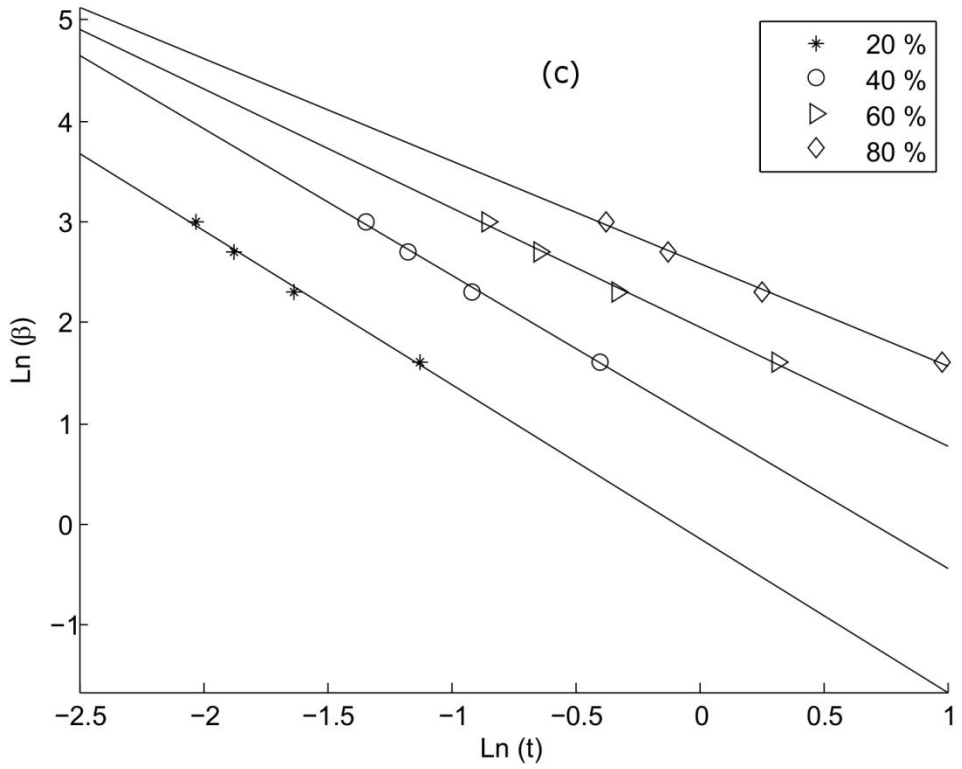

Figure 4-4 c. Mo-analysis plots for E-H-15

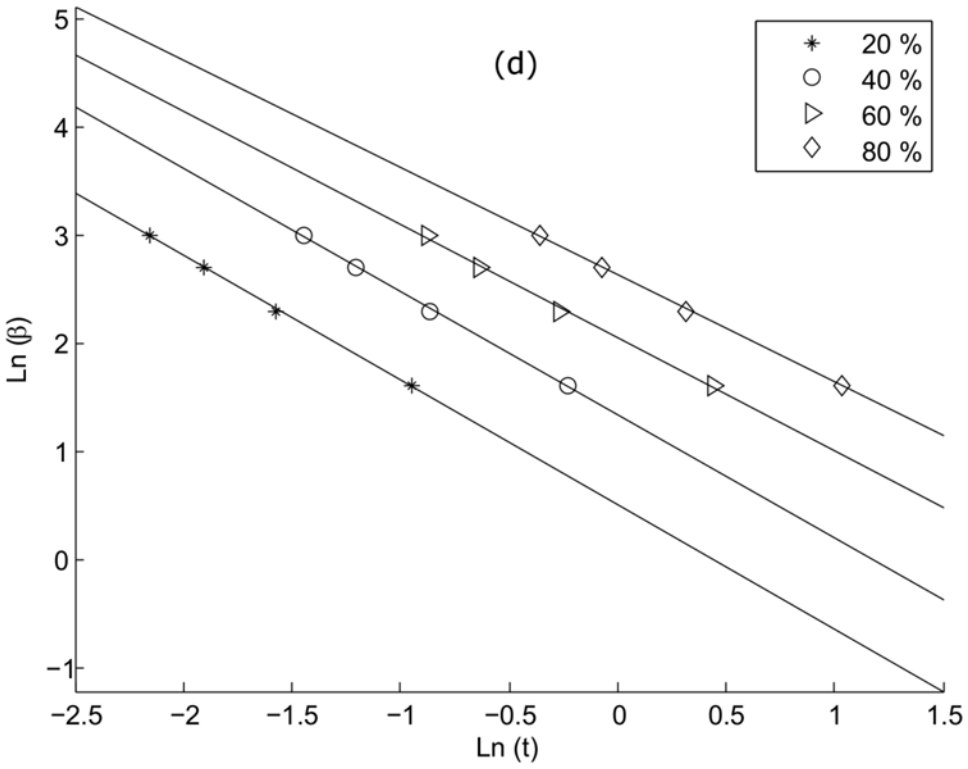

Figure 4-4 d. Mo-analysis plots for E-H-30

Table 4-4. Summarized Mo-model results

SAMPLE	X_t	F(T)	α(T)
E-H-0	0.2	0.80	0.21
	0.4	2.18	0.22
	0.6	5.83	0.30
	0.8	12.12	0.36
E-H-5	0.2	1.48	0.30
	0.4	3.38	0.31
	0.6	7.35	0.35
	0.8	13.17	0.38
E-H-15	0.2	0.87	0.21
	0.4	2.75	0.23
	0.6	7.1	0.30
	0.8	13.32	0.36
E-H-30	0.2	1.67	0.31
	0.4	3.52	0.32
	0.6	7.83	0.35
	0.8	13.9	0.37

4.3.4 Activation energy (EA)

E_A is related to the energy required for transporting the crystalline chains of polymer through the phase [39]. One approach to determine this energy is by taking into account the variation in peak temperature for crystallization (T_P) with the cooling rate, according to the following relationship [40].

$$\frac{d\left(Ln\left(\frac{\beta}{T_p{}^2}\right)\right)}{d\left(\frac{1}{T_p}\right)} = -\frac{E_A}{R} \qquad (8)$$

Where, R is the universal gas constant. E_A can be evaluated from the slope of $Ln\left(\frac{\beta}{T_p{}^2}\right)$ vs. $\frac{1}{T_p}$ shown in Figure 4-5. E_A turned out to be -603.86, -589.32, -559.35 and -556.53 kJ/mol, for E-H-0, E-H-5, E-H-15 and E-H-30 respectively. Since the crystallization process is exothermic i.e. transformation from melt to crystalline form, so the greater magnitude of absolute E_A favors the process [36, 41]. For the present case it is found that with the addition of nano-TiO_2/Mn, E_A is increased, indicating a difficulty in the crystallization process. This phenomenon can be attributed to adsorption of polymer segments by the nano filler, which then prevents the movement of molecular segments and thus makes the crystallization difficult. Similar observations were also made in the case of HDPE/nano-SiO_2 nanocomposites [42].

The current study only considers the laboratory work and is aimed to obtain a better idea about the role of nano-TiO_2/Mn upon the activity of the metallocene catalyst,

microstructural behavior of the copolymer and non-isothermal crystallization kinetics. It is necessary at this stage to evaluate other physical properties, including mechanical properties and calorimetric properties.

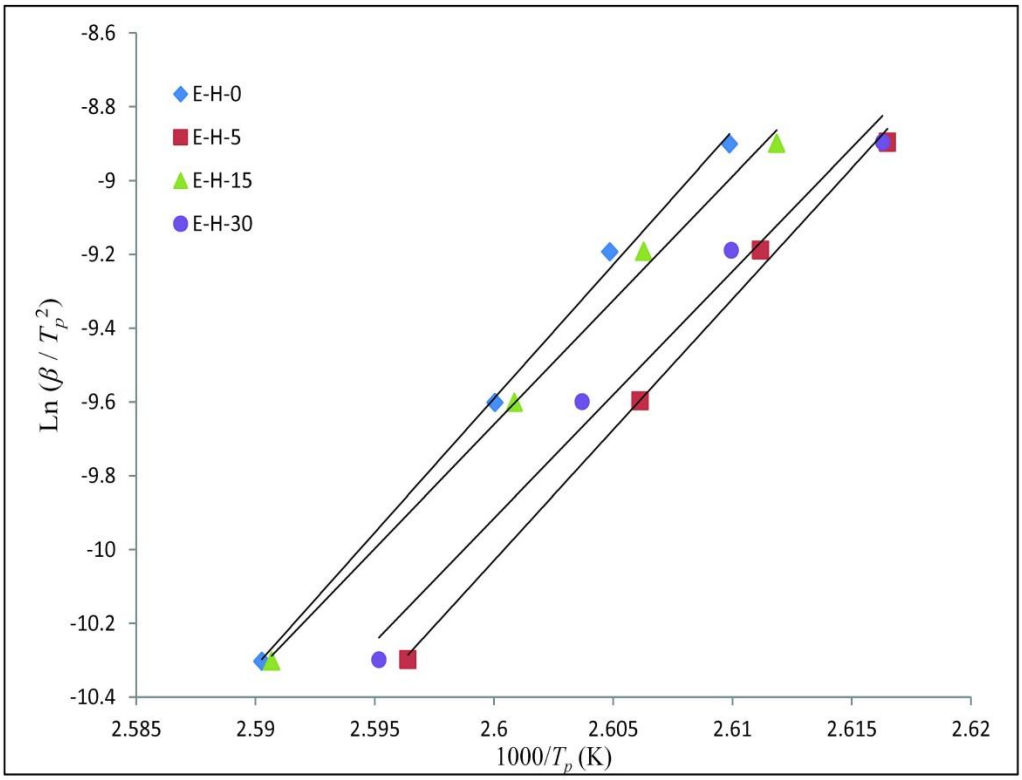

Figure 4-5. Kissinger Plots for LLDPE and LLDPE-TiO_2/Mn nanocomposites

4.4 CONCLUSION

Nano-TiO_2/Mn significantly influences the catalytic activity as well as the percentage crystallinity but it has very minimal effect on T_m. The optimum dose is found to be 15 mg of the nano filler to give the maximum catalytic activity. The drop in nano-TiO_2/Mn alters the polymer structure by adding more short chain branching to its backbone, thus decreasing the DOC. 1-hexene incorporation is determined by ^{13}C NMR which clearly indicates that, 1-hexene incorporation is increased by filler addition. The Ozawa-method and Mo-method successfully described the non-isothermal crystallization of LLDPE and LLDPE-TiO_2/Mn nanocomposites. E_A was calculated from Kissinger method. It was found that the crystallization process is retracted by presence of the nano filler due to steric hindrance, as indicated by an increase of cooling function and E_A, and decrease in the crystallization rate constant.

4.5 REFERENCES

1. Kontou E, Niaounakis M (2006) Thermo-mechanical properties of LLDPE/SiO_2 nanocomposites. Polymer (Guildf) 47:1267–1280. doi: 10.1016/j.polymer.2005.12.039

2. Kaminsky W (1998) Highly active metallocene catalysts for olefin polymerization. J Chem Soc Dalt Trans 1413–1418. doi: 10.1039/A800056E

3. Kaminsky W, Piel C, Scharlach K (2005) Polymerization of Ethene and Longer Chained Olefins by Metallocene Catalysis. Macromol Symp 226:25–34. doi: 10.1002/masy.200550803

4. Kaminsky W, Funck A, Klinke C (2008) In-situ Polymerization of Olefins on Nanoparticles or Fibers by Metallocene Catalysts. Top Catal 48:84–90. doi: 10.1007/s11244-008-9044-9

5. Choi Y, Soares JBP (2012) Supported single-site catalysts for slurry and gas-phase olefin polymerisation. Can J Chem Eng 90:646–671. doi: 10.1002/cjce.20583

6. Fónagy T, Schulze U, Komber H, et al. (2007) Poly(propylene- g -styrene) Graft Copolymers with Well-Defined Microstructure by Metallocene Catalyzed Copolymerization of Propylene with Allyl-Terminated Polystyrene Macromonomers. Macromolecules 40:1401–1407. doi: 10.1021/ma062511x

7. Wang H, Ma Z, Ke Y, Hu Y (2003) Synthesis of linear low density polyethylene (LLDPE) byin situ copolymerization with novel cobalt and zirconium catalysts. Polym Int 52:1546–1552. doi: 10.1002/pi.1282

8. Pérez O, Soares JBP, García M, et al. (2013) Heterogeneous Ethylene and Alpha-Olefin Copolymerization Using Zirconocene Aluminohydride Complexes. Macromol Symp 325-326:71–76. doi: 10.1002/masy.201200041

9. Wang Z, Wang X, Xie G, et al. (2006) Preparation and characterization of polyethylene/TiO_2 nanocomposites. Compos Interfaces 13:623–632. doi: 10.1163/156855406778440730

10. Abdul Kaleel SH, Kottukkal Bahuleyan B, De SK, et al. (2012) Effect of Mn doped-titania on the activity of metallocene catalyst by in situ ethylene polymerization. J Ind Eng Chem 18:1836–1840. doi: 10.1016/j.jiec.2012.04.010

11. Jordan J, Jacob KI, Tannenbaum R, et al. (2005) Experimental trends in polymer nanocomposites a review. Mater Sci Eng A 393:1–11. doi: 10.1016/j.msea.2004.09.044

12. Zou H, Wu S, Shen J (2008) Polymer/silica nanocomposites: preparation, characterization, properties, and applications. Chem Rev 108:3893–957. doi: 10.1021/cr068035q

13. Li K-T, Dai C-L, Kuo C-W (2007) Ethylene polymerization over a nano-sized silica supported Cp_2ZrCl_2/MAO catalyst. Catal Commun 8:1209–1213. doi: 10.1016/j.catcom.2006.11.011

14. Chaichana E, Pathomsap S, Mekasuwandumrong O, et al. (2012) LLDPE/TiO_2 nanocomposites produced from different crystallite sizes of TiO_2 via in situ polymerization. Chinese Sci Bull 57:2177–2184. doi: 10.1007/s11434-012-5021-6

15. Wang Z, Li G, Xie G, Zhang Z (2005) Dispersion Behavior of TiO_2 Nanoparticles in LLDPE/LDPE/TiO_2 Nanocomposites. Macromol Chem Phys 206:258–262. doi: 10.1002/macp.200400309

16. Shafiq M, Yasin T, Saeed S (2012) Synthesis and characterization of linear low density polyethylene/sepiolite nanocomposites. J Appl Polym Sci 123:1718–1723. doi: 10.1002/app.34633

17. Kuo MC, Tsai CM, Huang JC, Chen M (2005) PEEK composites reinforced by nano-sized SiO_2 and Al_2O_3 particulates. Mater Chem Phys 90:185–195. doi: 10.1016/j.matchemphys.2004.10.009

18. Jongsomjit B, Panpranot J (2006) Characteristics of LLDPE/ZrO_2 Nanocomposite Synthesized by In-situ Polymerization using a Zirconocene/MAO Catalyst. Iran Polym J 15:433–439.

19. Sagmeister M, Brossmann U, List EJW, et al. (2009) Synthesis and optical properties of organic semiconductor: zirconia nanocomposites. J Nanoparticle Res 12:2541–2551. doi: 10.1007/s11051-009-9823-7

20. Patel R (2012) Crystallization kinetics modeling of high density and linear low density polyethylene resins. J Appl Polym Sci. doi: 10.1002/app.35177

21. Shi Y-H, Dou Q (2012) Non-isothermal crystallization kinetics of β-nucleated isotactic polypropylene. J Therm Anal Calorim 112:901–911. doi: 10.1007/s10973-012-2611-0

22. Pucciariello R, Villani V, Giammarino G (2010) Thermal behaviour of nanocomposites based on linear-low-density poly(ethylene) and carbon nanotubes prepared by high energy ball milling. J Polym Res 18:949–956. doi: 10.1007/s10965-010-9494-1

23. Lee S, Kim M, Ogale A (2007) Crystallization behavior of carbon nanofiber/linear low density polyethylene nanocomposites. J Appl Polym Sci 106:2605–2614. doi: 10.1002/app.26800

24. Liu T, Mo Z, Wang S, Zhang H (1997) Nonisothermal melt and cold crystallization kinetics of poly (aryl ether ether ketone ketone). Polym Eng Sci 37:568–575. doi: 10.1002/pen.11700

25. Avrami M (1939) Kinetics of Phase Change. I General Theory. J Chem Phys 7:1103. doi: 10.1063/1.1750380

26. Jeziorny A (1978) Parameters characterizing the kinetics of the non-isothermal crystallization of poly(ethylene terephthalate) determined by D.S.C. Polymer (Guildf) 19:1142–1144. doi: 10.1016/0032-3861(78)90060-5

27. Ozawa T (1971) Kinetics of non-isothermal crystallization. Polymer (Guildf) 12:150–158. doi: 10.1016/0032-3861(71)90041-3

28. Pooter M De, Smith P (1991) Determination of the composition of common linear low density polyethylene copolymers by ^{13}CNMR spectroscopy. J Appl Polym Sci 42:399–408. doi: 10.1002/app.1991.070420212

29. Sarzotti DM, Soares JBP, Penlidis A (2002) Ethylene/1-hexene copolymers synthesized with a single-site catalyst: Crystallization analysis fractionation, modeling, and reactivity ratio estimation. J Polym Sci Part B Polym Phys 40:2595–2611. doi: 10.1002/polb.10339

30. Owpradit W, Jongsomjit B (2008) A comparative study on synthesis of LLDPE/TiO_2 nanocomposites using different TiO_2 by in situ polymerization with zirconocene/dMMAO catalyst. Mater Chem Phys 112:954–961. doi: 10.1016/j.matchemphys.2008.07.050

31. Severn JR, Chadwick JC, Duchateau R, Friederichs N (2005) "Bound but not gagged" immobilizing single-site alpha-olefin polymerization catalysts. Chem Rev 105:4073–147. doi: 10.1021/cr040670d

32. Chaichana E, Jongsomjit B, Praserthdam P (2007) Effect of nano-SiO_2 particle size on the formation of LLDPE/SiO_2 nanocomposite synthesized via the in situ polymerization with metallocene catalyst. Chem Eng Sci 62:899–905. doi: 10.1016/j.ces.2006.10.005

33. Macko T, Schulze U, Brüll R, et al. (2008) Monitoring the Chemical Heterogeneity and the Crystallization Behavior of PP-g-PS Graft Copolymers Using SEC-FTIR and CRYSTAF. Macromol Chem Phys 209:404–409. doi: 10.1002/macp.200700398

34. Bruaseth I, Rytter E (2003) Dual Site Ethene / 1-Hexene Copolymerization with MAO Activated Polymer Chains between the Sites. macro 36:3026–3034. doi: 10.1021/ma025832r

35. Zhang Z, Xiao C, Dong Z (2007) Comparison of the Ozawa and modified Avrami models of polymer crystallization under nonisothermal conditions using a computer simulation method. Thermochim Acta 466:22–28. doi: 10.1016/j.tca.2007.10.004

36. Shehzad F, Thomas SSP, Al-Harthi MA, Harthi M (2014) Non-isothermal crystallization kinetics of high density polyethylene/graphene nanocomposites prepared by in-situ polymerization. Thermochim Acta 589:226–234. doi: 10.1016/j.tca.2014.05.039

37. Apiwanthanakorn N, Supaphol P, Nithitanakul M (2004) Non-isothermal melt-crystallization kinetics of poly(trimethylene terephthalate). Polym Test 23:817–826. doi: 10.1016/j.polymertesting.2004.03.001

38. Ozawa T (1970) Kinetic analysis of derivative curves in thermal analysis. J Therm Anal Calorim 2:301–324. doi: 10.1007/BF01911411

39. Joshi M, Butola BS (2004) Studies on nonisothermal crystallization of HDPE/POSS nanocomposites. Polymer (Guildf) 45:4953–4968. doi: 10.1016/j.polymer.2004.04.057

40. Kissinger H (1957) Reaction kinetics in differential thermal analysis. Anal Chem 29:1702–1706. doi: 10.1021/ac60131a045

41. Ferreira CI, Dal Castel C, Oviedo M a. S, Mauler RS (2013) Isothermal and non-isothermal crystallization kinetics of polypropylene/exfoliated graphite nanocomposites. Thermochim Acta 553:40–48. doi: 10.1016/j.tca.2012.11.025

42. Jiasheng Q, Pingsheng H (2003) Non-isothermal crystallization of HDPE / nano-SiO_2 composite. J Mater Sci 38:2299–2304. doi: 10.1023/A:1023968026684

CHAPTER 5

Graphene/layered double hydroxides nanocomposites: A review of recent progress in synthesis and applications

Muhammad Daud [1], Muhammad Shahzad Kamal [2], Farrukh Shehzad [1], Mamdouh A. Al-Harthi [1,3*]

[1] Department of Chemical Engineering, King Fahd University of Petroleum and Minerals, Dhahran 31261, Saudi Arabia

[2] Center for Integrative Petroleum Research (CIPR), King Fahd University of Petroleum and Minerals, Dhahran 31261, Saudi Arabia

[3] Center for Research Excellence in Nanotechnology (CENT), King Fahd University of Petroleum & Minerals, 31261, Dhahran, Saudi Arabia

[*]Corresponding Author: Mamdouh A. Al-Harthi

E-mail address: mamdouh@kfupm.edu.sa

This chapter has been published in "CARBON" on 26th March 2016

Abstract

Hybrids of graphene (G) and layered double hydroxides (LDHs) are promising nanomaterials due to their versatile properties and the large number of composition/preparation variables available for fine-tuning. Several techniques are available for the synthesis of these novel G/LDHs nanocomposites. This article reviews the recent developments in their synthesis and applications in the oxygen evolution reaction, supercapacitors, hybrid sensors, adsorption, catalysis, water purification, and flame retardant materials.

5.1 Introduction

Graphene (G) and chemically modified graphene such as graphene oxide (GO) have special and much desired characteristics due to their unique electrical, mechanical, thermal, and surface properties [1–3]. Layered double hydroxides (LDHs) are inorganic materials with a 2D highly tunable brucite-like layered crystal structure. These inorganic clays contain layers of positively charged metal hydroxides with multivalent anions for neutrality. The LDHs are generally represented by formula $[M^{2+}_{(1-X)}M^{3+}_{(X)}(OH)_2]^{X+}(A^{n-})_{X/n}.\ mH_2O$. Where, M^{2+} and M^{3+} represents the di and trivalent metallic cations (M^{+2} can be Mg^{2+}, Ni^{2+}, Co^{2+}, Zn^{2+} *etc.* whereas M^{3+} can be Al^{3+}, Fe^{3+} *etc.*) and A^{n-} is an anion such as OH^-, F^-, NO_3^-, Cl^-, CO_3^{2-} or SO_4^{2-}. The water molecules embedded between the lamellar structures are initiating the synthesis process. Typically, x varies in the range 0.22 to 0.33 [4,5]. The LDHs can be used in a variety of potential applications due to their low cost, facile synthesis, thermal stability, and chemical versatility [6].

Hybrid nanomaterials developed using LDHs and carbon based materials such as carbon nanotubes (CNTs), carbon nanofibers, and graphene has invoked a great deal of interest lately because they have unique properties due to the combination of the special properties of the parent materials. Of particular interest is graphene sandwiched between two cationic layers of LDHs to yield a new material with improved properties as compared to the pristine graphene [7,8]. The layered structure of LDHs not only prevents the restacking of graphene but also improves the catalytic activity and thermal stability of the composite [9]. The general schematic of a sandwich assembly is shown in Figure 5-1.

The novel G/LDHs nanocomposites can be used in a variety of applications such as supercapacitors [11–13], as magnets [14,15], catalysis [10,16], electrochemistry [17], as nanofillers for polymer nanocomposites [18–20], in water treatment [21,22], in medical applications [23–25] and in many other areas.

A few review articles that focus on the synthesis and applications of individual LDHs, graphene nanocomposites, and carbon/LDHs are available [26–30]. Zhao et al. reviewed the research progress and new developments in the area of hierarchical nanocomposites derived from nanocarbon and LDHs [30]. Shao et al. highlighted the progress in the design, synthesis and characterization of LDHs for applications in electrochemical energy storage and conversion [29]. In this paper, the methods used for the synthesis of G/LDHs nanocomposites and their novel and potential applications in the areas of oxygen evolution reaction, supercapacitors, catalysis, sensors and polymer nanocomposites are reviewed. To the best of our knowledge, this is the first review dealing with the latest developments in the field of G/LDHs nanocomposites.

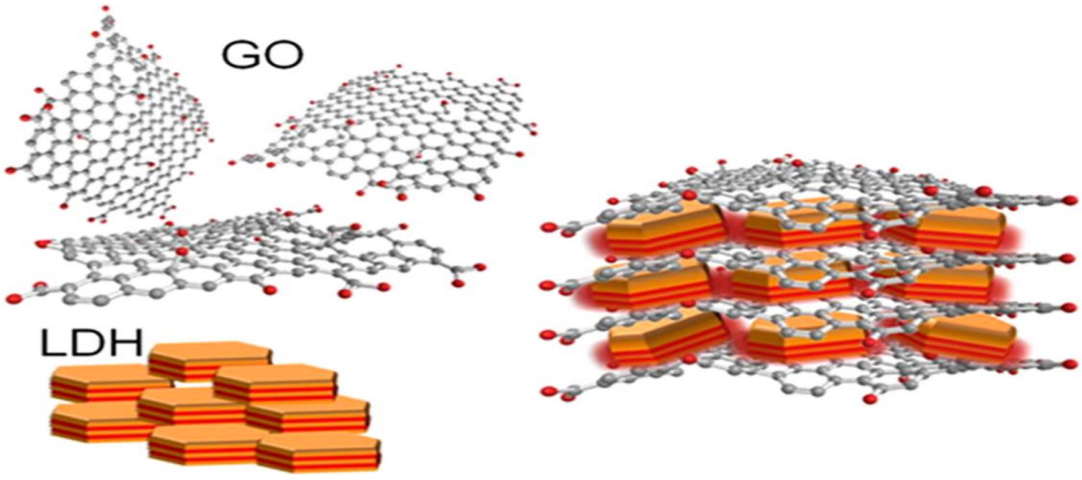

Figure 5-1. Schematic of the sandwich arrangement of LDHs and GO [10] with permission from ACS

5.2 SYNTHESIS OF G/LDHs NANOCOMPOSITES

5.2.1 Co-precipitation synthesis

The co-precipitation method is a method that is used extensively for the synthesis of a variety of LDHs and their novel carbon based hybrids such as CNT/LDHs and G/LDHs [31–33]. A schematic of the formation of a hybrid is shown in Figure 5-2. Initially, graphene nanosheets (GNS) or GO are ultrasonicated in deionized water (DI) and are mixed with a solution of the precursor salts (M^{2+}: M^{3+}) prepared under vigorous stirring at a controlled pH. Reducing agents are primarily used to adjust the pH and reduce GO to reduced graphene oxide (rGO) or GNS [23]. Commonly used reducing agents include urea, hydrazine, glucose, and sodium sulfide. Though, glucose is preferred over hydrazine because it is less toxic and environmental friendly [34]. The suspension is then allowed to reflux for 24-48 h at 90 $\pm$ 10 °C with continuous magnetic stirring followed by centrifuging and washing with DI water and pure ethanol to remove any impurities. The G/LDHs nanocomposites thus obtained are dried for 48 h at 60 °C. In this method, the charge densities of matrix cations within the hydroxide layers are maintained. The pH must be controlled in order to precipitate both M^{2+}/M^{3+} cations simultaneously to prevent $M(OH)_2$ remaining as an impurity [35]. However, a wide range of crystallite sizes are obtained due to the complex aging process [36]. Several G/LDHs nanocomposites along with their synthesis parameters are tabulated in Table 5-1.

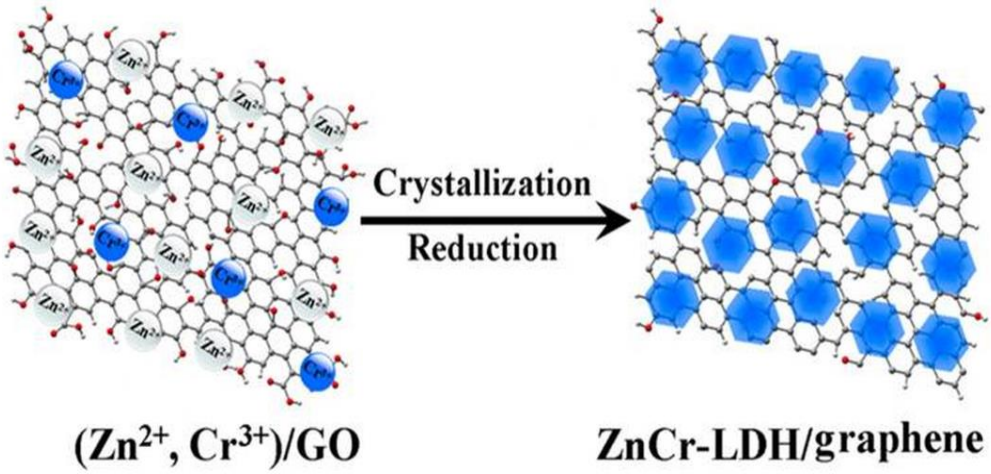

Figure 5-2. Schematic illustration of the assembly process of a ZnCr/graphene nanocomposite [37] with permission from ACS

Table 5-1. Graphene based nanocomposites synthesized using the co-precipitation method

Nanocomposite	Precursor salts	Molar ratio of precursor salts (M^{2+}: M^{3+})	Ultrasonication of GO suspension (mg-mL)/min	pH	Reducing agents	Applications	Ref
GO/MgAl	Nitrates	2:1	[a] 100-50/60	10	None	CO_2 adsorbent	[10]
rGO/ZnAl	Chlorides	2:1	100-500/60	9.0	Urea	DNA sensor	[23]
G/NiAl	Nitrates	3:1	[b] 60-50/30	10.5	[c] Sodium sulfide	Dopamine sensor	[24]
[d] G/CNTs/NiAl	Nitrates	3:1	[e] 60-50/30	10	Glucose	Glucose sensor	[25]
rGO/NiAl	Nitrates	3:1	[b] 320-150/60	10.5	Hydrazine	Flame retardant	[33]
G/ZnCr	Nitrates	2:1	-	9.0	None	Photocatalyst	[37]
[f] rGO/ ZnCo	Sulfates	1:1	60-100/30	9.0	Glucose	Water oxidation	[34]
G/NiAl	Nitrates	3:1	[b] 220-100/60	10.5	[c] Sodium sulfide	Immunosensor	[38]
G/CoAl	Chlorides	2:1	[g] GO-100/60	-	Urea	Supercapacitor	[39]

[a] GO is ultrasonicated in NaOH (4.8 M) and Na_2CO_3 (1.2 M)
[b] GO is ultrasonicated in NaOH (0.20 M) and Na_2CO_3 (0.05 M)
[c] Sodium sulfide as the reductant (34 mg mL^{-1})
[d] Decorated with Au nanoparticles with GO/CNTs mass ratio 1:1
[e] GO is ultrasonicated in $Ni(NO_3)_2$ (6 mmol) and $Al(NO_3)_3$ (2 mmol)
[f] H_2O_2 as the oxidant (0.2 mL, 35 wt %) and glucose assisted with ammonia as the reductant (0.5 mg mL^{-1} of GO)
[g] Varying GO contents i.e. 5.5, 11, 22 and 33 mg with 45, 55, 75 and 95 mM urea solution, respectively

5.2.2 One-pot hydrothermal synthesis

Hydrothermal synthesis method, also known as the urea-hydrolyzed method, is also used for the synthesis of G/LDHs nanocomposites. This technique involves the mixing of urea with a solution of precursor salts, followed by the addition of an ultrasonicated suspension of GO. The resultant mixture is then transferred to a Teflon-lined stainless steel jacketed autoclave reactor and heated at a desired temperature for an extended period to allow reduction of GO. Although, Although, LDHs and their GO or rGO hybrids with a uniform crystallite size and shape have been successfully synthesized using the urea-hydrolyzed method, the resultant product is typically contaminated with carbonate ions. Moreover, this method is of limited application in some cases, especially for preparing Cu^{+2} and Cr^{3+} cationic LDHs [40]. Hexamethylenetetramine (HMT) has been used instead of urea for selected applications. The high temperature of the hydrothermal process favors the formation of ammonia from HMT, making the aqueous solution more alkaline [41]. The advantage of hydrothermal synthesis over co-precipitation is that it yields a well crystallized nanocomposite with uniform morphology [7,42]. These rGO/LDHs nanocomposites with a uniform crystallite size and morphology have displayed superior properties over pristine LDHs in the field of supercapacitors. However, using a large amount of rGO tends to decrease the crystallinity of the nanocomposites [43]. A schematic illustration of a typical hydrothermal one-pot synthesis is shown in Figure 5-3. Experimental conditions that have been used for one-pot synthesis are summarized in Table 5-2. There is a need to develop a continuous flow process, which is rapidly gaining the interest and attention of researchers [44].

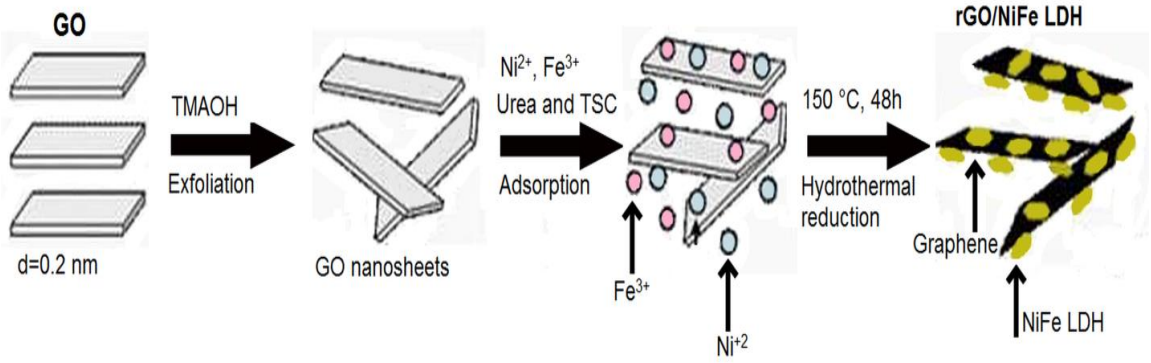

Figure 5-3. Schematic illustration of the formation of a rGO/NiFe composite [45] with permission from Elsevier

Table 5-2. G/LDHs nanocomposites synthesized using the hydrothermal approach

Nanocomposites	Precursor salts	Molar ratio of precursor salts (M^{2+}: M^{3+})	Autoclave parameters (°C / h)	Applications	Ref
G/MgAl	Nitrates	2:1	[a] 140 / 10	-	[7]
G/NiFe	Nitrates	3:1	[b] 150 / 48	Flame retardant	[18]
G/MgAl	Nitrates	2:1	[c] 140 / 12	Dielectric nanoplates	[46]
rGO/NiFe	Nitrates	[d] Varying concentration	[b] 150 / 48	-	[45]
G/MgAl	Nitrates	3:1	[b] 120 / 24	Cr removal from water	[22]
G/NiAl	Nitrates	2:1	95 / 24	Supercapacitor	[47]
[e] GO/MgAl	Chlorides	3:1	[c] 140 / 12	Arsenic removal from water	[48]
[f] GO/ MgAl/Fe_3O_4	Hydroxides	3.3:1	[b] 100 / 24	Lead removal from water	[49]
rGO/NiCo	Nitrates	[g] Varying concentration	[b] 180 / 12	Supercapacitor	[50]
[e] rGO/CoAl	Chlorides	2:1	[a] 100 / 4	Electrocatalytic reduction of oxygen	[51]
[e] rGO /CoAl	Nitrates	-	[b] 180 / 18	Supercapacitor	[52]
[h] rGO/NiCo	Nitrates	[i] 1:1	[j] Varying conditions	Supercapacitor	[43]

[a] NaOH hydrolyzed hydrothermal reaction
[b] Urea-hydrolyzed hydrothermal reaction
[c] HMT hydrolyzed hydrothermal reaction
[d] 2, 4, 16 and 35 mmol/L precursor salts concentration
[e] Varying GO contents were used
[f] 4 wt % of Fe_3O_4 with Varying GO contents were used
[g] 1:0, 1:1, 2:1, 0:1 molar ratio of precursor salts
[h] GO to metal precursor ratio were selected 1:5, 1:7.5 and 1: 10
[i] Ammonium hydroxide was used as a precipitant and hydrazine monohydrate (1 mL mg^{-1} GO) as a reductant
[j] 90, 120, 150, and 180 °C for 10 h, then 150 °C for 12 h were used

5.2.3 Exfoliation-restacking synthesis

This method involves the delamination of LDHs (intercalated with nitrates or chlorides) and the subsequent attachment of these exfoliated LDHs through self-assembly to the surface of GO due to electrostatic interactions [9]. The presence of functional groups attached to GO makes their colloidal solutions strongly negative, while LDHs, which are positively charged metallic hydroxides with replaceable anions, can form positively charged species through exfoliation. Thus, exfoliation and restacking is a good route to obtain nanocomposites of GO/LDHs or chemically modified G/LDHs [11]. These exfoliated 2D LDHs provide nucleation sites for the growth of graphene. Homogenous anchoring of GNS and uniform crystal growth are key factors for the successful application of these nanocomposites [53]. However, exfoliation of LDHs is difficult due to the strong electrostatic forces between the metallic hydroxides and intercalated anionic layers. These forces can be weakened by introducing solvents such as formamide [11,54], water [55], and sodium dodecyl sulfate (SDS) [56]. Typically, the LDHs are ultrasonicated in formamide solution initially and then added to an ultrasonicated GO suspension for the restacking process. The resultant mixture is stirred at least for 12 h and then centrifuged and washed. Washing 4-5 times with DI water followed by washing with pure ethanol is required to remove all the impurities. The resulting solid is then dried in a vacuum oven at 80 °C overnight [54]. The nanocomposites obtained through this process possess high phase purity and relatively high crystallinity [41]. A schematic illustration of the formation of the hybrid G/NiAl complex through exfoliation-restacking is presented in Figure 5-4. Table 5-3 summarizes the exfoliation-restacking methods reported in the literature and the conditions used in them.

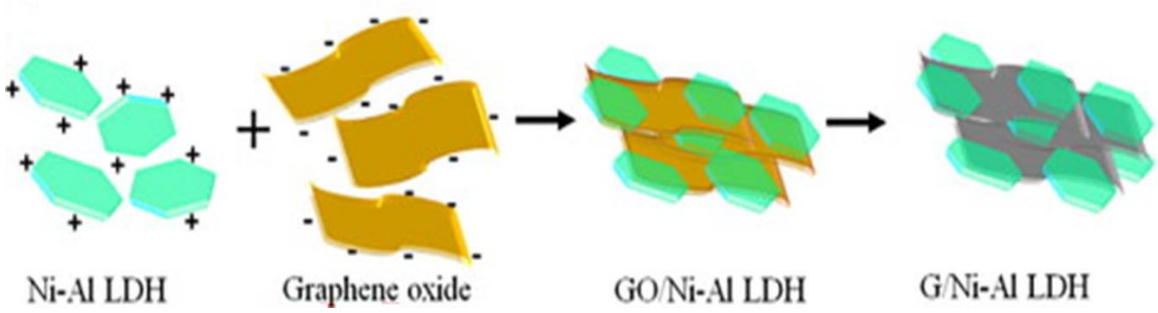

Figure 5-4. Schematic representation of the synthesis of G/NiAl through exfoliation-restacking [9] with permission from Elsevier

Table 5-3. Graphene based nanocomposites synthesized using the exfoliation and restacking approach

LDHs synthesis method	Thermal parameters	Constituents		Nanocomposite	Applications	Ref
		Component : A (+ve charged)	Component : B (-ve charged)			
Co-precipitation	-	CoAl LDHs	rGO	rGO/CoAl LDHs	Supercapacitor	[11]
Co-precipitation	Refluxing at 90 °C for 24 h	[a] NiTi LDHs	rGO	rGO/NiTi LDHs	Photocatalyst	[55]
-	-	CoAl LDHs	GO	GO/CoAl LDHs	Supercapacitor	[54]
Co-precipitation	Refluxing at 120 °C overnight	MgAl LDHs	GO	GO/MgAl LDHs	CO_2 adsorbent	[57]
Hydrothermal	Autoclave at 95 °C for 24 h	NiAl LDHs	GO	[b] G/NiAl LDHs	Supercapacitor	[9]
HMT-AQS hydrothermal	Autoclave at 120 °C for 6 h	[c] NiFe LDHs-AQS	GO	[d] rGO/NiFe LDHs	Oxygen evolution reaction	[58]
Hydrothermal	Autoclave at 160 °C for 12 h	CoAl LDHs	[e] GO	rGO/CoAl LDHs	Supercapacitor	[59]

[a] NiTi LDHs are ultrasonicated in DI water

[b] GO is reduced using hydrazine monohydrate at 80 °C for 2.5 h

[c] 2:1, 3:1, 4:1 molar ratio of precursor salts

[d] GO is reduced using HMT hydrothermal process and anthraquinone-2-sulfonate anions (AQS) transforms ferric (Fe^{+2}) to ferrous (Fe^{+3}) anions. SDS is used to increase the interlayer spacing of NiFe-LDHs from 2 to 2.4 nm

[e] Varying GO content

5.2.4 Characterization of DSSCs

G/LDHs nanocomposites can be formed by layer-by-layer (LBL) assembly using the electrostatic attractions between the negatively charged GO and positively charged materials [53]. Polymeric solutions such as poly(diallyldimethylammonium chloride) (PDDA), polyaniline (PANI), poly (ethylene imine) (PEI) and poly (vinyl alcohol) (PVA) etc. can be used to obtain a cationic surface required for LBL assembly. The product exhibits a highly tunable hybrid architecture with nanoscale precision, uniform particle size, and a film morphology. [60,61]. Furthermore, a variety of substrate supports can be used for the deposition of negatively charged GO and positively charged LDHs. Dong et al. formed multilayered composites containging CoAl LDHs and GO by LBL assembly using a PDDA-coated indium tin oxide (ITO) substrate. The CoAl LDHs were synthesized using the co-precipitation method followed by exfoliation using formamide solution. The exfoliated GO, obtained via the modified Hummer's method, is ultrasonicated to obtain a uniform dispersion. The coated substrate was then immersed in the GO dispersion followed by immersion in the exfoliated LDHs dispersion. After each immersion, the coated substrate was washed and dried with nitrogen to remove impurities and un-exfoliated components. The process was repeated several times to achieve the desired number of layers [61]. A similar procedure, schematically depicted in Figure5-5, was also adopted by Chen et al. for the formation of the CoAl/GO/PVA hybrid by LBL assembly. The CoAl-LDHs, obtained from the hydrothermal treatment of precursor salts, were exfoliated using formamide solution. The quartz glass sheets (substrate) were thoroughly washed with DI water and dried in a nitrogen stream. The cleaned glass substrate was coated with hybrid films by repeated cyclic immersion for 10 minutes each

in the three media to obtain the desired number of layers. After each immersion step the coated substrate was washed and dried with nitrogen. These immersion steps included the following: (a) dipping of the substrate in the exfoliated CoAl-LDHs suspension; (b) dipping of the substrate in the aqueous PVA solution (1 wt. %); and (c) dipping in the ultrasonicated GO suspension. The thin films thus formed contained GO, which was further reduced to films of CoAl/G/PVA nanocomposites by immersing the coated substrate in hydrazine/N,N-dimethylformamide (0.5/30 vol. ratio) solution [20].

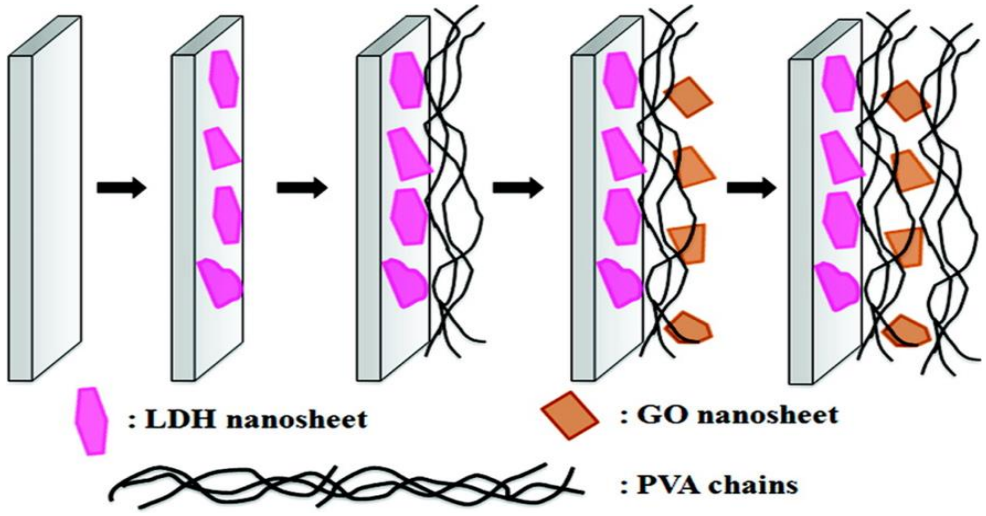

Figure 5-5. Schematic representation of the layer-by-layer assembly procedure [20] with permission from ACS

5.2.5 In-situ synthesis

The *in-situ* synthesis, also referred as surface synthesis, typically involves two steps. Initially, the boehmite (AlOOH) primer solution is obtained by hydrolyzing aluminum isopropoxide, followed by LBL assembly of the AlOOH gel on GO [12,62]. The precursor, denoted by GO/AlOOH, is known as the base or substrate. The AlOOH gel helps reduce surface roughness and enhances the adhesion properties. Typically, cobalt or nickel based asymmetric 3D nanocomposites are formed by this technique. The activated surface provides Al sites which are utilized as the source of the trivalent cations[62]. The GO/AlOOH solution is typically formed by adding 20 mL of the AlOOH solution to 6 mL of an ultrasonicated GO suspension followed by vigorous mixing for 12 h. Solid is separated by centrifugation, washed with ethanol several times to remove impurities and dried at room temperature. The dried GO/AlOOH sheets are then dispersed in DI water and ultrasonicated for 0.5-1 h. The suspension is then transferred to an autoclave along with the precursor salt solution of 0.5 molar $Ni(NO_3)_2$ and 0.3 g urea for hydrothermal reaction. Finally, the resultant product is centrifuged and washed with DI water and ethanol to remove any traces of impurities and subsequently oven dried for 48 h at 80 °C [12,21]. *In-situ* growth process has been used to fabricate a hierarchical 3D nanocomposite, in which arrays of LDHs are grown on both sides of the substrate [12]. The uniform size and morphology of the nanocomposites are attributed to the *in-situ* growth of the arrays of LDHs on the surface of graphene sheets during the hydrothermal process [12,41,62]. The schematic illustration of the LBL process is shown in Figure 5-6 and a summary of methods used is listed in Table 5-4.

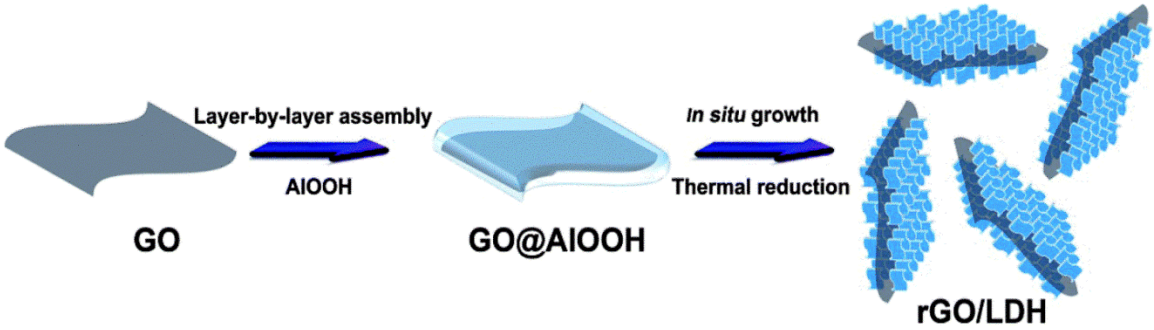

Figure 5-6. Schematic illustration of the formation of hybrid rGO/NiAl composites using the *in-situ* method [12] with permission from RSC

Table 5-4. G/LDHs nanocomposites synthesized by *in-situ* approach

Constituents		Autoclave parameters for one-step hydrothermal treatment (°C / h)	Nanocomposite	Applications	Ref
Component: A	Component: B (from LBL assembly)				
$Ni(NO_3)_2$	GO/AlOOH	120 / 24	rGO /NiAl LDHs	Uranium(VI) removal	[21]
$Ni(NO_3)_2$	GO/AlOOH	100 / 24	rGO /NiAl LDHs	Supercapacitor	[12]
[a] Co/Ni chlorides	[b] GP/AlOOH	120 / 24	[c] GP /NiCoAl LDHs	Supercapacitor	[62]
$CoCl_2.6H_2O$	rGO/AlOOH	80 / 24	rGO /CoAl LDHs	Supercapacitor	[63]

[a] 1:1 molar ratio of Co:Ni was used

[b] Graphite paper (GP) was used as substrate

[c] Flexible 3D architecture material made of NiCoAl LDHs coupled with NiCo carbonate hydroxide grown on GP

5.2.6 Others

Solvothermal technique is a modified form of the urea-hydrolyzed method in which DI water is replaced with other non-aqueous solvents. The precursor salts are first dissolved in a non-aqueous solvent followed by addition of an ultrasonicated GO suspension. The final step involves treatment in an autoclave reactor. The remaining steps and the operating parameters are similar to those of urea-hydrolyzed synthesis [13,64]. Microwave technology can be used as an alternate for the traditional hydrothermal synthesis using an autoclave for the rapid synthesis of G/LDHs nanocomposite shown schematically in Figure 5-7 [8]. Recent studies describe the use of potentiostatic deposition of LDHs on the rGO electrode to form G/LDHs nanocomposites with a unique 3D morphology [65]. Other methods used for the synthesis of G/LDHs nanocomposites are listed in Table 5-5.

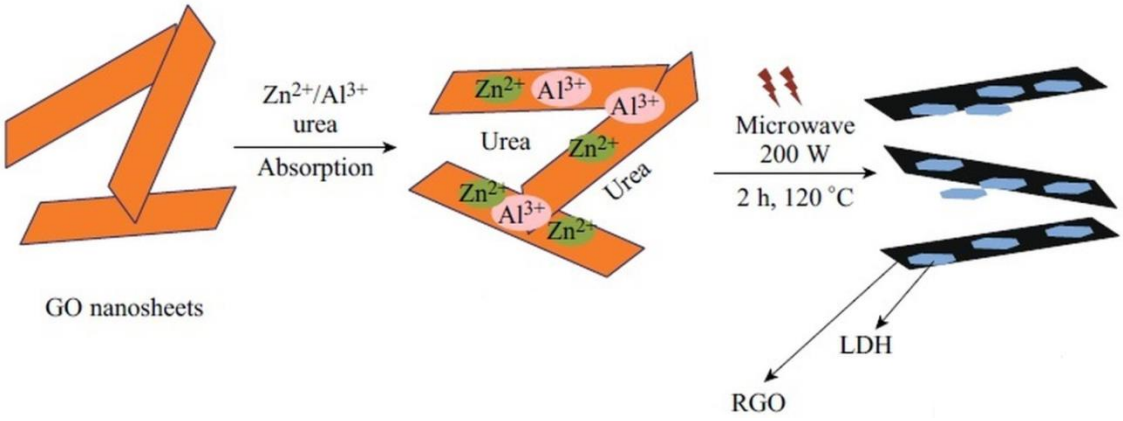

Figure 5-7. Schematic representation of the synthesis of G/LDHs nanocomposites using the microwave technique [8] with permission from Springer

Table 5-5. Synthesis of G/LDHs nanocomposites using different approaches

Synthesis technique	Nanocomposite	Precursor salts/solvent used	Molar ratio of precursor salts (M^{2+}: M^{3+})	Experimental conditions	Applications	Ref
Solvothermal	rGO/NiCo LHDs	Chlorides/Methanol	3:2	180 °C / 24 h	Supercapacitor	[13]
Solvothermal	rGO/NiAl LDHs	Nitrates/Ethanol	3:1	140 °C / 14 h	Supercapacitor	[64]
Microwave-assisted hydrothermal synthesis	G/ZnAl LDHs	Nitrates/DI water (urea assisted)	3:1	Microwave conditions 150 °C / 2 h (200 W)	-	[8]
	G/CoAl LDHs	Nitrates/DI water (urea assisted)	2:1	100 °C / 2 h (1000 W)	Supercapacitor	[66]
[a] rGO electrode deposition method	rGO/NiFe LDHs	Nitrates/DI water	4:1	[b] Potentiostat-galvanostat conditions -1.2V / 10s	Water oxidation	[65]

[a] Electrolyte used is 0.1 M $LiClO_4$

[b] Working electrode - Au (5mm diameter); Counter electrode - Pt foil

5.3 Results and Discussion

Currently, G/LDHs nanocomposites are of increased scientific interest. These materials are being tested for their applications in catalysis, oxygen evolution reaction (OER), supercapacitors, flame retardant materials, nanofillers, photo-catalysts, and sorbents. This section highlights the performance of various G/LDHs nanocomposites used in different applications.

5.3.1 Oxygen evolution reaction

The oxygen evolution reaction plays an important role in sustainable energy systems such as fuel cells, solar cells and metal-air batteries [67]. Molecular oxygen is generated in the OER, which is highly influenced by the sluggish kinetics due to the high overpotential [34]. Thus, cost-effective and efficient electrocatalysts are critically important as they reduce the large overpotential and accelerate the reaction. Although metal oxides such as IrO2 and RuO2 are very active and durable electrocatalysts for OER, however, the high cost and scarcity considerably limit their applications [68,69]. Transition metal oxides are a viable alternative due to their abundance and high stability [70–73]. A range of carbon materials such as CNTs, graphene, carbon quantum dots and nitrogen doped graphite have been recently identified as good OER catalysts with a multifunctional framework [74–76]. Due to the electrostatic interactions between two oppositely charged nanosheets LDHs can act as effective electrocatalysts. Introducing graphene into monolayers of LDHs enhances their OER performance in three ways. First, graphene provides a large surface area, thereby increasing the available number of active sites. Secondly, graphene provides electrically conductive pathways for the LDHs and control the aggregation of LDHs crystals. Thirdly, the electrostatic interactions between the positively charged

LDHs and negative charged GO at molecular scale provides direct contact between the transition metal and carbon, thus shortening the diffusion distance [56,67,77].

The onset overpotential (η¬onset), the overpotential required to reach a current density of 10 mA cm^{-2} (η10) and the Tafel slope are important parameters which determine whether OER can be used in a water splitting device [67]. The OER data for different G/LDHs nanocomposites are given in Table 5-6. Among them, NiFe LDHs are the most promising catalysts for future OER systems [78]. The hybrid formed by the combination of NiFe LDHs with GO was recently reported as a potential electrocatalyst for OER. The synergy between the catalytic activity of NiFe LDHs and the electrical conductivity of graphene makes these nanocomposites excellent electrocatalysts for OER [58,79]. A G/NiFe LDHs nanocomposite possessing an overpotential of 0.195V and a turnover frequency at overpotential of 0.98 s-1 was synthesized by Long et al. to overcome the limitations of specific surface area and conductivity [80]. Wang et al. reported that nanocomposite of G/NiFe LDHs possess a remarkably low overpotential of 324 mV at 10 mA cm^{-2} [67]. Youn et al. synthesized GO/NiFe LDHs nanocomposites using the solvothermal method. GO/NiFe LDHs nanocomposites showed superior properties compared to NiFe and IrO_2. The GO/NiFe LDHs nanocomposites possesses a lower value of η10 (245 v) which is much lower than that of bare NiFe [77]. Ma et al. studied the effect of the Ni and Fe content on the properties of GO/NiFe LDHs nanocomposites and showed that the performance improved with increasing Fe content. An overpotential as low as 210 mV was achieved for GO/NiFe LDHs nanocomposites [58]. Xia et al. used a hree-step process to form GO/NiFe LDHs nanocomposites. The resulting nanocomposite exhibited excellent OER activity [81]. Zhu et al. introduced a mildly oxidized graphene/ CNT

hybrid to improve the properties of NiFe LDHs [82]. The resulting material contains a porous structure with a more hydrophilic surface, which enhances the smooth permeation of electrolytes. The nanocomposite also exhibited superior OER performance with an η¬onset of 240 mV. Most of the scientific work in OER applications is limited to G/NiFe LDHs nanocomposites. Other G/LDHs nanocomposites have to be investigated for their potential use in OER applications.

Table 5-6. OER data for different LDHs nanocomposites

Nanocomposites	η_{onset}[a] (mV)	η_{10}[b] (mV)	Tafel slope (mV decade^{-1})	Ref
G/Ni	300	399	52	[67]
NiFe LDHs	250	350	51	[67]
G/NiFe LDHs	240	325	44	[67]
GO/NiFe LDHs (6:1)	240	280	-	[77]
GO/NiFe LDHs (5:1)	230	245	-	[77]
GO/NiFe LDHs (4:1)	232	253	-	[77]
GO/NiFe LDHs	-	210	40	[58]
GO/CNT/NiFe LDHs	240	350	54	[82]
GO/NiFe LDHs	-	250	33	[81]

[a]Onset overpotential
[b]Overpotential required to reach a current density of 10 mA cm^{-2}

5.3.2 Supercapacitors

Supercapacitors are high-capacity energy devices that have attracted attention due to their high power density, energy density, low maintenance cost, and long life cycle [83–85]. Super capacitors are divided into two main categories of redox electrochemical capacitors and electric double layer capacitors. Due to the presence of both double-layered capacitance and Faradaic pseudo-capacitance simultaneously, LDHs are thus attractive materials that can be used as supercapacitors. However, the performance is affected by their low electrical conductivity. A specific capacitance of 552 F g^{-1} at a current density of 1 A g^{-1} with a lower specific capacitance retention rate of 31.9 % at 8 A g^{-1} have been recorded for pure CoAl LDHs [59]. Owing to the ease of chemical modification, graphene can be coupled with a various LDHs and the resulting nanocomposites have great potential for supercapacitor applications [1,3]. Graphene can be used to overcome the poor high-rate charge and discharge capability resulting from the low electrical conductivity. The addition of graphene into LDHs provides a large surface area, high electrical conductivity, mechanical flexibility, and thermal/chemical stability [11,12]. Thus, due to the synergetic effects the hybrid material containing LDHs and graphene has better capacitance with a notable improvement in the capacitance retention rate at higher current densities than the parent materials [11,13,39,59,85–89]. Other than graphene activated carbon, porous carbon, CNTs, carbon onions, and nanohorns are also used in electric double layer capacitors [3,9,90,91]. The energy storage capability of supercapacitors is still low compared to ion batteries, and efforts are underway to improve the energy density [54].

Huang et al. evaluated the electrochemical properties of GO/CoAl LDHs nanocomposites and obtained a specific capacitance of 1296 F g^{-1} at a current density of 1 A g^{-1}. In addition, 90.5% of the initial capacitance was retained at a high current density (15 A g^{-1}) after 1000 cycles [11]. Wang et al. synthesized hybrid GO/CoAl LDHs nanocomposites with a specific capacitance of 1031 F g^{-1} at 1 A g^{-1} [54], indicating that the GO/CoAl LDHs nanocomposites are well suited to be used as supercapacitor electrodes. Xu et al. synthesized and used 3D G/NiAl LDHs nanocomposites as a supercapacitor electrode with a specific capacitance of 1329 F g-1 at a current density of 3.57 A g^{-1}. After 500 cycles at 15.30 A g^{-1}, the specific capacitance was remained at 91% of the initial value. However, a similar treatment of pure NiAl LDHs resulted in a retained specific capacitance of 74 % [12]. Yang et al. developed ternary nanocomposites containing GO/CNT/NiAl LDHs which possess a 3D structure with enhanced supercapacitor capabilities [64]. The specific capacitance and the current density of some G/LDHs are listed and compared with the parent LDHs in Table 5-7.

Table 5-7. Summary of specific capacitances and cyclic performance of G/ LDHs nanocomposites

Nanocomposite	Amount of GO used	Specific capacitance ($F\ g^{-1}$)	Current density ($A\ g^{-1}$)	No. of cycles	Current density ($A\ g^{-1}$)	Specific capacitance retained %	Ref
G/NiAl LDHs	100 mg	915	2	1500	10	95	[9]
		154	10				
rGO/NiAl LDHs	6 mg	1329	3.57	500	15.30	91	[12]
		851	17				
	0	379	15	500	15.30	74	
[a] rGO/NiAl LDHs	200 mg	2712	1	5000	30	98.9	[92]
		1820	10				
	0	366	1	-	-	-	
		116	10				
G/CNT/NiAl LDHs	10 wt.%	1869	[f] 1	1000	[f]10	96.5	[64]
		1562	[f] 5				
G/NiAl LDHs	50 mg	1081	[f] 5	-	-	-	
NiAl LDHs	0	484	[f] 5				
[b] rGO/NiCo LDHs	30 mg	1911	2	1000	20	74	[13]
		1469	20				
	0	898	2	1000	20	51	
		500	20				
rGO/NiCo LDHs	[c] 1:5	811	0.5	5000	[h]70	77	[43]
		730	2				
[d] rGO/NiCo LDHs	80 mg	2130	2	10,000	10	80	[86]
		1000	10				

	0	678	2	-	-	-	
		148	10				
rGO/CNT/NiCoAl LDHs	10.8 wt.%	1188	1	1000	6	100	
		850	10				
rGO/NiCoAl LDHs	10 wt. %	936	1	1000	6	88	[93]
		437	10				
NiCoAl LDHs	0	950	1	-	-	-	
		232	10				
GP/NiCoAl LDHs	[i] CH-NWs	1297	1	10,000	10	97	[62]
		764	30				
	[j] LDHs	1129	1	-	-	-	
		666	15				
rGO/NiMn LDHs	10 mg	[g] 217	[f] 2	10,000	[f] 4	95	[94]
		[g] 163	[f] 16				
G/CoAl LDHs	9.3 wt.%	711	1	2000	10	81	[39]
		517	10				
	0	641	1	2000	10	64	
		421	10				
rGO/CoAl LDHs	7 mg	1296	1	1000	15	90.5	[11]
		554	10				
	0	682	1	-	-	-	
		313	10				
GO/CoAl LDHs	12.9 wt.%	772	1	10,000	6	73	[89]
		617	20				
	0	704	1	10,000	6	54	

		373	20				
GO/CoAl LDHs	5 mg	1031	1	6000	20	100	[54]
		250	20				
rGO/CoAl LDHs	12 wt. %	825	1	4000	4	89.3	[59]
		514	8				
	0	552	1	4000	4	60.4	
		176	8				
rGO / CoAl LDHs	3 mg	628	2	5000	4	92.4	[95]
		599	4				
	0	340	2	-	-	-	
G/CoAl LDHs	2 mg	1043	1	3000	[h]100	88	[96]
		912	20				
	0	756	1	3000	[h]100	76	
		332	20				
rGO/CoAl LDHs	13.7 wt.%	640	1	10,000	20	97	[88]
		530	10				
		305	20				
	0	320	1	-	-	-	
		80	10				

[a] Activated reduced graphene oxide having Ni and Al molar ratio 2.25:1

[b] 3:2 molar ratio of (Ni:Co) precursor salts having $Ni(NO_3)_2.6H_2O$ concentration 0.84 mmole

[c] GO to metal precursor ratio (synthesis time 12h)

[d] 1:2 molar ratio of (Ni:Co) precursor salts were used at 150 °C for 12 h using hydrothermal treatment

[f] Units are reported in mA/cm^2

[g] Units are reported in mF/cm^2

[h] Scan rate reported in $mV.\ s^{-1}$

[i] LDHs coupled with NiCo-carbonate hydroxide nanowires (CH-NWs) grown on graphite paper (GP)

[j] NiCoAl LDHs grown on GP

5.3.3 Catalysts and sorbents

The high interlayer spacing, high surface area, positive charge on the surface, high anion exchange capacity, and the high number of active sites allow LDHs to be used as anion exchangers, catalysts, and adsorbents [4–6,26,27]. The adsorption capacity of LDHs can be enhanced by decreasing the particle size, by techniques such as delamination [97]. As they can easily pile up and restack [6,9] due to the strong surface charge density between the LDHs monolayers, it is difficult to keep the LDHs in an orderly and uniform manner. The restacking can be minimized by introducing negatively charged GO into the layers of LDHs which provide the required support and stability to the LDHs sheets [9,57]. The nanocomposites of GO or rGO supported LDHs can thus be used for the adsorption of CO2 [57], removal of heavy metals from water [22], and photo-catalysis [55]. Forming graphene nanocomposites with pure LDHs exponentially increases its adsorption capabilities. Garcia-Gallastegui et al. showed that the adsorption capacity of MgAl LDHs increased by 62 % with the addition of only 7 wt. % of GO [10]. Wang and co-workers showed that the CO2 adsorption significantly improved with the incorporation of 6.54 wt. % of GO in a MgAl LDHs as compared to the pure material [57]. G/LDHs nanocomposites have been used for the removal of heavy metals such as uranium (U(VI)) [21], chromium (Cr(VI)) [22], arsenic (As(V)) [48], Cd2+ [98], lead (Pb(II)) and 2, 4 dichlorophenoxyacetic acid [49] from water. Tan et al. studied the removal of uranium (VI) from water using the rGO/NiAl LDHs nanocomposites [21]. As this nanocomposite has a large surface area and mesoporous characteristics, it shows enhanced adsorption of contaminants from aqueous media. The nanohybrid adsorbent can also be regenerated [21]. In another similar study hexa-valent chromium was successfully removed from

wastewater using the G/MgAl LDHs. The adsorption capacity of the G/LDHs nanocomposites can be further enhanced by calcination at high temperature which eliminates the "memory effects" of parent LDHs [5,22]. Fang and Chen used the GO/LDHs nano-aerogel for the removal of methylene blue and Cd2+ from water. The aerogel exhibited high structural stability and a high number of active sites to capture Cd2+ ions. The hydrophilic surface of the aerogel helps retain the active sites in polar solvents [98]. Wen et al. used hybrids of MgAl LDHs with graphene synthesized by the hydrothermal route for the efficient removal of toxic As(V) from polluted water. The high Brunauer−Emmett−Teller (BET) surface area of these hybrids containing only 6.0 % of GO leads to an adsorptive capacity of 2.44 mmol/g [49]. In another study methyl orange was successfully adsorbed by rGO/NiCr from an aqueous solution containing organic matter, demonstrating its promise as an adsorbent for the removal of anionic dyes from wastewaters [99]. A few published studies on the application of G/LDHs nanocomposites for photocatalysis are also available. rGO/NiTi LDHs can be used for photocatalytic oxidation of water under visible light [55]. Lan et al. reported the degradation of rhodamine-B under visible light using the G/ZnCr LDHs with a remarkable photocatalytic activity (88% photodegradation of rhodamine after five regeneration cycles) [37]. The studies conducted by Miao et al. showed the superior catalytic activity and stability of rGO/NiAl LDHs as a support for Au nanoparticles in the selective oxidation of benzyl alcohol. The improved catalytic activity was attributed to the size of the Au nanoparticles and the number of basic sites on NiAl LDHs, while the defect sites and oxygen containing functional groups attached to rGO led to the catalytic stability [100]. Song et al. used G/CoAl LDHs for the hydrogenation of p-nitrophenol in

presence of excess sodium hydroxide and found excellent catalytic activity and stability [16]. These nanocomposites also reduces the emission of toxic CO and volatile organic compounds from the decomposition of the epoxy resin [101].

5.3.4 Nanofiller

These materials are promising nanofillers for polymers mainly to enhance the flame retardant characteristics. Good flame retardant properties of G/LDHs nanocomposites are attributed due to the complementary flame retardant properties of graphene and LDHs. Graphene is known to impart good flame retardant properties to polymers such as high density polyethylene, poly(methyl methacrylate) (PMMA), and polystyrene [2,28,102]. The flame retardant properties are due to the physical barrier formed by the layered structure of graphene which slows down the release of flammable gases, thus preventing the polymer matrix from burning [33,103]. On the other hand, LDHs are also used as flame retardants in polymer nanocomposites [104,105]. The LDHs helps to lower the temperature of the substrate by releasing H2O and CO_2 produced during the burning process. The porous structure of the thermally decomposed products of LDHs can suppress smoke due to the large specific surface area [103]. However, the following major shortcomings restrict the use of bare graphene as a flame retardant: (1) homogeneous dispersion of graphene in the polymer matrix: and (2) relatively lower efficiency as a fire retardant, when bare graphene is used [106]. These shortcomings can be overcome by taking advantage of the synergic properties of LDHs and graphene [19]. Thermal stability of PMMA is reported to be improved by addition of rGO/NiAl LDHs. The heat release rate, smoke and carbon monoxide production rate of the resulting nanocomposites are relatively lower as compared to those of LDHs or rGO polymer

nanocomposites [33]. Wang et al. synthesized G/NiFe LDHs epoxy nanocomposites to reduce the fire hazards associated with the epoxy [18]. Incorporating 2% G/LDHs nanocomposites enhanced the degradation onset temperature of epoxy by 25 °C. Combustion and cone calorimetric data demonstrate a significant decrease in the peak heat release rate (PHRR) and the total heat release (THR) values of epoxy. The decrease in these parameters as compared to those of pure epoxy is an indication of the improvement in the flame retardant properties. Graphene retards the thermal degradation of the epoxy matrix via the adsorption and barrier effects, while LDHs increase the thermal oxidative resistance [18]. Recently, Huang et al. reported that the flame retardant properties of intumescent flame-retardant (IFR) PMMA nanocomposites improve significantly when G/LDHs nanomaterials are incorporated [103]. The authors have also reported 45% decrease in the PHRR for the PMMA/IFR/rGO/LDH nanocomposites, when filled with 10 wt. % IFRs, 1 wt. % graphene, and 5 wt. % LDHs [103].

Apart from imparting flame retardant properties, these nanomaterials can also be used as reinforced fillers in polymer nanocomposites. The LDHs hybrids with multi walled carbon nanotubes (MWCNTs) are also used as reinforced fillers in polymer nanocomposites [32,107]. Furthermore, these nanomaterials have been used as nanofillers in the development of silicon rubber nanocomposites with improved mechanical properties. The maximum increase in the tensile strength was achieved using 1 wt. % MgAl/MWCNTs LDHs, which resulted in a 134% increase in the tensile strength of the silicon rubber and better swelling behavior [108]. Chen et al. prepared poly(vinyl alcohol) hybrid films by orienting graphene and CoAl LDHs, which resulted in polymer

nanofilms with improved electrical conductivity [20]. However, an improved dispersion of the G/LDHs in polymers must be achieved.

5.3.5 Miscellaneous

Due to the conducting properties and capacitance of the G/LDHs nanocomposites, they have been used in sensing applications and medical diagnostics. G/NiAl LDHs along with hollow gold nanospheres have been used in the fabrication of an electrochemical immunosensor [38]. G/NiAl LDHs was also used in the detection of dopamine [24]. Non-enzymatic sensors are based on the direct electrocatalytic oxidation and typically use noble metal, metal oxide, metal hydroxide, and metal complexes along with the appropriate matrix [109]. Therefore, these G/LDHs nanocomposites can be used in biological sensing applications. For example, Fu et al. studied non-enzymatic glucose sensors based on ternary G/CNT/NiAl LDHs coated Gold (Au) nanoparticles [25]. The authors reported superior catalytic performance for oxidation of glucose with highly sensitive sensing of glucose even at lower concentration of glucose. These sensors also exhibited reproducibility, repeatability, stability and anti-interference characteristics. These characteristics were ascribed to the better conductivity and abundant active sites. In another study, G/ZnAl LDHs nanocomposites were used as a luminescent sensor for the detection of deoxyribonucleic acid (DNA) [23]. The nanocomposite can efficiently quench the emission of Ru(phen)3Cl2. A seventeen times enhancement of the luminescence was observed after the addition of DNA, which indicates that the luminescence enhancement and DNA count are directly proportional. The nanocomposite also helped in the luminescence recovery of the sensor. A hybrid 2D electrical-mechanical interface of G/MgAl LDHs has demonstrated a much stronger electro-

rheological results in a device with a quick response and low power consumption [46]. An electro-rheological suspensions exhibit electrically tunable rheology, mainly consisting of polarizable particles in electrically insulating oil, they are of great importance in applications such as electrical-mechanical interfaces for better controlling the device. These hybrid nanocomposites have also found applications in nickel plating. The G/NiAl LDHs nanocomposites have been successfully employed to recover nickel, phosphorous, and sulfur from a spent electrode-less nickel plating bath [110].

5.4 CONCLUSIONS AND PERSPECTIVES

Graphene hybridized layered double hydroxides (G/LDHs) are a valuable addition to the field of nanomaterials. They can be used as supercapacitors, sorbents, and heterogeneous catalysts because of their unique inherent properties. Their synthesis techniques, however, are delicate and sensitive, making it difficult to get a uniform size distribution in batch processes. The high surface area and the excellent thermal and catalytic stability make the G/LDHs nanocomposites a promising choice for catalysis. Superior capacitance properties of G/LDHs make them favorable materials for applications in supercapacitors. Furthermore, their pH responsive solubility, ability to form co-precipitates, and higher active sites make them capable for applications in highly selective extraction applications. The synergetic properties of hybrid material also contribute to enhance mechanical and fire retardant properties of polymer nanocomposites.

The synthesis and application of G/LDHs nanocomposites are new and emerging areas, worth further investigation for various applications that are not yet investigated in detail. For example, owing to their mesoporous structure and the potential of graphene to increase the molecular weight of polymers, these materials can be used as supports for

single site heterogeneous catalysts used in polymerization. Therefore, the use of G/LDH is expected to produce interesting results. The anisotropic properties and good dispersion ability make them suitable to be used as particulates in the dispersion phase of electro-responsive and electro-rheological fluids. The potential use of these materials in thin conducting films for applications in solar cells should also be investigated. Although these materials have been tested for the removal of contaminants from single component solutions in water, it is necessary to evaluate their performance in the removal of contaminants from multi-components solutions. Research on the use of these materials in sensing and drug delivery applications are rare. There are opportunities to investigate their potential in these areas in detail, taking into consideration their side effects and the toxicity of nanomaterials. Moreover, the potential use of these materials in the areas of biomedicine, nanoreactors, ion exchangers, and corrosion resistant coatings should also be studied. Establishing the structure property relationship of these materials is essential to understand the effects of various factors such as functionalization or doping of graphene. Finally, the challenges in obtaining material with precisely controlled particle sizes and morphology must be addressed.

5.5 REFERENCES

[1] W.L. Zhang, H.J. Choi, Graphene/graphene oxide: A new material for electrorheological and magnetorheological applications, J. Intell. Mater. Syst. Struct. 26 (2015) 1826–1835.

[2] F. Shehzad, M. Daud, M.A. Al-Harthi, Synthesis, characterization and crystallization kinetics of nanocomposites prepared by in situ polymerization of ethylene and graphene, J. Therm. Anal. Calorim. 123 (2016) 1501–1511.

[3] J.J. Yoo, K. Balakrishnan, J. Huang, V. Meunier, B.G. Sumpter, A. Srivastava, et al., Ultrathin planar graphene supercapacitors, Nano Lett. 11 (2011) 1423–1427.

[4] K.H. Goh, T.T. Lim, Z. Dong, Application of layered double hydroxides for removal of oxyanions: a review., Water Res. 42 (2008) 1343–68.

[5] M. Sajid, C. Basheer, Layered double hydroxides: Emerging sorbent materials for analytical extractions, TrAC - Trends Anal. Chem. 75 (2016) 174–182.

[6] S. Tang, H.K. Lee, Application of dissolvable layered double hydroxides as sorbent in dispersive solid-phase extraction and extraction by co-precipitation for the determination of aromatic acid anions, Anal. Chem. 85 (2013) 7426–7433.

[7] X. Zhao, J.P. Cao, J. Zhao, G.H. Hu, Z.M. Dang, A hybrid Mg–Al layered double hydroxide/graphene nanostructure obtained via hydrothermal synthesis, Chem. Phys. Lett. 605-606 (2014) 77–80.

[8] S.P. Lonkar, J.M. Raquez, P. Dubois, One-Pot Microwave-Assisted Synthesis of Graphene/Layered Double Hydroxide (LDH) Nanohybrids, Nano-Micro Lett. 7 (2015) 332–340.

[9] Y. Wimalasiri, R. Fan, X.S. Zhao, L. Zou, Assembly of Ni-Al layered double hydroxide and graphene electrodes for supercapacitors, Electrochim. Acta. 134 (2014) 127–135.

[10] A. Garcia-Gallastegui, D. Iruretagoyena, V. Gouvea, M. Mokhtar, A.M. Asiri, S.N. Basahel, et al., Graphene Oxide as Support for Layered Double Hydroxides: Enhancing the CO2 Adsorption Capacity, Chem. Mater. 24 (2012) 4531–4539.

[11] Z. Huang, S. Wang, J. Wang, Y. Yu, J. Wen, R. Li, Exfoliation-restacking synthesis of coal-layered double hydroxide nanosheets/reduced graphene oxide composite for high performance supercapacitors, Electrochim. Acta. 152 (2015) 117–125.

[12] J. Xu, S. Gai, F. He, N. Niu, P. Gao, Y. Chen, et al., A sandwich-type three-dimensional layered double hydroxide nanosheet array/graphene composite: fabrication and high supercapacitor performance, J. Mater. Chem. A. 2 (2014) 1022–1031.

[13] X. Cai, X. Shen, L. Ma, Z. Ji, C. Xu, A. Yuan, Solvothermal synthesis of NiCo-layered double hydroxide nanosheets decorated on RGO sheets for high performance supercapacitor, Chem. Eng. J. 268 (2015) 251–259.

[14] G. Abellán, E. Coronado, C. Martí-Gastaldo, A. Ribera, T.F. Otero, Magnetic Nanocomposites Formed by FeNi3 Nanoparticles Embedded in Graphene. Application as Supercapacitors, Part. Part. Syst. Charact. 30 (2013) 853-863.

[15] G. Abellán, C. Martí-Gastaldo, A. Ribera, E. Coronado, Hybrid Materials Based on Magnetic Layered Double Hydroxides: A Molecular Perspective, Acc. Chem. Res. 48 (2015) 1601–1611.

[16] J.M. Song, J.J. Ni, J. Zhang, D. Ling, H.L. Niu, C.J. Mao, et al., A facile synthesis of graphene-like cobalt–nickel double hydroxide nanocomposites at room temperature and their excellent catalytic and adsorption properties, J. Nanoparticle Res. 16 (2014) 1–15.

[17] G. Abellán, J.G. Martínez, T.F. Otero, A. Ribera, E. Coronado, A chemical and electrochemical multivalent memory made from FeNi3-graphene nanocomposites, Electrochem. Commun. 39 (2014) 15–18.

[18] X. Wang, S. Zhou, W. Xing, B. Yu, X. Feng, L. Song, et al., Self-assembly of Ni–Fe layered double hydroxide/graphene hybrids for reducing fire hazard in epoxy composites, J. Mater. Chem. A. 1 (2013) 4383.

[19] B. Yuan, C. Bao, X. Qian, S. Jiang, P. Wen, W. Xing, et al., Synergetic Dispersion Effect of Graphene Nanohybrid on the Thermal Stability and Mechanical Properties of Ethylene Vinyl Acetate Copolymer Nanocomposite, Ind. Eng. Chem. Res. 53 (2014) 1143–1149.

[20] D. Chen, X. Wang, T. Liu, X. Wang, J. Li, Electrically Conductive Poly(vinyl alcohol) Hybrid Films Containing Graphene and Layered Double Hydroxide Fabricated via Layer-by-Layer Self-Assembly, ACS Appl. Mater. Interfaces. 2 (2010) 2005–2011.

[21] L. Tan, Y. Wang, Q. Liu, J. Wang, X. Jing, L. Liu, et al., Enhanced adsorption of uranium (VI) using a three-dimensional layered double hydroxide/graphene hybrid material, Chem. Eng. J. 259 (2015) 752–760.

[22] X. Yuan, Y. Wang, J. Wang, C. Zhou, Q. Tang, X. Rao, Calcined graphene/MgAl-layered double hydroxides for enhanced Cr(VI) removal, Chem. Eng. J. 221 (2013) 204–213.

[23] H. Li, J. Wen, R. Yu, J. Meng, C. Wang, C. Wang, et al., Facile synthesis of a nanocomposite based on graphene and ZnAl layered double hydroxides as a portable shelf of a luminescent sensor for DNA detection, Rsc Adv. 5 (2015) 9341–9347.

[24] M. Li, J.E. Zhu, L. Zhang, X. Chen, H. Zhang, F. Zhang, et al., Facile synthesis of NiAl-layered double hydroxide/graphene hybrid with enhanced electrochemical properties for detection of dopamine, Nanoscale. 3 (2011) 4240.

[25] S. Fu, G. Fan, L. Yang, F. Li, Non-enzymatic glucose sensor based on Au nanoparticles decorated ternary Ni-Al layered double hydroxide/single-walled carbon nanotubes/graphene nanocomposite, Electrochim. Acta. 152 (2015) 146–154.

[26] X. Guo, F. Zhang, D.G. Evans, X. Duan, Layered double hydroxide films: synthesis, properties and applications., Chem. Commun. (Camb). 46 (2010) 5197–210.

[27] Q. Wang, D. O'Hare, Recent advances in the synthesis and application of layered double hydroxide (LDH) nanosheets., Chem. Rev. 112 (2012) 4124–55.

[28] P. Avouris, C. Dimitrakopoulos, Graphene: synthesis and applications, Mater. Today. 15 (2012) 86–97.

[29] M. Shao, R. Zhang, Z. Li, M. Wei, D.G. Evans, X. Duan, Layered double hydroxides toward electrochemical energy storage and conversion: design, synthesis and applications., Chem. Commun. (Camb). 51 (2015) 15880–93.

[30] M.Q. Zhao, Q. Zhang, J.Q. Huang, F. Wei, Hierarchical Nanocomposites Derived from Nanocarbons and Layered Double Hydroxides - Properties, Synthesis, and Applications, Adv. Funct. Mater. 22 (2012) 675–694.

[31] E.L. Crepaldi, P.C. Pavan, J.B. Valim, Comparative Study of the Coprecipitation Methods for the Preparation of Layered Double Hydroxides, J. Braz. Chem. Soc. 11 (2000) 64–70.

[32] S. Mallakpour, M. Dinari, Hybrids of Mg-Al-layered double hydroxide and multiwalled carbon nanotube as a reinforcing filler in the l-phenylalanine-based polymer nanocomposites, J. Therm. Anal. Calorim. 119 (2015) 1905–1912.

[33] N. Hong, L. Song, B. Wang, A.A. Stec, T.R. Hull, J. Zhan, et al., Co-precipitation synthesis of reduced graphene oxide/NiAl-layered double hydroxide hybrid and its application in flame retarding poly(methyl methacrylate), Mater. Res. Bull. 49 (2014) 657–664.

[34] D. Tang, Y. Han, W. Ji, S. Qiao, X. Zhou, R. Liu, et al., A high-performance reduced graphene oxide/ZnCo layered double hydroxide electrocatalyst for efficient water oxidation., Dalton Trans. 43 (2014) 15119–25.

[35] S.P. Newman, W. Jones, Synthesis, characterization and applications of layered double hydroxides containing organic guests, New J. Chem. 22 (1998) 105–115.

[36] D.G. Evans, X. Duan, Preparation of layered double hydroxides and their applications as additives in polymers, as precursors to magnetic materials and in biology and medicine., Chem. Commun. (Camb). (2006) 485–96.

[37] M. Lan, G. Fan, L. Yang, F. Li, Significantly Enhanced Visible-Light-Induced Photocatalytic Performance of Hybrid Zn−Cr Layered Double Hydroxide / Graphene Nanocomposite and the Mechanism Study, Ind. Eng. Chem. Res. 53 (2014) 12943–12952.

[38] L. Qiao, Y. Guo, X. Sun, Y. Jiao, X. Wang, Electrochemical immunosensor with NiAl-layered double hydroxide/graphene nanocomposites and hollow gold nanospheres double-assisted signal amplification, Bioprocess Biosyst. Eng. (2015) 1–14.

[39] L. Zhang, X. Zhang, L. Shen, B. Gao, L. Hao, X. Lu, et al., Enhanced high-current capacitive behavior of graphene/CoAl-layered double hydroxide composites as electrode material for supercapacitors, J. Power Sources. 199 (2012) 395–401.

[40] U. Costantino, F. Marmottini, M. Nocchetti, R. Vivani, New Synthetic Routes to Hydrotalcite-Like Compounds − Characterisation and Properties of the Obtained Materials, Eur. J. Inorg. Chem. 1998 (1998) 1439–1446.

[41] J. He, M. Wei, B. Li, Y. Kang, D.G. Evans, X. Duan, Preparation of Layered Double Hydroxides, in: Layer. Double Hydroxides, Springer-Verlag, Berlin/Heidelberg, 2006: pp. 89–119.

[42] T. Hibino, H. Ohya, Synthesis of crystalline layered double hydroxides: Precipitation by using urea hydrolysis and subsequent hydrothermal reactions in aqueous solutions, Appl. Clay Sci. 45 (2009) 123–132.

[43] S.N. Tiruneh, B.K. Kang, Q.T. Ngoc, D.H. Yoon, Enhanced electrochemical performance of lamellar structured Co–Ni(OH) 2 /reduced graphene oxide (rGO) via hydrothermal synthesis, RSC Adv. 6 (2016) 4764–4769.

[44] H. Liang, F. Meng, M. Cabán-Acevedo, L. Li, A. Forticaux, L. Xiu, et al., Hydrothermal continuous flow synthesis and exfoliation of NiCo layered double hydroxide nanosheets for enhanced oxygen evolution catalysis, Nano Lett. 15 (2015) 1421–1427.

[45] H. Li, G. Zhu, Z.H. Liu, Z. Yang, Z. Wang, Fabrication of a hybrid graphene/layered double hydroxide material, Carbon N. Y. 48 (2010) 4391–4396.

[46] Y. Dong, Y. Liu, J. Yin, X. Zhao, Preparation and enhanced electro-responsive characteristic of graphene/layered double-hydroxide composite dielectric nanoplates, J. Mater. Chem. C. 2 (2014) 10386–10394.

[47] Z. Gao, J. Wang, Z. Li, W. Yang, B. Wang, M. Hou, et al., Graphene nanosheet/Ni2+/Al3+ layered double-hydroxide composite as a novel electrode for a supercapacitor, Chem. Mater. 23 (2011) 3509–3516.

[48] T. Wen, X. Wu, X. Tan, X. Wang, A. Xu, One-pot synthesis of water-swellable Mg-Al layered double hydroxides and graphene oxide nanocomposites for efficient removal of As(V) from aqueous solutions., ACS Appl. Mater. Interfaces. 5 (2013) 3304–11.

[49] F. Zhang, Y. Song, S. Song, R. Zhang, W. Hou, Synthesis of magnetite-graphene oxide-layered double hydroxide composites and applications for the removal of Pb(II) and 2,4-dichlorophenoxyacetic acid from aqueous solutions., ACS Appl. Mater. Interfaces. 7 (2015) 7251–63.

[50] H. Ma, J. He, D.-B. Xiong, J. Wu, Q. Li, V. Dravid, et al., Nickel Cobalt Hydroxides @Reduced Graphene Oxide Hybrid Nanolayers for High Performance Asymmetric Supercapacitors with Remarkable Cycling Stability, ACS Appl. Mater. Interfaces. 8 (2016) 1992-2000.

[51] Y. Wang, Z. Wang, X. Wu, X. Liu, M. Li, Synergistic effect between strongly coupled CoAl layered double hydroxides and graphene for the electrocatalytic reduction of oxygen, Electrochim. Acta. (2016). doi:10.1016/j.electacta.2016.01.201.

[52] A. Zhang, C. Wang, Q. Xu, H. Liu, Y. Wang, Y. Xia, A hybrid aerogel of Co–Al layered double hydroxide/graphene with three-dimensional porous structure as a novel electrode material for supercapacitors, RSC Adv. 5 (2015) 26017–26026.

[53] J.L. Gunjakar, I.Y. Kim, J.M. Lee, Y.K. Jo, S.J. Hwang, Exploration of Nanostructured Functional Materials Based on Hybridization of Inorganic 2D Nanosheets, J. Phys. Chem. C. 118 (2014) 3847–3863.

[54] L. Wang, D. Wang, X.Y. Dong, Z.J. Zhang, X.F. Pei, X.J. Chen, et al., Layered assembly of graphene oxide and Co–Al layered double hydroxide nanosheets as electrode materials for supercapacitors, Chem. Commun. 47 (2011) 3556–3558.

[55] B. Li, Y. Zhao, S. Zhang, W. Gao, M. Wei, Visible-Light-Responsive Photocatalysts toward Water Oxidation Based on NiTi-Layered Double Hydroxide / Reduced Graphene Oxide Composite Materials, ACS Appl. Mater. Interfaces. 5 (2013) 10233–10239.

[56] W. Ma, R. Ma, C. Wang, J. Liang, X. Liu, K. Zhou, et al., A superlattice of alternately stacked Ni-Fe hydroxide nanosheets and graphene for efficient splitting of water., ACS Nano. 9 (2015) 1977–84.

[57] J. Wang, X. Mei, L. Huang, Q. Zheng, Y. Qiao, K. Zang, et al., Synthesis of layered double hydroxides/graphene oxide nanocomposite as a novel high-temperature CO2 adsorbent, J. Energy Chem. 24 (2015) 127–137.

[58] W. Ma, R. Ma, C. Wang, J. Liang, X. Liu, K. Zhou, et al., A superlattice of alternately stacked Ni-Fe hydroxide nanosheets and graphene for efficient splitting of water, ACS Nano. 9 (2015) 1977–1984.

[59] Y. Zhong, Y. Liao, A. Gao, J. Hao, D. Shu, Y. Huang, et al., Supercapacitive behavior of electrostatic self-assembly reduced graphene oxide/CoAl-layered double hydroxides nanocomposites, J. Alloys Compd. (2016). doi:10.1016/j.jallcom.2016.01.251.

[60] T. Lee, S.H. Min, M. Gu, Y.K. Jung, W. Lee, J.U. Lee, et al., Layer-by-Layer Assembly for Graphene-Based Multilayer Nanocomposites: Synthesis and Applications, Chem. Mater. 27 (2015) 3785–3796.

[61] X. Dong, L. Wang, D. Wang, C. Li, J. Jin, Layer-by-layer engineered Co-Al hydroxide nanosheets/graphene multilayer films as flexible electrode for supercapacitor., Langmuir. 28 (2012) 293–298.

[62] J. Yang, C. Yu, X. Fan, J. Qiu, 3D architecture materials made of NiCoAl-LDH nanoplates coupled with NiCo-carbonate hydroxide nanowires grown on flexible graphite paper for asymmetric supercapacitors, Adv. Energy Mater. 4 (2014). doi:10.1002/aenm.201400761.

[63] J. Hao, W. Yang, Z. Zhang, B. Lu, X. Ke, B. Zhang, et al., Facile synthesis of three dimensional hierarchical Co-Al layered double hydroxides on graphene as high-performance materials for supercapacitor electrode., J. Colloid Interface Sci. 426 (2014) 131–136.

[64] W. Yang, Z. Gao, J. Wang, J. Ma, M. Zhang, L. Liu, Solvothermal one-step synthesis of Ni-Al layered double hydroxide/carbon nanotube/reduced graphene oxide sheet ternary nanocomposite with ultrahigh capacitance for supercapacitors, ACS Appl. Mater. Interfaces. 5 (2013) 5443–5454.

[65] X. Yu, M. Zhang, W. Yuan, G. Shi, A high-performance three-dimensional Ni–Fe layered double hydroxide/graphene electrode for water oxidation, J. Mater. Chem. A. 3 (2015) 6921–6928.

[66] J. Fang, M. Li, Q. Li, W. Zhang, Q. Shou, F. Liu, et al., Microwave-assisted synthesis of CoAl-layered double hydroxide/graphene oxide composite and its application in supercapacitors, Electrochim. Acta. 85 (2012) 248–255.

[67] H.F. Wang, C. Tang, Q. Zhang, Towards superior oxygen evolution through graphene barriers between metal substrates and hydroxide catalysts, J. Mater. Chem. A. 3 (2015) 16183–16189.

[68] T. Nakagawa, N.S. Bjorge, R.W. Murray, Electrogenerated IrO(x) nanoparticles as dissolved redox catalysts for water oxidation., J. Am. Chem. Soc. 131 (2009) 15578–9.

[69] Y. Lee, J. Suntivich, K.J. May, E.E. Perry, Y. Shao-Horn, Synthesis and Activities of Rutile IrO2 and RuO2 Nanoparticles for Oxygen Evolution in Acid and Alkaline Solutions., J. Phys. Chem. Lett. 3 (2012) 399–404.

[70] Z. Zhao, H. Wu, H. He, X. Xu, Y. Jin, A high-performance binary Ni-Co hydroxide-based water oxidation electrode with three-dimensional coaxial nanotube array structure, Adv. Funct. Mater. 24 (2014) 4698–4705.

[71] C.C.L. McCrory, S. Jung, J.C. Peters, T.F. Jaramillo, Benchmarking Heterogeneous Electrocatalysts for the Oxygen Evolution Reaction, J. Am. Chem. Soc. 135 (2013) 16977–16987.

[72] F. Song, X. Hu, Ultrathin cobalt-manganese layered double hydroxide is an efficient oxygen evolution catalyst., J. Am. Chem. Soc. 136 (2014) 16481–4.

[73] X. Lu, C. Zhao, Electrodeposition of hierarchically structured three-dimensional nickel-iron electrodes for efficient oxygen evolution at high current densities., Nat. Commun. 6 (2015) 6616.

[74] G.L. Tian, M.-Q. Zhao, D. Yu, X.-Y. Kong, J.-Q. Huang, Q. Zhang, et al., Nitrogen-doped graphene/carbon nanotube hybrids: in situ formation on bifunctional catalysts and their superior electrocatalytic activity for oxygen evolution/reduction reaction., Small. 10 (2014) 2251–9.

[75] J. Geng, L. Kuai, E. Kan, Q. Wang, B. Geng, Precious-metal-free Co-Fe-O/rGO synergetic electrocatalysts for oxygen evolution reaction by a facile hydrothermal route., ChemSusChem. 8 (2015) 659–64.

[76] D. Tang, J. Liu, X. Wu, R. Liu, X. Han, Y. Han, et al., Carbon quantum dot/NiFe layered double-hydroxide composite as a highly efficient electrocatalyst for water oxidation., ACS Appl. Mater. Interfaces. 6 (2014) 7918–25.

[77] D.H. Youn, Y. Bin Park, J.Y. Kim, G. Magesh, Y.J. Jang, J.S. Lee, One-pot synthesis of NiFe layered double hydroxide/reduced graphene oxide composite as an efficient electrocatalyst for electrochemical and photoelectrochemical water oxidation, J. Power Sources. 294 (2015) 437–443.

[78] Z. Lu, W. Xu, W. Zhu, Q. Yang, X. Lei, J. Liu, et al., Three-dimensional NiFe layered double hydroxide film for high-efficiency oxygen evolution reaction., Chem. Commun. (Camb). 50 (2014) 6479–6482.

[79] C. Tang, H.S. Wang, H.F. Wang, Q. Zhang, G.L. Tian, J.Q. Nie, et al., Spatially Confined Hybridization of Nanometer-Sized NiFe Hydroxides into Nitrogen-Doped Graphene Frameworks Leading to Superior Oxygen Evolution Reactivity., Adv. Mater. (2015). doi:10.1002/adma.201501901.

[80] X. Long, J. Li, S. Xiao, K. Yan, Z. Wang, H. Chen, et al., A strongly coupled graphene and FeNi double hydroxide hybrid as an excellent electrocatalyst for the oxygen evolution reaction, Angew. Chemie - Int. Ed. 53 (2014) 7584–7588.

[81] D. Xia, L. Zhou, S. Qiao, Y. Zhang, D. Tang, J. Liu, et al., Graphene/Ni–Fe layered double-hydroxide composite as highly active electrocatalyst for water oxidation, Mater. Res. Bull. 74 (2016) 441–446.

[82] X. Zhu, C. Tang, H.F. Wang, Q. Zhang, C. Yang, F. Wei, Dual-sized NiFe layered double hydroxides in situ grown on oxygen-decorated self-dispersal nanocarbon as enhanced water oxidation catalysts, J. Mater. Chem. A. 3 (2015) 24540–24546.

[83] L.L. Zhang, R. Zhou, X.S. Zhao, Graphene-based materials as supercapacitor electrodes, J. Mater. Chem. 20 (2010) 5983–5992.

[84] L.L. Zhang, X.S. Zhao, Carbon-based materials as supercapacitor electrodes., Chem. Soc. Rev. 38 (2009) 2520–3.

[85] L. Zhang, J. Wang, J. Zhu, X. Zhang, K. San Hui, K.N. Hui, 3D porous layered double hydroxides grown on graphene as advanced electrochemical pseudocapacitor materials, J. Mater. Chem. A. 1 (2013) 9046.

[86] M. Jana, S. Saha, P. Samanta, N.C. Murmu, N.H. Kim, T. Kuila, et al., Growth of Ni–Co binary hydroxide on a reduced graphene oxide surface by a successive ionic layer adsorption and reaction (SILAR) method for high performance asymmetric supercapacitor electrodes, J. Mater. Chem. A. 4 (2016) 2188–2197.

[87] X. Wu, L. Jiang, C. Long, T. Wei, Z. Fan, Dual Support System Ensuring Porous Co-Al Hydroxide Nanosheets with Ultrahigh Rate Performance and High Energy Density for Supercapacitors, Adv. Funct. Mater. 25 (2015) 1648–1655.

[88] A. Zhang, C. Wang, Q. Xu, H. Liu, Y. Wang, Y. Xia, A hybrid aerogel of Co-Al layered double hydroxide/graphene with three-dimensional porous structure as a novel electrode material for supercapacitors., RSC Adv. 5 (2015) 26017–26026.

[89] J. Fang, M. Li, Q. Li, W. Zhang, Q. Shou, F. Liu, et al., Microwave-assisted synthesis of CoAl-layered double hydroxide/graphene oxide composite and its application in supercapacitors, Electrochim. Acta. 85 (2012) 248–255.

[90] C. Du, J. Yeh, N. Pan, High power density supercapacitors using locally aligned carbon nanotube electrodes, Nanotechnology. 16 (2005) 350–353.

[91] G. Wang, L. Zhang, J. Zhang, A review of electrode materials for electrochemical supercapacitors, Chem. Soc. Rev. 41 (2012) 797–828.

[92] L. Yan, R. Li, Z. Li, J. Liu, Y. Fang, G. Wang, et al., Three-dimensional activated reduced graphene oxide nanocup/nickel aluminum layered double hydroxides composite with super high electrochemical and capacitance performances, Electrochim. Acta. 95 (2013) 146–154.

[93] C. Yu, J. Yang, C. Zhao, X. Fan, G. Wang, J. Qiu, Nanohybrids from NiCoAl-LDH coupled with carbon for pseudocapacitors: understanding the role of nano-structured carbon., Nanoscale. 6 (2014) 3097–104.

[94] W. Quan, Z.L. Tang, S.T. Wang, Y. Hong, Z.T. Zhang, Facile preparation of free-standing rGO paper-based Ni-Mn LDH/graphene superlattice composites as a pseudocapacitive electrode., Chem. Commun. (Camb). (2016). doi:10.1039/c5cc08744a.

[95] J. Hao, W. Yang, Z. Zhang, B. Lu, X. Ke, B. Zhang, et al., Facile synthesis of three dimensional hierarchical Co-Al layered double hydroxides on graphene as high-performance materials for supercapacitor electrode, J. Colloid Interface Sci. 426 (2014) 131–136.

[96] X. Wu, L. Jiang, C. Long, T. Wei, Z. Fan, Dual Support System Ensuring Porous Co-Al Hydroxide Nanosheets with Ultrahigh Rate Performance and High Energy Density for Supercapacitors, Adv. Funct. Mater. 25 (2015) 1648–1655.

[97] W. Hou, L. Kang, R. Sun, Z.H. Liu, Exfoliation of layered double hydroxides by an electrostatic repulsion in aqueous solution, Colloids Surfaces A Physicochem. Eng. Asp. 312 (2008) 92–98.

[98] Q. Fang, B. Chen, Self-assembly of graphene oxide aerogels by layered double hydroxides cross-linking and their application in water purification, J. Mater. Chem. A. 2 (2014) 8941.

[99] X. Ruan, Y. Chen, H. Chen, G. Qian, R.L. Frost, Sorption Behavior of Methyl Orange from Aqueous Solution on Organic matter and Reduced Graphene Oxides

Modified Ni-Cr Layered Double Hydroxides, Chem. Eng. J. (2016). doi:10.1016/j.cej.2016.01.041.

[100] M.Y. Miao, J.T. Feng, Q. Jin, Y.F. He, Y.N. Liu, Y.Y. Du, et al., Hybrid Ni–Al layered double hydroxide/graphene composite supported gold nanoparticles for aerobic selective oxidation of benzyl alcohol, RSC Adv. 5 (2015) 36066–36074.

[101] S.D. Jiang, L. Song, W.R. Zeng, Z.Q. Huang, J. Zhan, A.A. Stec, et al., Self-assembly fabrication of hollow mesoporous silica@Co-Al layered double hydroxide@graphene and application in toxic effluents elimination., ACS Appl. Mater. Interfaces. 7 (2015) 8506–14.

[102] G. Huang, J. Gao, X. Wang, H. Liang, C. Ge, How can graphene reduce the flammability of polymer nanocomposites, Mater. Lett. 66 (2012) 187–189.

[103] G. Huang, S. Chen, P. Song, P. Lu, C. Wu, H. Liang, Combination effects of graphene and layered double hydroxides on intumescent flame-retardant poly(methyl methacrylate) nanocomposites, Appl. Clay Sci. 88-89 (2014) 78–85.

[104] Y. Gao, J. Wu, Q. Wang, C.A. Wilkie, D. O'Hare, Flame retardant polymer/layered double hydroxide nanocomposites, J. Mater. Chem. A. 2 (2014) 10996.

[105] C.M. Becker, A.D. Gabbardo, F. Wypych, S.C. Amico, Mechanical and flame-retardant properties of epoxy/Mg–Al LDH composites, Compos. Part A Appl. Sci. Manuf. 42 (2011) 196–202.

[106] X. Wang, L. Song, H. Yang, W. Xing, B. Kandola, Y. Hu, Simultaneous reduction and surface functionalization of graphene oxide with POSS for reducing fire hazards in epoxy composites, J. Mater. Chem. 22 (2012) 22037.

[107] S. Roy, S.K. Srivastava, J. Pionteck, V. Mittal, Assembly of layered double hydroxide on multi-walled carbon nanotubes as reinforcing hybrid nanofiller in thermoplastic polyurethane/nitrile butadiene rubber blends, Polym. Int. (2015). doi:10.1002/pi.5032.

[108] B. Pradhan, S.K. Srivastava, Layered double hydroxide/multiwalled carbon nanotube hybrids as reinforcing filler in silicone rubber, Compos. Part A Appl. Sci. Manuf. 56 (2014) 290–299.

[109] J. Wang, Electrochemical glucose biosensors, Electrochem. Sensors, Biosens. Their Biomed. Appl. 108 (2008) 57–69.

[110] X.H. Zhu, F. Xie, J. Li, G.P. Jin, Simultaneously recover Ni, P and S from spent electroless nickel plating bath through forming graphene/NiAl layered double-hydroxide composite, J. Environ. Chem. Eng. 3 (2015) 1055–1060.

CHAPTER 6

Graphene/MgAl layered double hydroxides nanofillers as reinforcing agent for LLDPE nanocomposites prepared via *in-situ* polymerization

Muhammad Daud [1], Farrukh Shehzad [1], Mamdouh A. Al-Harthi [1,2*]

[1] Department of Chemical Engineering, King Fahd University of Petroleum and Minerals, Dhahran 31261, Saudi Arabia

[2] Center for Research Excellence in Nanotechnology (CENT), King Fahd University of Petroleum & Minerals, 31261, Dhahran, Saudi Arabia

[*]Corresponding Author: Mamdouh A. Al-Harthi

E-mail address: mamdouh@kfupm.edu.sa

Target journal for the submission of this chapter is "Composite science and Technology"

Abstract

Hybrid nanofiller based on graphene and MgAl layered double hydroxides (G/LDHs) were synthesized successfully by co-precipitation method. The *in situ* polymerization technique was adopted using 1-hexene as comonomer, zirconocene as a catalyst and hybrid as drop-in nanofiller. An increase catalytic activity was recorded due to the addition of hybrid nanofiller. Further, a maximum catalytic activity was observed for nanofiller hybridized with 100 mg of graphene. However, higher graphene contents reduce the activity due to agglomeration process. Moreover, the degree of crystallinity (DOC) decreases due to the addition of short chain branching (SCB) in the copolymers. The thermal stability of the copolymers was analyzed using TGA. The activation energy E_A profiles thus obtained has revealed that the polymer nanocomposites having hybrid 100 mg of graphene have imparted hgiher thermal stability to the copolymers.

Keywords: Graphene, Layered double hydroxides, Hybrid materials, Polymer nanocomposites, Catalytic activity

6.1 INTRODUCTION

Recently, polymer nanocomposites have gained great interest due to their potential applications, especially in energy storage applications [1,2], supercapacitors [3–5], sensors [6–8], drug delivery [9,10], water purification [11,12] and food packaging [13]. Nanofillers efficiently dispersed and interact with the polymer matrix by attributing the polymer with high mechanical strength, thermal stability and enhanced electrical properties, depending on the nature of the filler [14,15]. Carbon based nanofillers especially; carbon nanotubes (CNTs) and graphene are mostly used nanofillers to prepare polymer nanocomposites [16,17]. Though, the high production cost and low dispersive index of CNTs have limited its use in polymer nanocomposites. On the contrary, graphene has a two dimensional (2D) monolayer carbon assembly, arranged in honeycomb structure with high surface area [17]. Thermal and mechanical properties of the polymers are dramatically enhanced even with low graphene contents [18]. However, the pristine graphene is not compatible with organic polymers and need to be functionalized or hybridized with the other 2D nanomaterials [9,19].

On the other hand, layered double hydroxides (LDHs) have 2D highly tunable brucite-like lamellar crystal structure [20]. Like graphene, LDHs are also employed as nanofillers for the synthesis of polymer nanocomposites [21]. These LDHs based polymer nanocomposites have shown better thermal stability and flame retardancy [22,23]. However, in order to maintain the properties inherited by the LDHs and uniform dispersion in the polymer matrices, the LDHs undergo anionic modification or hybridization with others 1D or 2D nanofillers [24,25].

Of particular, hybrid nanomaterials fabricated using LDHs and graphene (G/LDHs), is of great importance because of the superior intrinsic properties inherited by them due to the combination of the special properties of the parent materials [26,27]. G/LDHs nanofillers can be used in variety of applications due to their versatile properties and flexibility in the composition/preparation for fine-tuning [28]. These future generation nanomaterials have thus a great potential to be used as supercapacitors [29], nanofillers for polymer nanocomposites [30], medical applications [31] and hybrid sensors [32] *etc.* In addition, the polymer nanocomposites developed using G/LDHs nanofillers have shown significant improvement in mechanical, thermal and electrical properties [30].

Linear low density polyethylene (LLDPE) is an important resin of polyethylene (PE), synthesized by the copolymerization of ethylene with comonomers [33]. Because of their low production cost and promising properties, make them of great importance among the consumers [34]. The most prominent applications of LLDPE include food packaging, plastic bags and pipes etc. [35].

In the present study, G/LDHs hybrid nanofillers were successfully synthesized by co-precipitation method. Different ratios of composition/preparation of G/LDHs were obtained by varying the ultrasonicated graphene contents in the feed. The hybrid G/LDHs nanofillers were than employed for the *in-situ* copolymerization of the LLDPE based polymer nanocomposites, using metallocene/MAO as a catalyst/cocatalyst complex. G/LDHs nanofillers have a noteworthy effect on the catalytic activity, short chain branching (SCB) and thermal stability of the copolymers.

6.2 EXPERIMENTAL

6.2.1 Chemical Reagents

Bis(cyclopentadienyl zirconium (IV) dichloride) > 98 % ($C_{10}H_{10}C_{l2}Zr$), Methylaluminoxane (MAO), Aluminum(III) nitrate nonahydrate [$Al(NO_3)_3.9H_2O$], magnesium(II) nitrate hexahydrate [$Mg(NO_3)_2.6H_2O$] and all other chemicals and solvents were provided by Sigma Aldrich Co. Graphene (96–99%, 50–100 nm) was purchased from Grafen Chemical Industries Co. (Turkey).

6.2.2 Preparation of MgAl LDHs

The standard co-precipitation method was adopted for the preparation of pure MgAl LDHs [36]. Briefly, precursor salts solution of both $Mg(NO_3)_2.6H_2O$ (0.03M) and $Al(NO_3)_3.9H_2O$ (0.01M) were initially well-mixed in 50mL of deionized (DI) water. Subsequently, the pH was adjusted at 10 ± 0.1 using 1M NaOH solution under vigorous stirring condition at 60 °C. After stabilizing the desired pH, the suspension was kept for reflux for 24h at 95 °C. The resultant white slurry was then centrifuge and washed with DI water and ethanol to remove any impurity. Lastly, the dense suspension was dried in vacuum oven at 60 °C for 24h. Approximately, 2.5 g of pure LDHs was synthesized with 3:1 molar ratio of precursor salts (Mg^{+2}: Al^{+3}).

6.2.3 Synthesis of Hybrid G/MgAl LDHs

The hybrids of G/MgAl LDHs were synthesized using co-precipitation method, already explained in our previous study [28]. Initially, graphene was ultrasonicated in 50ml solution of NaOH (0.20M) solution for 30min. Two different amounts of graphene were employed during this study i.e. 100 mg and 300 mg abbreviated as 100LDHs and

300LDHs respectively. The ultrasonicated graphene was then mixed with 3:1 molar precursor salt solution under continuous vigorous stirring. Consequently, the pH of the mixture was maintained at 10 ± 0.1 using 1M NaOH solution. The resultant hybrid solution was then kept for reflux at 95°C for 24h with subsequent centrifuging and washing. Finally the black dense suspension was dried in oven and characterized using different techniques. The weight percent of graphene were calculated to be 4 % and 12 % for 100LDHs and 300LDHs respectively from yield analysis.

6.2.4 *In-situ* polymerization

In-situ polymerization of ethylene-co-1-hexene was carried out in Schlenk reactor, according to the procedure, previously described in our work [37]. Briefly, the reactor was initially charged with 6mg (20 μmol) of zirconocene catalyst, 75 mg of hybrid G/LDHs nanofiller, 1 mL of comonomer (1-hexene) and 100mL of solvent (toluene) under nitrogen environment, inside the glove box. The reactor was then connected to ethylene feed line (1.3 bar gauge pressure) and maintained at a temperature of 30 °C using oil bath and hot plate. Subsequently, 5ml of MAO was introduced to the reactor after 5min of saturation with ethylene. The reaction was then stopped after 30min of reaction time and quenched with acidified methanol under vigorous stirring. The polymerization product was then filtered and dried in oven for 12h at 60 °C. After drying, the polymer was weighted to calculate the activity, before subjected to other characterization steps. Four samples were synthesized using no-filler (control), pure LDHs, 100LDHs and 300LDHs represented by PC, PC-LDH, PC-100 and PC-300 respectively.

6.2.5 Characterizations

1. The purity and crystalline phases of the as-synthesized hybrid nanofillers were investigated using room temperature wide-angle XRD. The sampling were carried out using Mini-Flex XRD (from Rigaku) operated at 40 kV and 15 mA with CuK alpha radiation (λ = 1.54060). The diffraction angle was selected in the range of 5 to 70 degrees (2θ) at a scanning rate of 2 degree per minute.

2. Fourier transform infrared spectra (FT-IR) spectra of the G/LDHs nanofillers were recorded with a PerkinElmer FT-IR spectrometer (model 16F-PC) using KBr pellet technique in the range of 4000 to 400 cm^{-1}.

3. Surface morphology of the as-synthesized nanofillers was observed using TESCAN Lyra-3 Field Emission Dual Beam (Electron/Focused Ion Beam) system combined with high resolution field emission scanning electron microscope (FE-SEM).

4. The dispersion of graphene and structural analysis of the as-synthesized hybrid nanofillers were observed with JEOL, JEM-2100F (USA) Transmission electron microscope (TEM).

5. The melting and crystallization behavior of the polymer nanocomposites were investigated using differential scanning calorimetry (DSC Q-1000) TA instrument using third heating cycle (30° to 160 °C).

6. Thermo-gravimetric analysis (TGA) was performed to study the thermal stability of the as-synthesized polymer nanocomposites. SDT-Q600 TGA by TA instruments was utilized at three different heating rates i.e. 10, 15, and 20 °C/min.

7. Crystallization analysis fractionation (CRYSTAF) supplied by Polymer Char (model-200) was employed to find the micro-structure and chemical composition distribution (CCD) of the polymer nanocomposites. Initially, the samples were dissolved in 1, 2, 4 trichlorobenzene (0.1 mg/mL), with subsequent cooling at 0.1 °C /min, with built-in infrared sensor detecting the crystallized portion of the polymer.

8. To find the comonomer incorporation analysis, 13 carbon nuclear magnetic resonance (^{13}C NMR) was conducted. ASTM method 5017-96 [38], based on integration of peaks relative to main methylene resonance at 30.0 ppm on x-axis was employed to compute the effect of nanofiller on the comonomer incorporation.

6.3 Results and Discussion

6.3.1 Establishment of hybrid G/LDHs nanofillers

XRD Patterns

XRD patterns of pure MgAl LDHs, pristine graphene (PG), 100LDHs and 300LDHs are depicted in Figure 6-1. The PG has shown an intense crystalline characteristic peak around $2\theta \approx 26°$ which corresponds to C(002) plane obtained from graphene reflection [39]. Moreover, the sharp diffraction peaks inherited by pure LDHs, 100LDHs and 300LDHs indicate their good lamellar structure and high crystalline nature. The diffraction peaks are approximately at ($2\theta \approx$) 11°, 23°, 35°, 39°, 60° and 62° which relates to the (003), (006), (009), (012), (110) and (113) crystal structure planes respectively, and is in consistent with the reported data [40,41]. As expected, the pure MgAl LDHs had more intense peaks at (003) and (006) planes compared to 100LDHs and 300LDHs. Moreover, at higher contents of graphene in the sample corresponds to intense (002) peak

(See Figure 6-1d). Furthermore, the XRD patterns have concluded that the G/LDHs hybrid nanofillers are less crystalline in nature than pure LDHs. In addition, the width of the XRD spectral peaks increases with the addition of graphene compared to pure LDHs [42]. Notably, the consistent appearance of (110) and (113) planes of almost same intensity has confirmed the well maintain crystal structure of LDHs [43,44].

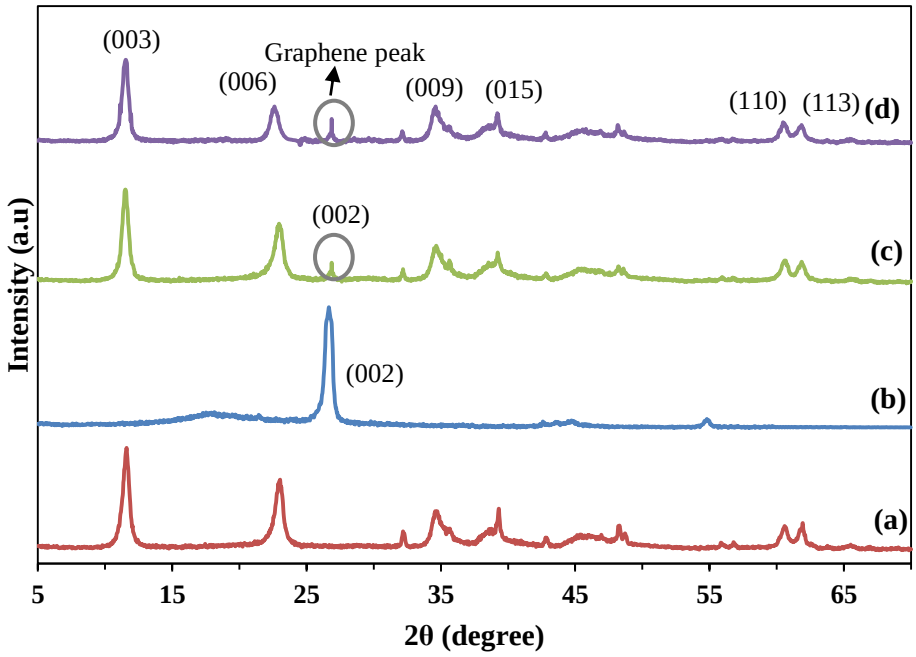

Figure 6-1. XRD patterns of (a) MgAl LDHs (b) PG (c) 100LDHs (c) 300LDHs

FT-IR Spectroscopy

The FT-IR spectra for pure LDHs, PG, 100LDH and 300LDH are presented in Figure 6-2. The characteristic peaks for the LDHs have shown a broad band at 3470 cm^{-1} which is due to the stretching vibration of hydrogen bonding and intercalated traces of water molecules that comes from synthesis process. Whereas, the weak band at peak position 1630 cm^{-1} is representing the bending modes of these intercalated water molecules [25]. Furthermore, the stretching vibration of the interlayer anions (NO_3^{-1}) of MgAl LDHs (1384 cm^{-1}) and metal-oxygen metal (400-810 cm^{-1}) are consistent with the reported data [45]. The PG absorption spectrum (See Figure 6-2) shows two weak band regions i.e. at position ≈1608 cm^{-1} (due to skeleton vibration of the graphene nanosheets) and ≈ 3423 (due to structural –OH groups and vibration of water molecules) [39].

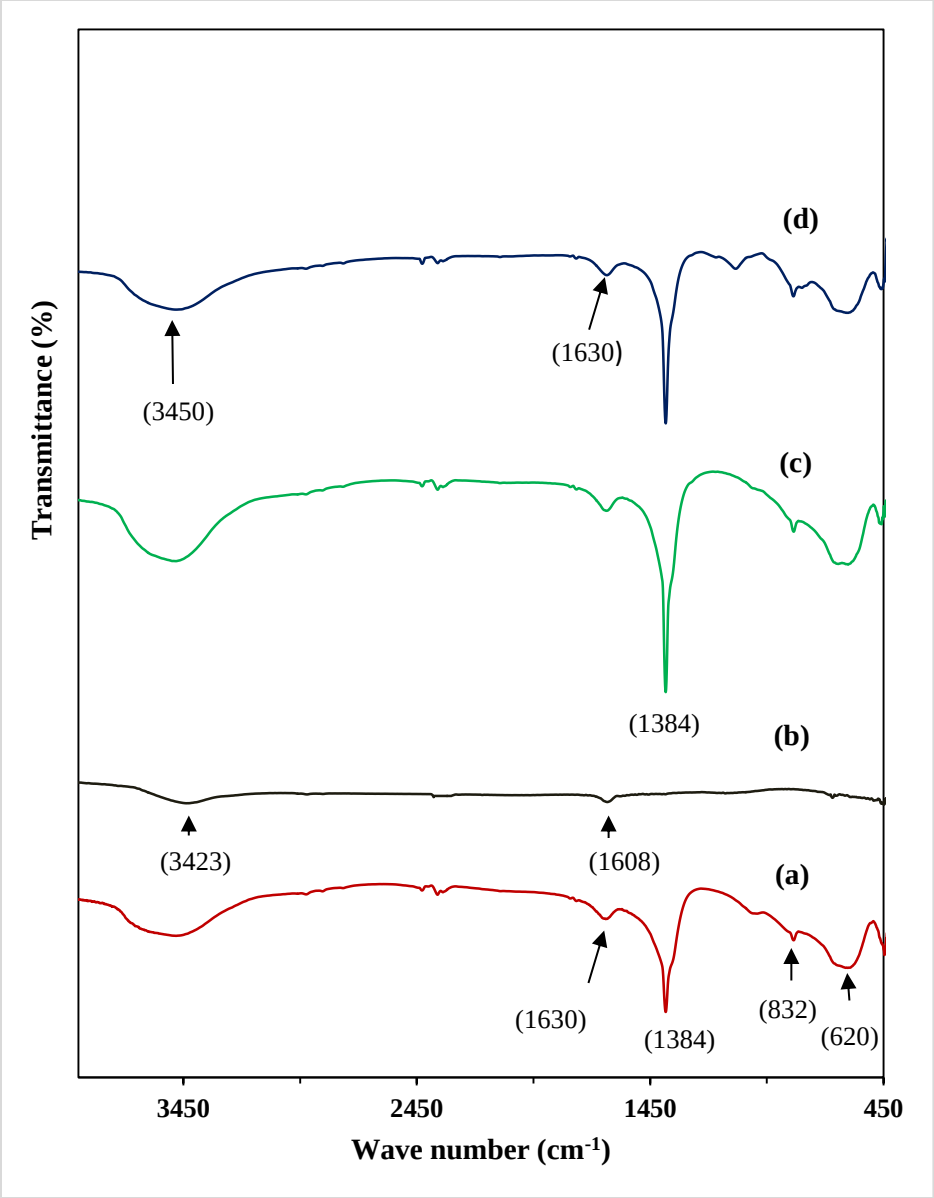

Figure 6-2. FT-IR spectra of (a) MgAl LDHs (b) PG (c) 100LDHs (c) 300LDHs

FE-SEM analysis

In order to study the morphology and microstructure of the hybrid nanofillers, PG, pure LDHs, 100LDs and 300LDHs were characterized using FE-SEM (See Figure 6-3). As expected, the PG is found to exist as smooth flat nanosheets, whereas, the occurrence of LDHs are as aggregates. The FE-SEM images for pure LDHs have revealed their lamellar surface morphology, stacked on top of each other. The hybrid images clearly indicated the synergy of graphene nanosheets inside the layered structure of LDHs.

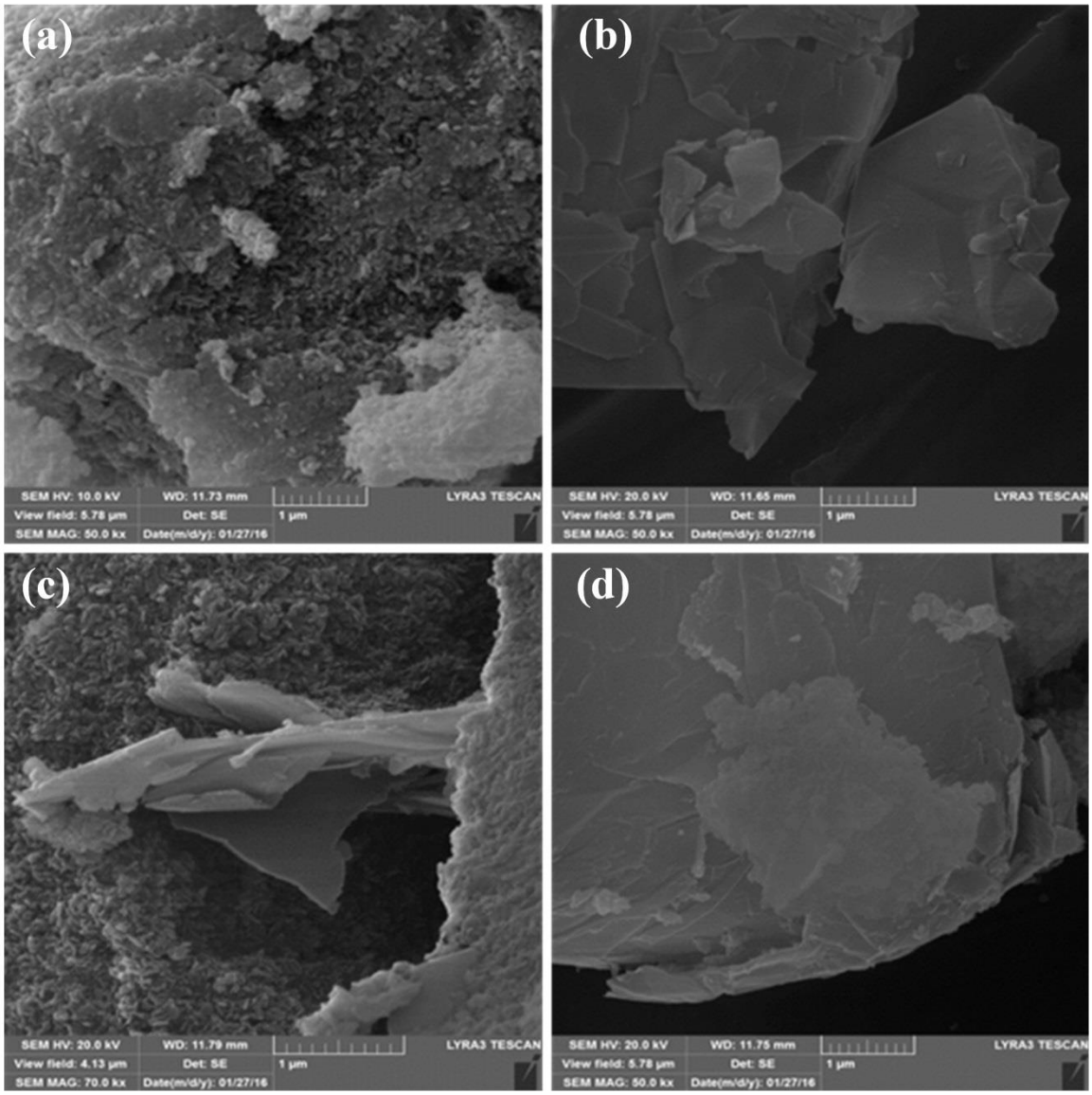

Figure 6-3. FE-SEM images of (a) MgAl LDHs (b) PG (c) 100LDHs (c) 300LDHs

TEM analysis

TEM images of PG, pure LDHs, 100LDHs and 300LDHs are displayed in Figure 6-4. The customary hexagonal nanoscale platelet structure of LDHs can be clearly seen from HR-TEM images. Further, the hexagons are stacked and strongly adhere to each other [41]. The hybrid G/LDHs shows homogeneous dispersion of graphene inside the nanofiller and a synergistic effect is observed in Figure 6-4 (c, d).

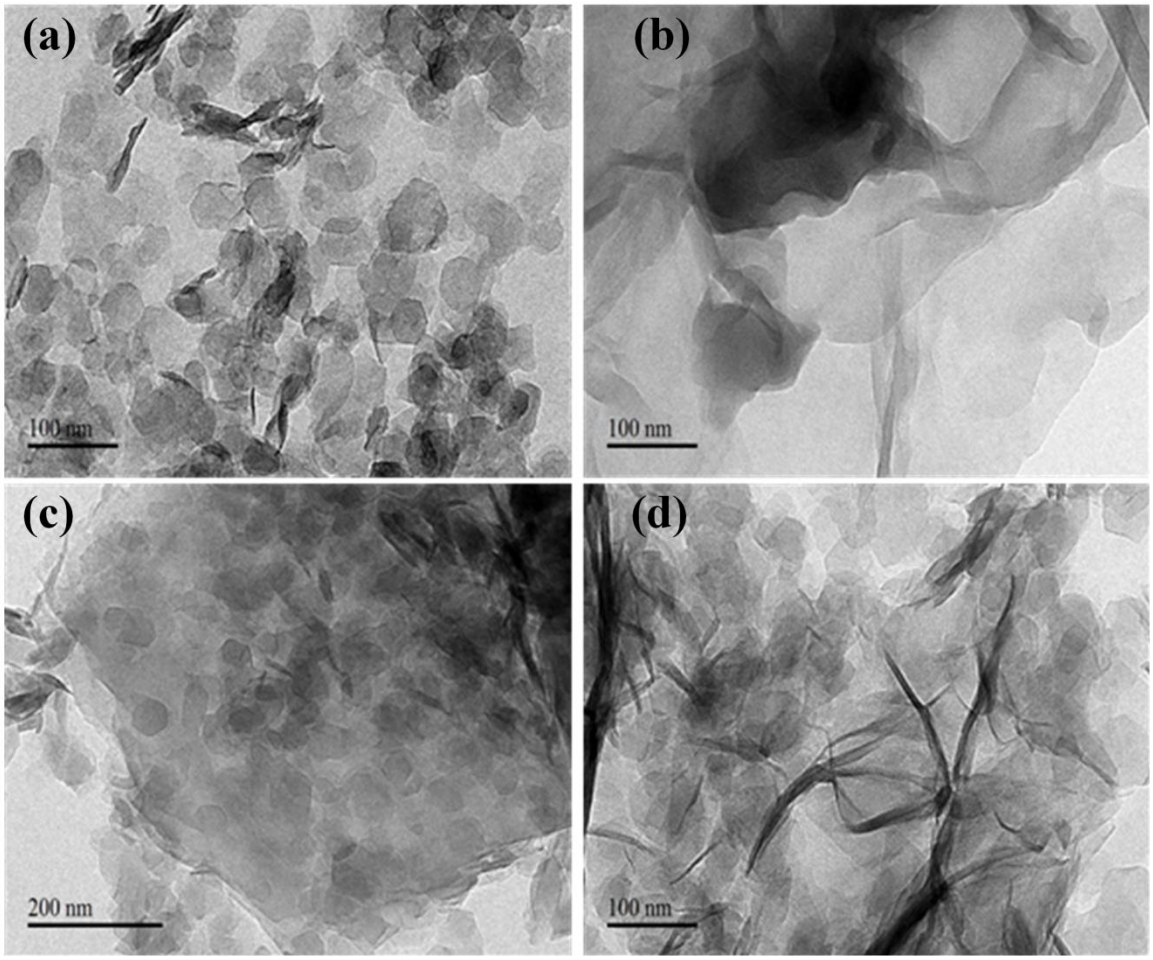

Figure 6-4. HR-TEM images of (a) MgAl LDHs (b) PG (c) 100LDHs (c) 300LDHs

6.3.2 Characterization of LLDPE-G/LDHs nanocomposites

Catalytic activity

The activity of the catalyst was calculated from the obtained yield and the corresponding polymerization results are summarized in Table 6-1. The addition of these nanofillers significantly influences the catalytic activities. The PC-LDHs has shown better catalytic activity (See Table 6-1) compared to control polymer sample (PC). Since, LDHs provide easier access to the active sites of the metallocene catalyst with relatively less agglomerated and spherical polymer particles. Moreover, the LDHs supported metallocene catalysts has shown more stability and higher catalytic activity towards ethylene polymerization [46]. The PC-100LDHs has maximum yield compared to all ethylene-co-1-hexene copolymers under study. This increase in activity is due to the hybridization of LDHs with 100 mg of graphene. The high surface area provided by 100LDHs hybrid nanofillers compared to pure LDHs, enables ethylene monomers with an easy access towards the active sites of zirconocene catalyst. However, further addition of graphene causes agglomeration around the catalyst, which reduces the active sites availability and thus causing decrease in the activity of zirconocene [47]. This phenomena is termed as “steric hindrance” [15]. Thus PC-300LDHs has relatively less catalytic activity than PC-100LDHs. However, minimal effects in molecular weights of the as-synthesized copolymers were observed due to the filler addition.

Table 6-1. Effect of hybrid G/LDHs nanofillers on the catalytic activity and other properties of LLDPE nanocomposites

S/no.	Sample code	Filler type/Amount (mg)	Activity [a] (kg PE mole^{-1} hr^{-1} bar^{-1})	DOC [b]	T_m [c] (°C)	M_w [d] (g/mol)
1	PC (control)	No filler	246.03 ± 3.29	39.02	122.27	22,141
2	PC-LDHs	Pure LDHs/75	299.83 ± 4.33	34.46	116.36	19,266
3	PC-100LDHs	100LDHs/75	389.67 ± 7.49	32.93	114.33	20,944
4	PC-300LDHs	300LDHs/75	362.20 ± 2.50	29.88	116.79	22,748

Reaction Temperature = 30 °C; solvent used= toluene (100 mL); zirconocene amount = 6 mg (20 μmol); comonomer used = 1-hexene (1 mL); polymerization time = 30 min

[a] calculated from yields

[b] determined by DSC

[c] determined by DSC

[d] determined by GPC

Crystallinity and 1-hexene incorporation

The degrees of crystallinity (DOC) of the copolymers were greatly influenced due to nanofiller addition (See Table 6-1). CRYSTAF is being utilized to figure out the CCD of the as-synthesized polymer nanocomposites, as depicted in Figure 6-5. As observed that a much wider profiles are obtained for the polymer nanocomposites compared to the PC (control). This change occurred in CCD and microstructure of the polymer samples were due to SCB (1-hexene incorporation), that were being induced by the nanofiller. In case of LLPDE, the comonomer incorporation has a very obvious effect on the DOC. Higher 1-hexene incorporation leads to lower DOC and vice versa [37]. The peak crystallization temperature (Tpeak) obtained from CRYSTAF results are tabulated in Table 6-2. The decrease in Tpeak temperatures indicates that nanofiller inducing more SCB to the polymer backbone thus decreasing the DOC. The CRYSTAF results were validated by ^{13}C NMR analysis (See Table 6-2). The maximum 1-hexene incorporation was recorded for PC-300LDHs, indicating more SCB added to the backbone structure of PE. On the other hand the melting temperatures (T_m) were also affected by SCB. A decrease in Tm was recorded for higher 1-hexene incorporation. However, a slight increase in T_m for PC-300LDHs nanocomposites was observed due to the presence of higher graphene contents.

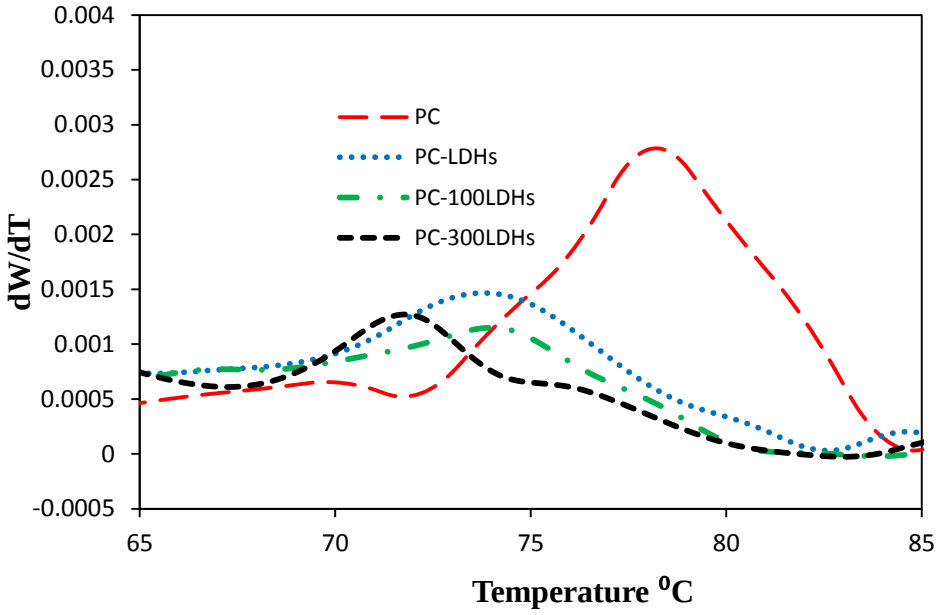

Figure 6-5. CRYSTAF profiles of LLDPE-hybrid G/LDHs polymer nanocomposites

Table 6-2. Effect of hybrid nanofillers on CRYSTAF curves

Sample ID	PC	PC-LDHs	PC-100LDHs	PC-300LDHs
T_{Peak} (°C)	78.2	73.4	73	71.1
1-hexene incorporation (^{13}C NMR)	3.30	5.1	5.3	5.8

Thermal Stability

The TGA curves of the all the samples are shown in Figure 6-6 at 10 °C /min and the selected results are listed in Table 6-3. The degradation curve is shifted to the right i.e. increasing temperature with the addition of the nano-filler. For example the, temperature at 5 wt. % (T5%) loss is increased from 379 °C for neat polymer to 397 °C for PC-LDH nanocomposites. Similarly, for the PC-100LDHs the T5% increased to 414 °C, the highest in this case. The T5% for PC-300LDHs is observed to be slightly lower that of PC-100LDHs i.e. 409 °C. This can be due to higher SCB as well as the high content of graphene within the hybrid nanofillers, which can increase the thermal conductivity of the nanocomposites, consequently providing better heat conduction and relatively faster degradation. The increase in the T5% indicates the nanocomposites are thermally more stable as compared to the neat polymer. A similar increasing trend for T50% and peak decomposition temperature (T_p) is also observed. However, the difference for T50% and Tp between the neat polymer and nanocomposites is reduced as compared to the T5%. The higher thermal stability of the nanocomposites, especially in the initials stages can be attributed to the layered structure and gas barrier characteristics of the nanofillers, which inhibits the evolution of the combustion gases [15,45]. Figure 6-7 shows the derivative of weight loss against temperature for all the samples.

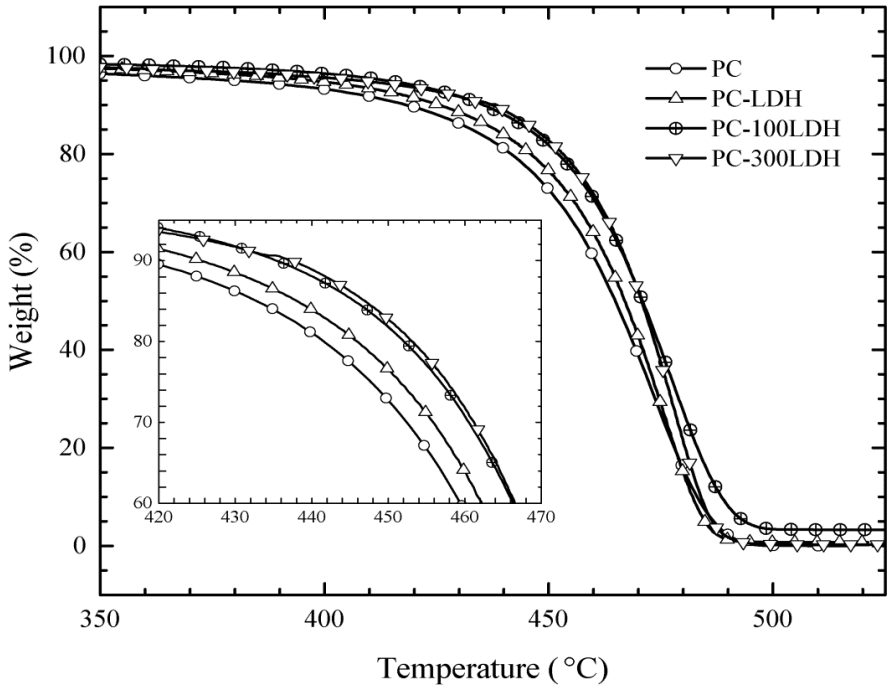

Figure 6-6. Weight loss with temperature ramp at 10 °C /min for polymer and its nanocomposites

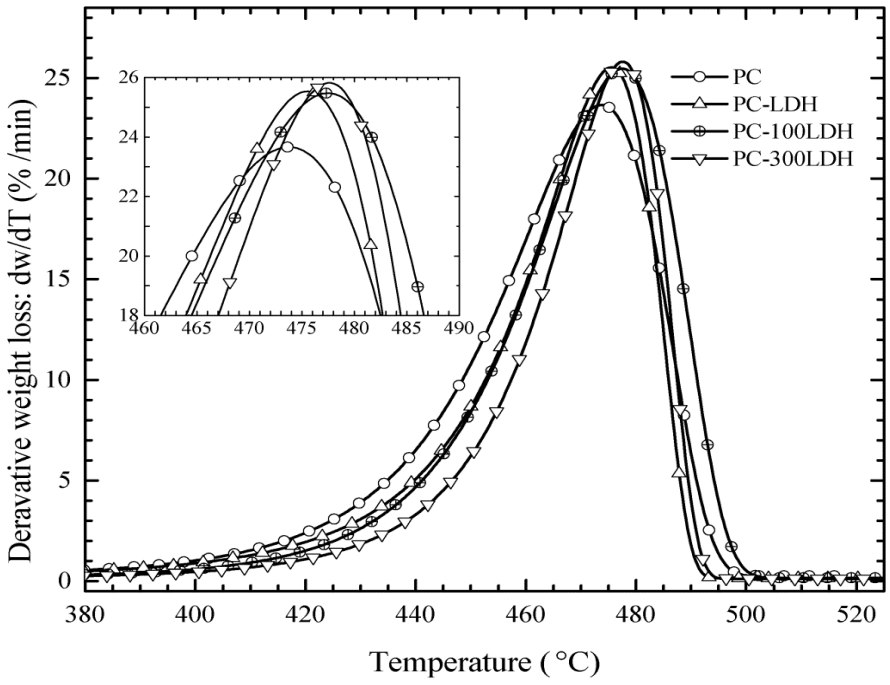

Figure 6-7. Derivative of weight loss with temperature ramp at 10 °C /min for polymer and its nanocomposites

Table 6-3. TGA analysis results for polymer and the nanocomposites at 10 °C /min

Sample	$T_{5\%}$ (°C)	$T_{50\%}$ (°C)	T_p (°C)
PC	379	464	474
PC-LDHs	397	468	476
PC-100LDHs	414	471	479
PC-300LDHs	409	470	478

A further insight of the thermal degradation was analyzed by calculating the apparent activation energy of degradation. As already reported in literature that the degradation of PE is a complex process i.e. it involves multiple kinetics steps [46]. Therefore, we have use iso-conversional Friedman method for the calculation of activation energy. Friedman method given by equation1, is an accurate differential method and provides the correct values of activation energy even if it is conversion dependent [47,48]. For this purpose each sample was heated with three heating rates 5, 10, and 15 °C /min under nitrogen flow of 100 mL/min.

$$\ln\left(\beta_i\left(\frac{d\alpha}{dT}\right)\right)_{\alpha_j} = -\left[lnf(\alpha) + \frac{E_A}{RT_i}\right] \qquad (1)$$

Whereas, β is the heating rate, α is the fractional conversion, E_A is the activation energy, R is gas constant and T is the temperature corresponding to the fractional conversion. E_A at specific values of α can be calculated from the slope of the straight line of $\beta_i\left(\frac{d\alpha}{dT}\right)$ vs $\frac{1}{RT_i}$, whereas, i represents the heating rate. Figure 6-8 shows the activation energy for all samples as a function of α. It can be observed that for all the samples the E_A changes with α, indicating a multiple step degradation mechanism. The degradation of polyethylene is known to start at the weak link by the reaction of a radical with the hydrogen atom on the fifth carbon atom. This free radical then degrades into either propene or 1-hexene. The initial lower values of the E_A correspond to this starting initiation reaction at the weak links. Later on, the degradation process is governed by the random scission process which demands a comparatively higher E_A [46]. As it can be seen from Figure 6-8 (a-d), the initial values of E_A increased with the addition of the nanofiller, from around 155 for PC to 169, 186, and 216, (kJ/mol) for PC-LDHs, PC-100LDHs, and

PC-300LDHs respectively. This increase can be attributed to higher thermal stability due to the addition of nanofillers. For the PC-300LDHs nanocomposites, average E_A is slightly lower as compared to the PC-100LDHs; this is due to the higher SCB content of the former, which provides more favorable links for the degradation to occur.

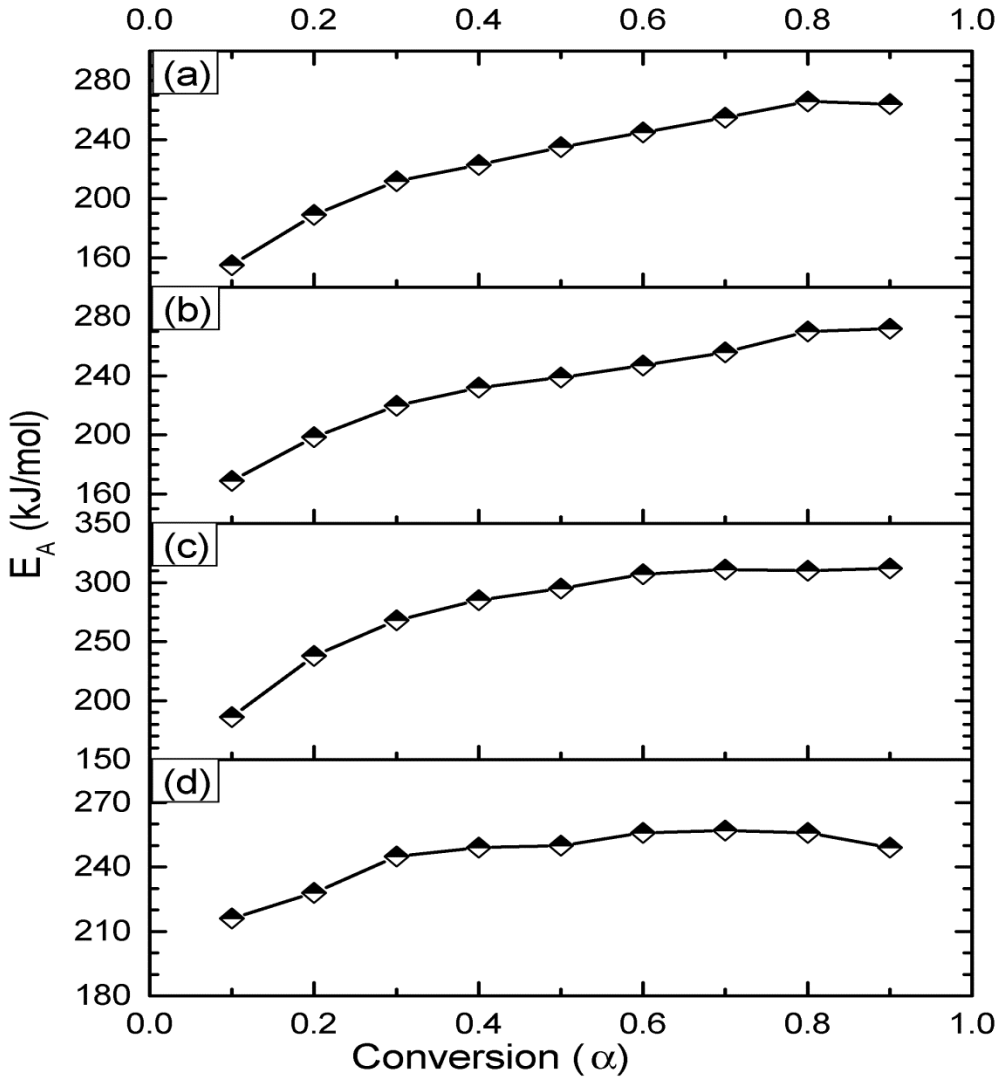

Figure 6-8. E_A as a function of the fractional conversion for (a) PC, (b) PC-LDHs, (c) PC-100LDHs, and (d) PC-300LDHs

6.4 Conclusion

Hybrid G/LDHs nanofillers were used for the synthesis of LLDPE nanocomposites. High catalytic activities and lower DOC were recorded for the as-synthesized polymer nanocomposites due to the nanofiller addition. 1-hexene incorporation was also increased due to more SCB in the polymer matrix. The PC-100LDHs nanocomposites have maximum catalytic activity (Approx. 36 % increased). A slight increase in the T_m of the PC-300LDHs was attributed due to presence of high graphene contents. Activation Energy (E_A) for the as-synthesized polymer nanocomposites were calculated using iso-conversional Friedman method. A higher average E_A was obtained for PC-100LDHs (≈ 270 kJ/mol), indicating its higher thermal stability. Moreover, the improvements observed in catalytic activity, comonomer incorporation and thermal properties of these polymer nanocomposites, indicating better dispersion of nanofillers in the polymer matrix

6.5 References

[1] V.K. Thakur, M.R. Kessler, Polymer Nanocomposites: New Advanced Dielectric Materials for Energy Storage Applications, in: Adv. Energy Mater., Wiley Blackwell, 2014: pp. 207–257.

[2] X. Huang, P. Jiang, Core-shell structured high- k polymer nanocomposites for energy storage and dielectric applications, Adv. Mater. 27 (2015) 546–554.

[3] Z. Zhang, M. Liao, H.-Y. Zeng, S. Xu, X. Liu, J. Du, et al., Temperature effect on chromium(VI) removal by Mg/Al mixed metal oxides as adsorbents, Appl. Clay Sci. 102 (2014) 246–253. doi:10.1016/j.clay.2014.10.005.

[4] W. Wu, Y. Li, L. Yang, Y. Ma, D. Pan, Y. Li, A facile one-pot preparation of dialdehyde starch reduced graphene oxide/polyaniline composite for supercapacitors, Electrochim. Acta. 139 (2014) 117–126.

[5] F. Chen, P. Liu, Q. Zhao, Well-defined graphene/polyaniline flake composites for high performance supercapacitors, Electrochim. Acta. 76 (2012) 62–68.

[6] L. Al-Mashat, K. Shin, K. Kalantar-Zadeh, J.D. Plessis, S.H. Han, R.W. Kojima, et al., Graphene/polyaniline nanocomposite for hydrogen sensing, J. Phys. Chem. C. 114 (2010) 16168–16173.

[7] S. Konwer, A.K. Guha, S.K. Dolui, Graphene oxide-filled conducting polyaniline composites as methanol-sensing materials, J. Mater. Sci. 48 (2013) 1729–1739.

[8] S.K. Kumar, M. Castro, A. Saiter, L. Delbreilh, J.F. Feller, S. Thomas, et al., Development of poly(isobutylene-co-isoprene)/reduced graphene oxide

nanocomposites for barrier, dielectric and sensingapplications, Mater. Lett. 96 (2013) 109–112.

[9] M. Zhang, Y. Li, Z. Su, G. Wei, Recent advances in the synthesis and applications of graphene–polymer nanocomposites, Polym. Chem. 6 (2015) 6107–6124. doi:10.1039/C5PY00777A.

[10] T. Kavitha, I.K. Kang, S.Y. Park, Poly(N-vinyl caprolactam) grown on nanographene oxide as an effective nanocargo for drug delivery, Colloids Surfaces B Biointerfaces. 115 (2014) 37–45.

[11] C.A. Crock, A.R. Rogensues, W. Shan, V. V. Tarabara, Polymer nanocomposites with graphene-based hierarchical fillers as materials for multifunctional water treatment membranes, Water Res. 47 (2013) 3984–3996.

[12] R. Li, L. Liu, F. Yang, Preparation of polyaniline/reduced graphene oxide nanocomposite and its application in adsorption of aqueous Hg(II), Chem. Eng. J. 229 (2013) 460–468.

[13] A.M. Youssef, Polymer Nanocomposites as a New Trend for Packaging Applications, Polym. Plast. Technol. Eng. 52 (2013) 635–660.

[14] J.R. Potts, D.R. Dreyer, C.W. Bielawski, R.S. Ruoff, Graphene-based polymer nanocomposites, Polymer (Guildf). 52 (2011) 5–25.

[15] F. Shehzad, M. Daud, M.A. Al-Harthi, Synthesis, characterization and crystallization kinetics of nanocomposites prepared by in situ polymerization of ethylene and graphene, J. Therm. Anal. Calorim. 123 (2016) 1501–1511.

doi:10.1007/s10973-015-5087-x.

[16] G. Mittal, V. Dhand, K.Y. Rhee, S.-J. Park, W.R. Lee, A review on carbon nanotubes and graphene as fillers in reinforced polymer nanocomposites, J. Ind. Eng. Chem. 21 (2015) 11–25. doi:10.1016/j.jiec.2014.03.022.

[17] H. Kim, A.A. Abdala, C.W. MacOsko, Graphene/polymer nanocomposites, Macromolecules. 43 (2010) 6515–6530.

[18] F. Shehzad, S.P. Thomas, M.A. Al-Harthi, Non-isothermal crystallization kinetics of high density polyethylene/graphene nanocomposites prepared by in-situ polymerization, Thermochim. Acta. 589 (2014) 226–234. doi:10.1016/j.tca.2014.05.039.

[19] H. Kim, S. Kobayashi, M.A. Abdurrahim, M.J. Zhang, A. Khusainova, M.A. Hillmyer, et al., Graphene/polyethylene nanocomposites: Effect of polyethylene functionalization and blending methods, Polymer (Guildf). 52 (2011) 1837–1846.

[20] Q. Wang, D. Ohare, Recent advances in the synthesis and application of layered double hydroxide (LDH) nanosheets, Chem. Rev. 112 (2012) 4124–4155. doi:10.1021/cr200434v.

[21] F.R. Costa, M. Saphiannikova, U. Wagenknecht, G. Heinrich, Layered double hydroxide based polymer nanocomposites, Wax Cryst. Control Nanocomposites, Stimuli-Responsive Polym. 210 (2008) 101–168. doi:10.1007/12_2007_123.

[22] C. a. W. and D.O. Yanshan Gao, Jingwen Wu,QiangWang, Flame retardant polymer/layered double hydroxide nanocomposites, J. Mater. Chem. A. (2014)

10996–11016. doi:10.1039/c4ta01030b.

[23] Z. Matusinovic, C. a. Wilkie, Fire retardancy and morphology of layered double hydroxide nanocomposites: a review, J. Mater. Chem. 22 (2012) 18701.

[24] B. Pradhan, S.K. Srivastava, A.K. Bhowmick, A. Saxena, Effect of bilayered stearate ion-modified Mg-Al layered double hydroxide on the thermal and mechanical properties of silicone rubber nanocomposites, Polym. Int. 61 (2012) 458–465. doi:10.1002/pi.3218.

[25] S. Mallakpour, M. Dinari, Hybrids of Mg–Al-layered double hydroxide and multiwalled carbon nanotube as a reinforcing filler in the l-phenylalanine-based polymer nanocomposites, J. Therm. Anal. Calorim. 119 (2015) 1905–1912. doi:10.1007/s10973-014-4270-9.

[26] Y. Cao, G. Li, X. Li, Graphene/layered double hydroxide nanocomposite: Properties, synthesis, and applications, Chem. Eng. J. 292 (2016) 207–223. doi:10.1016/j.cej.2016.01.114.

[27] M.-Q. Zhao, Q. Zhang, J.-Q. Huang, F. Wei, Hierarchical Nanocomposites Derived from Nanocarbons and Layered Double Hydroxides - Properties, Synthesis, and Applications, Adv. Funct. Mater. 22 (2012) 675–694. doi:10.1002/adfm.201102222.

[28] M. Daud, M.S. Kamal, F. Shehzad, M.A. Al-Harthi, Graphene/layered double hydroxides nanocomposites: A review of recent progress in synthesis and applications, Carbon N. Y. 104 (2016) 241–252.

doi:10.1016/j.carbon.2016.03.057.

[29] Y. Zhong, Y. Liao, A. Gao, J. Hao, D. Shu, Y. Huang, et al., Supercapacitive behavior of electrostatic self-assembly reduced graphene oxide/CoAl-layered double hydroxides nanocomposites, J. Alloys Compd. 669 (2016) 146–155.

[30] B. Yuan, C. Bao, X. Qian, S. Jiang, P. Wen, W. Xing, et al., Synergetic dispersion effect of graphene nanohybrid on the thermal stability and mechanical properties of ethylene vinyl acetate copolymer nanocomposite, Ind. Eng. Chem. Res. 53 (2014) 1143–1149.

[31] S. Fu, G. Fan, L. Yang, F. Li, Non-enzymatic glucose sensor based on Au nanoparticles decorated ternary Ni-Al layered double hydroxide/single-walled carbon nanotubes/graphene nanocomposite, Electrochim. Acta. 152 (2015) 146–154.

[32] H. Li, J. Wen, R. Yu, J. Meng, C. Wang, C. Wang, et al., Facile synthesis of a nanocomposite based on graphene and ZnAl layered double hydroxides as a portable shelf of a luminescent sensor for DNA detection, Rsc Adv. 5 (2015) 9341–9347.

[33] M. Daud, F. Shehzad, M.A. Al-Harthi, Crystallization behaviour and lamellar thickness distribution of metallocene-catalyzed polymer: Effect of 1-alkene comonomer and branch length, Can. J. Chem. Eng. (2016). doi:10.1002/cjce.22711.

[34] P.S. Chum, K.W. Swogger, Olefin polymer technologies—History and recent

progress at The Dow Chemical Company, Prog. Polym. Sci. 33 (2008) 797–819. doi:10.1016/j.progpolymsci.2008.05.003.

[35] S.T. Harini, S. Padmavathi, A. Satish, B. Raj, Food compatibility and degradation properties of pro-oxidant-loaded LLDPE film, J. Appl. Polym. Sci. 131 (2014) n/a-n/a. doi:10.1002/app.39756.

[36] E.L. Crepaldi, P.C. Pavan, J.B. Valim, Comparative study of the coprecipitation methods for the preparation of Layered Double Hydroxides, J. Braz. Chem. Soc. 11 (2000) 64–70. doi:10.1590/S0103-50532000000100012.

[37] M. Daud, F. Shehzad, M.A. Al-Harthi, Non-isothermal crystallization kinetics of LLDPE prepared by in situ polymerization in the presence of nano titania, Polym. Bull. 72 (2015) 1233–1245. doi:10.1007/s00289-015-1335-2.

[38] ASTM D5017-96(2009)e1, Standard Test Method for Determination of Linear Low Density Polyethylene (LLDPE) Composition by Carbon-13 Nuclear Magnetic Resonance, ASTM Int. West Conshohocken, PA, 2003. (2009).

[39] S. Roy, S.K. Srivastava, J. Pionteck, V. Mittal, Mechanically and Thermally Enhanced Multiwalled Carbon Nanotube-Graphene Hybrid filled Thermoplastic Polyurethane Nanocomposites, Macromol. Mater. Eng. 300 (2015) 346–357. doi:10.1002/mame.201400291.

[40] V. Rives, Characterisation of layered double hydroxides and their decomposition products, Mater. Chem. Phys. 75 (2002) 19–25. doi:10.1016/S0254-0584(02)00024-X.

[41] S. Roy, S.K. Srivastava, J. Pionteck, V. Mittal, Assembly of layered double hydroxide on multi-walled carbon nanotubes as reinforcing hybrid nanofiller in thermoplastic polyurethane/nitrile butadiene rubber blends, Polym. Int. 65 (2016) 93–101. doi:10.1002/pi.5032.

[42] M.G. Álvarez, D. Tichit, F. Medina, J. Llorca, Role of the synthesis route on the properties of hybrid LDH-graphene as basic catalysts, Appl. Surf. Sci. (2016). doi:10.1016/j.apsusc.2016.11.037.

[43] R. Ma, X. Liu, J. Liang, Y. Bando, T. Sasaki, Molecular-Scale Heteroassembly of Redoxable Hydroxide Nanosheets and Conductive Graphene into Superlattice Composites for High-Performance Supercapacitors, Adv. Mater. 26 (2014) 4173–4178. doi:10.1002/adma.201400054.

[44] W. Ma, R. Ma, C. Wang, J. Liang, X. Liu, K. Zhou, et al., A Superlattice of Alternately Stacked Ni–Fe Hydroxide Nanosheets and Graphene for Efficient Splitting of Water, ACS Nano. 9 (2015) 1977–1984. doi:10.1021/nn5069836.

[45] S. Tang, H.K. Lee, Application of Dissolvable Layered Double Hydroxides As Sorbent in Dispersive Solid-Phase Extraction and Extraction by Co-Precipitation for the Determination of Aromatic Acid Anions, Anal. Chem. 85 (2013) 7426–7433. doi:10.1021/ac4013573.

[46] J.-C. Buffet, C.F.H. Byles, R. Felton, C. Chen, D. O'Hare, Metallocene supported core@LDH catalysts for slurry phase ethylene polymerisation, Chem. Commun. 52 (2016) 4076–4079. doi:10.1039/C6CC00280C.

[47] H.-X. Zhang, E.-B. Ko, J.-H. Park, Y.-K. Moon, X.-Q. Zhang, K.-B. Yoon, Fabrication of polyethylene/graphene nanocomposites through in situ polymerization with a spherical graphene/MgCl2-supported Ziegler-Natta catalyst, Compos. Sci. Technol. 136 (2016) 61–66. doi:10.1016/j.compscitech.2016.10.005.

[48] G. Huang, S. Chen, P. Song, P. Lu, C. Wu, H. Liang, Combination effects of graphene and layered double hydroxides on intumescent flame-retardant poly(methyl methacrylate) nanocomposites, Appl. Clay Sci. 88–89 (2014) 78–85. doi:10.1016/j.clay.2013.11.002.

[49] J.D. Peterson, S. Vyazovkin, C.A. Wight, Kinetics of the Thermal and Thermo-Oxidative Degradation of Polystyrene, Polyethylene and Poly(propylene), Macromol. Chem. Phys. 202 (2001) 775–784. doi:10.1002/1521-3935(20010301)202:6<775::AID-MACP775>3.0.CO;2-G.

[50] H.L. Friedman, Kinetics of thermal degradation of char-forming plastics from thermogravimetry. Application to a phenolic plastic, J. Polym. Sci. Part C Polym. Symp. 6 (1964) 183–195. doi:10.1002/polc.5070060121.

[51] M. Zubair, F. Shehzad, M.A. Al-Harthi, Impact of modified graphene and microwave irradiation on thermal stability and degradation mechanism of poly (styrene-co-methyl meth acrylate), Thermochim. Acta. 633 (2016) 48–55.

CHAPTER 7

CONCLUSIONS AND RECOMMENDATIONS

7.1 Conclusion

The *in-situ* polymerization of ethylene-co-α-olefin were carried out in slurry phase polymerization using zirconocene complex and Schlenk techniques. These α-olefin (comonomers) significantly influenced the catalytic activity, melt crystallization and lamellar thickness distribution. Approx. 18 %, 19 % and 15 % increased catalytic activities were recorded with the addition of just 1 mL of 1-hexene, 1-octene and 1-decene comonomers respectively. Mo-model successfully covered the melt crystallization behavior of copolymers used under this study. The activation energies (E_A), calculated for the fabricated copolymers has shown that the crystallization behavior is more affected by comonomer contents rather than its type for same feed ratios.

The drop in nanofiller (TiO_2/Mn) significantly increased the catalytic activity (approx. ≈ 44 %) for ethylene-co-1-hexene at an optimum dose of 15 mg. The filler also increased the 1-hexene incorporation by imparting more SCB to the polymer structure and hence decreased the DOC and T_m. An increased E_A was recorded for the as-synthesized LLDPE nanocomposites, which indicates slow crystal growth rate in the presence of nanofiller.

G/LDHs hybrid nanofillers were synthesized in house by co-precipitation route. The hybrid fillers were then used as a drop in filler during *in-situ* ethylene polymerization in the presence of 1-hexene as a comonomer. The polymer nanocomposites synthesized

with 100 mg of hybridized graphene and LDHs have shown maximum catalytic activity (approx. 36% increased) and is more thermally stable ($E_A \approx 270$ kJ/mol) compared to the control ethylene-co-1-hexene copolymer ($E_A \approx 155$ kJ/mol).

The research outcomes are four ISI indexed (peer reviewed) research publications. The details of these manuscripts are as under:

1. **Muhammad Daud**, Muhammad Shahzad Kamal, Farrukh Shehzad, Mamdouh A. Al-Harthi, "Graphene/layered double hydroxides nanocomposites: A review of recent progress in synthesis and applications" ***Carbon*** **2016**
2. **Muhammad Daud**, Farrukh Shehzad, Mamdouh A. Al-Harthi, "Non-isothermal crystallization kinetics of LLDPE prepared by *in-situ* polymerization in the presence of nano titania" ***Polymer Bulletin*** **2015**
3. **Muhammad Daud**, Farrukh Shehzad, Mamdouh A. Al-Harthi, "Crystallization behavior and lamellar thickness distribution of metallocene-catalyzed polymer: Effect of 1-alkene comonomer and branch length" ***The Canadian Journal of Chemical Engineering*** **2016**
4. **Muhammad Daud**, Faruukh Shehzad, Mamdouh A. Al-Harthi, "Graphene/MgAl layered double hydroxides nanofillers as reinforcing agent for LLDPE nanocomposites prepared via *in-situ* polymerization" submitted to, **Composite Science and Technology 2016**.

7.2 Future Recommendations

- The effect of different crystallite sizes of nano titania can be studied for the activity of zirconocene catalyst.
- The work can be extended to study the effect of hybrid nanofillers on the mechanical properties of the LLDPE nanocomposites.
- More combination of hybrid nanofillers should be synthesized and employed as a drop in nanofillers for the production of LLDPE nanocomposites.
- It is recommended to used LDHs as support material for zirconocene catalyst.
- It is highly recommended to synthesized Mn based hybrid nanofillers for LLDPE nanocomposites.

Vitae

MUHAMMAD DAUD

Department of Chemical Engineering,

King Fahd University of Petroleum & Minerals,

Dhahran, Kingdom of Saudi Arabia

Phone (M): +966-598902558
Phone (M): +92-3459111772
Nationality: Pakistani
Date of birth: 23-05-1983
Email: daud@uetpeshawar.edu.pk

EDUCATION

Ph.D **:** Chemical Engineering, 2012-2016
King Fahd University of Petroleum & Minerals, Saudi Arabia
Thesis: Effect of Nano Fillers on the Production and Properties of LLDPE using *in-situ* Polymerization

M.Sc **:** Advance Chemical Engineering
University of Engineering & Technology, Peshawar, Pakistan
Thesis: Coal Briquettes Analysis Using Different Binding Materials, For Khyber Pakhtunkhwa Coal

B.Sc**:**.Chemical Engineering (Gold Medalist), 2004-2007
University of Engineering & Technology, Peshawar, Pakistan

RESEARCH INTERESTS

- Polymer Synthesis
- Crystallization Kinetics
- Solid State Kinetics
- Nanocomposites

TEACHING INTERESTS

- Transport Phenomena
- Reaction Engineering
- Simultaneous Heat and Mass Transfer
- Poymer Material Testing and Characterization

PROFESSIONAL EXPERIENCE

- Lecturer, Department of Chemical Engineering, UET Peshawar, from 13th December, 2007 till date (on study leave).
- Lecturer-B, Department of Chemical Engineering KFUPM, KSA from January 2012 December 2016.

JOURNAL PUBLICATIONS

1. **Muhammad Daud**, Muhammad Shahzad Kamal, Farrukh Shehzad, Mamdouh A. Al-Harthi, "Graphene/layered double hydroxides nanocomposites: A review of recent progress in synthesis and applications" ***Carbon*** **2016**
2. **Muhammad Daud**, Farrukh Shehzad, Mamdouh A. Al-Harthi, "Non-isothermal crystallization kinetics of LLDPE prepared by *in-situ* polymerization in the presence of nano titania" ***Polymer Bulletin*** **2015**
3. **Muhammad Daud**, Farrukh Shehzad, Mamdouh A. Al-Harthi, "Crystallization behavior and lamellar thickness distribution of metallocene-catalyzed polymer: Effect of 1-alkene comonomer and branch length" ***The Canadian Journal of Chemical Engineering*** **2016**
4. Farrukh Shehzad, **Muhammad Daud**, Mamdouh A. Al-Harthi, "Synthesis, characterization and crystallization kinetics of nanocomposites prepared by in-situ polymerization of ethylene and graphene" ***Journal of Thermal Analysis and Calorimetry*** **2015**
5. **Muhammad Daud**, Faruukh Shehzad, Mamdouh A. Al-Harthi, "Graphene/MgAl layered double hydroxides nanofillers as reinforcing agent for LLDPE nanocomposites prepared via *in-situ* polymerization" submitted to, **Composite Science and Technology 2016**

6. Mukarram Zubair, Mamdouh Al-Harthi, Saood Manzar, **Muhammad Daud**, Nuhu Dalhat Mu'azu, Shamsudeen Haladu, "Adsorption of Eriochrome Black-T from Aqueous Phase on MgAl-, CoAl- and NiFe- Calcined Layered Double Hydroxides: Kinetic, Equilibrium and Thermodynamic Studies" Under Review, **Journal of Molecular Liquids**
7. Mukarram Zubair, **Muhammad Daud**, Gordon McKay, Farrukh Shehzad, Mamdouh Al-Harthi, "Recent progress in Layered double hydroxides (LDHs) nano-hybrids as adsorbents for water remediation" submitted to, **Environmental Science and Pollution Research**